Correlation of Distance and Damage in a Ballistic Setting

by

Nathan George Brooke

Canterbury Christ Church University

Thesis Submitted

For the degree of MSC by Research

2020

Abstract

Forensic Investigation is a discipline which relies on various fields in order to be able to reconstruct an incident. Forensic Ballistics focuses upon the mechanics of projectile launch, flight and the effects of the projectile when impacting a target as well as firearms and ammunition. One of the most common evidence types in firearms related events is Gun Shot Residue (GSR), where typical analysis methods involves chemical confirmatory tests. Therefore, the fields traditionally associated with forensic ballistics are chemistry and physics, however there are various other scientific fields which could potentially further knowledge in this area such as radiography and computational science.

Arguably one of the most important considerations within Forensic Ballistics is the ability to accurately reconstruct an incident. Currently there is limited literature aimed at understanding GSR spread at distances above 15 metres, which is a limitation for the criminal justice system *(chapter 1)*. This work aims to further this knowledge by gaining an understanding of GSR spread at various distances, both short and long range *(chapter 4)*, whilst combining this with Gun Shot Wound (GSW) damage using radiography *(chapter 3)*. The data obtained will then be used for computational modelling with the aim of predicting shooter distance *(chapter 5)*.

Acknowledgements

Summary of Figures

Summary of Tables

Table of Contents

Chapter 1
Introduction and Literature Review

1.1 Forensic Investigation & Ballistics

1.1.1 Introduction

Forensic Investigation is a broad and diverse field within the criminal justice system, involving many areas of science, such as Forensic Biology, Forensic Chemistry and Ballistics (Lyle, 2019). Each of these play an important role within forensic investigation, however the amount of research attention focussed upon each area differs greatly. The field of ballistics, while being as important as other specialisms does not share the same wealth of research. For example, in the 2018 – 2020 period, 20,700 research articles were published for Forensic Chemistry versus the 1,490 for Forensic Ballistics (Google Scholar, 2020).

Firearms identification is a specialist field within Forensic Investigation, which often combines with Forensic Ballistics. Forensic Ballistics is focussed upon the mechanics of projectile launch, flight and the effects of the projectile when impacting a target, such as damage caused to people and objects (Warlow, 2016). It also includes the study of firearms and ammunition.

1.1.2 History of Firearms

Some of the earliest forms of ballistic weapons were stones and spears, which were originally thrown before the introduction of launching apparatus such as bows and slingshots around 10,000 years ago (Marsden, 1999). Gunpowder was invented in the 9th century by China, with the first ever recorded

example of firearms coming in the 10th century, also from China (Andrade, 2017). At this time, the firearm was rudimentary, composed of a pipe filled with gunpowder and lead pellets, which was aimed in the direction of the enemy and ignited causing the lead pellets to fire out the end of the barrel.

As society progressed, so did the design and production of firearms. In the 1400's the matchlock firearm was invented, which worked by holding a burning wick, and was fired by holding the burning wick to a touch hole, causing the gunpowder in the barrel to ignite (Carman, 2015). The 1500's saw the invention of the wheel lock firearms which did not require a wick, like previous matchlock firearms, but a mechanically generated spark caused the gunpowder to ignite (Chase, 2009). The 1500's also saw the invention of rifling in the barrel of firearms. The first true flintlock was invented in 1600 along with the first use of firearms proof marks. Proof marks, still used to this day, are printed onto the firearm by the manufacturer as a sign of authentication of manufacturing (Carman, 2015). The 1800's saw the invention of the caplock mechanism which replaced the flintlock mechanism, with a hammer being used to strike a percussion cap to set off the charge in the firearm (Chase, 2009). The first revolver was also invented in 1835 by Colt, which allowed for multiple shots as opposed to a single shot at a time. At the end of the 1800's in 1893, the first automatic firearm was created in the form of a pistol, and this automatic method of loading and firing has been used since (Carman, 2015).

1.1.3 Firearm Crime

With the advancements in firearms, the field of ballistics is always evolving. This means that firearms are becoming more common in the hands of criminals, demonstrated by the large increase in confiscated illegal firearms, with one hundred and four being confiscated in 2017-2018, rising to four hundred and twenty-five illegal firearms confiscated in 2019-2020 (House of Commons Library, 2020). Other countries such as the United States of America (USA) also suffer with gun crime, with ten thousand, nine hundred and eighty-two firearms related murders being committed in 2017 according to the Federal Bureau of Investigation (Expanded Homicide Data, 2019).

With the increase in illegal firearms seizures also comes an increase in firearms related crimes meaning that the need for forensic ballistics has also increased. Aspects such as determining if the suspect was present within a scene and the shooters distance from the victim for example have become critical when reconstructing the crime. Reconstruction of crime scenes is a critical step in the process of securing a prosecution or in the exoneration of a suspect. Accurate reconstructions of shootings allow the investigating officers to begin building up the events of the shooting, which allows for accurate allocation of resources. When determining the shooters distance from the victim, the main

measurable evidence left at the scene is gunshot residue (GSR), which is a type of evidence of importance within an investigation.

1.2 Gunshot Residue

1.2.1 GSR Introduction

Gunshot residue (GSR) is the material left by the burnt and unburnt particles from the cartridge primer, propellant, fragments of the cartridge case, the bullet surface and lubricants that are used for the maintenance of the firearm (Wallace, 2018). Gunshot residue is categorised into Organic gunshot residue (OGSR) and Inorganic gunshot residue (IGSR). Inorganic GSR typically consists of the chemical elements of Barium (Ba), Antimony (Sb) and Lead (Pb). These primary components are commonly associated with GSR, but to positively identify GSR as present at the scene, a minimum of two of the aforementioned elements need to be present (Wallace, 2018).

Organic GSR is mainly composed of the residues from the additives and explosives such as nitro-glycerine and nitrocellulose. Nitro-glycerine and Nitrocellulose are organic components found inside of the propellant mixture which is mostly composed of nitrocellulose. These additives are added to improve the performance of the propellant, forcing the bullet down the barrel at a higher speed (Dalby, 2010).

The combination and quantities of propellants within a cartridge depends on the manufacturer and the purpose of the round, a factor which will affect the amount of GSR deposited at a scene (Campbell, 2018). The propellant is broken down into several sections which are, Propellants, Deterrents, Stabilisers, Decoppering, Flash reducers, Wear reduction and other additives.

- **Propellants** such as Nitrocellulose are the driving force that push the bullet down barrel after being ignited.
- **Deterrents** such as centralites are used to slow the burning rate of the propellant, causing a more gradual increase in pressure. This improves the acceleration of the bullet when leaving the barrel of the firearm.
- **Stabilisers** such as diphenylamine are used to slow and, in some cases, prevent the deterioration of the propellant mixture, allowing for stable long-term storage.
- **Decoppering agents** such as tin are added to the propellant mixture to prevent the build-up up of copper residues from the bullet travelling down the barrel.

- **Flash reducers** such as Potassium Chloride are used to reduce the brightness of the muzzle flash when shooting. The muzzle flash is caused from the burning propellant traveling down the barrel after the bullet.

- **Wear reducers** such as wax are used to lower the wear on the barrel of the firearm from firing.

- **Other additives** such as graphite may also be added to prevent the mixture from clumping together as well as to dissipate the build-up of static electricity.

1.2.2 Firing Mechanics

When the trigger is pulled on a loaded firearm, the firing pin strikes a primer cap *(figure 1.1 (a)),* which causes an explosion and flame. The resulting flame and explosion passes into the primers anvil *(figure 1.1 (b)),* which focuses the flame through the flash hole *(figure 1.1 (c)),* igniting the propellant (figure 1.1 (d)) in the casing causing a high temperature and pressure reaction to occur *(figure 1.1 (e)).* The high pressure causes the bullet *(figure 1.1 (f)),* to separate from the cartridge case *(figure 1.1 (e)).* The bullet *(figure 1.1 (f)),* is then pushed down the barrel of the firearm by the high pressure, accelerating and leaving the barrel of the firearm at high speed. As the bullet leaves the barrel, unburnt propellant, cartridge primer and fragments of the cartridge casing also exit the barrel of the firearm.
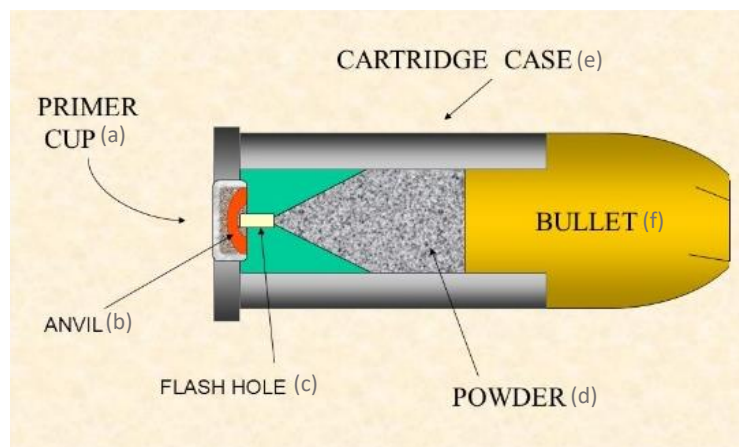
Figure 1.1: Diagram showing labelled bullet cross-section
(Saloom, 2015).

GSR leaving the barrel of the firearm does so in the form of a plume as seen in *figure 1.2*. Due to the propellant igniting and combusting, there is a lot of gas which is used to propel the bullet down the barrel (Blakey, 2019). Once the gasses reach the end of the barrel, they form a distinctive plume shape as these speed out and get sucked back in from behind as there is a negative pressure left in the trail

of the bullet (Blakey, 2019). This, therefore, creates a rolling effect on the GSR as it gets pulled in behind the bullet and propelled forward, as can be seen in *figure 1.2.*

Figure 1.2: GSR plume from handgun (Mythbusters, 2015).

1.2.3 Morphology and Quantification

Gunshot residue is small and spherical in shape, as seen in *figure 1.3* (Brożek-Mucha, 2014). A study by Brożek-Mucha (2014), used Scanning Electron Microscopy and X-Ray Microanalysis to research the morphology of GSR. The study found that GSR particles preserved a spherical shape in air, but when the particles did not solidify before the collisions, for example inside of the cartridge walls, more complex and flat shapes were observed. The study also discovered that irregularly shaped GSR had a higher level of persistence compared to spherical GSR on the shooter's hands, face, hair and garments.
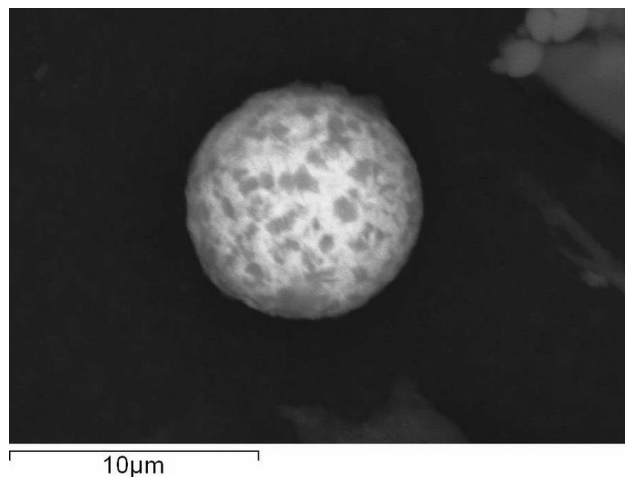
Figure 1.3: SEM Image of GSR particle (Spathis, 2017).

The quantity of GSR left around the target can give an indication of shooter distance (Santos et al., 2007). The more concentrated the GSR, then the closer the shooter to the target at the time of shooting. The further away the shooter from the victim, the larger the plume of GSR leaving the barrel of the firearm, causing the GSR from the shot to fall over a larger area (Brożek-Mucha, 2017). In cases of point-blank firing of the weapon, such as in executions, the barrel of the firearm is placed against the victim when fired. This can cause burning around the wound on the victim from the heat caused by the bullet firing, as seen in *figure 1.4*, giving investigators a strong indication of a close distance (Baptista, 2014).

A study conducted by Santos et al. (2007) looked at estimating shooters distance through analysis of GSR deposits. The study used cotton tissue targets shot by a 6.35 mm pistol to obtain data for modelling. The study was able to estimate the firing distances with intervals of between 20 - 80 cm. However, one of the limitations of the study was the material used as cotton tissue reacts and has different persistence than biological tissue, therefore limiting the application of the study in real world scenarios.

Figure 1.4: Image of gunshot suicide victim (Nikolić, 2017).

A study completed by Miranda (2019), was again looking at shooter distance estimation through the analysis of GSR. Different fabrics were shot at various ranges and immediately placed into petri dishes to prevent the loss of GSR from the fabric. The ammunition used was .38 calibre and was fired from two different Taurus revolvers. The study was able to accurately estimate the shooters distance despite only completing one shot per distance. The accuracy for GSR particle and detection was true across both of the Taurus revolvers used in the study. One of the limitations of the study was that the analytical method used was X-ray diffraction (XRD) over Scanning Electron Microscope (SEM). This is a limitation because the XRD is less sensitive and only detected metallic elements such as Lead.

1.2.4 GSR Transfer, Persistence and Retention

Dr Edmond Locard postulated the theory of *"every contact leaves a trace"* (Locard, 1920), meaning that when a person sits on a chair cushion, for example, a transfer of clothing fibres will occur between the persons clothing and the cushion as well as between the cushion and clothing. Therefore, an exchange of fibres occurs, and both types can be used as evidence in Forensic Investigation (Roux, 2018). This principle became widely accepted and applied in the field of forensic investigation, and still applies today. With this principle in mind, there are various types of transfer which can occur, and play an important role when reconstructing a scene. These are known as primary, secondary and tertiary transfer.

Primary transfer occurs between the suspect and object/person through direct contact. Secondary transfer occurs when GSR, is transferred from an object/person through an intermediate. Finally, tertiary transfer is an extension of secondary transfer, with the second person being able to then spread the GSR to other people and objects (Roux, 2018). The exchange principle is applied to investigations involving GSR, as it is possible for someone to touch the same object as the shooter and have GSR transfer onto themselves (Hofstetter et al., 2017). This could be done as simply as shaking hands to touching a light switch that had been previously touched by the shooter. Due to this a strong investigation is a key part of ensuring that the offender is brought to justice, and not an innocent person wrongfully convicted for a crime they did not commit (Roux, 2018).

Environmental factors such as rain and wind influence GSR transmission and retention. Shootings that happen outdoors are exposed to environmental factors such as wind, which can dissipate a large amount of GSR when the firearm is discharged causing this to change direction and be blown away from the victim or target in some cases. This can have a large negative effect on the investigation as there may be a lack of evidence present. Another external factor is the rain, which can also have a detrimental effect on the transmission and persistence of GSR at a crime scene. When rain is present at the scene of a shooting, GSR can be washed off and away by the rain from both victim and the suspect (Wallace, 2018).

Distance is also a contributing factor, as the closer the proximity of weapons and target, the less distance has to be covered by the GSR before impact occurs, meaning the time that GSR is exposed to external factors such as the wind is reduced (Wallace, 2018). When the shooter is further away, the time that the GSR has in flight before impacting with the target is greater, and therefore the time that the wind and other external factors have to interact with it is increased. As a result, the majority of the GSR will be blown away and not land on the victim (Wallace, 2018).

Location of GSR can also give an indication on the distance of the shooter from the victim. A study by Blakey et al, (2017) showed that GSR found on skin, such as the hands is not as persistent as GSR that is found on clothing. This is because people use and wash their many times during everyday life, causing GSR to wash/wear off. The study also found that hair (both body and facial) aids in the retention of OGSR as this adheres well to intertwined hair. Although there being GSR present on a potential suspect does not prove guilt. Transfer and persistence of evidence within Forensic Investigation is a key part of any investigation.

The persistence of GSR on clothing depends on the material used in the production of the clothing as well as the distance the shooter was from the victim. In the case of a woollen jumper shot closely, GSR particles work their way into the fibres of the jumper where they are captured (Blakey, 2017). This is because GSR leaving the barrel of the firearm has a large amount of force behind it which enables it to embed itself within the wool giving a high persistence of evidence. The particle size of the GSR is also a contributing factor in its retention on items of clothing. The sizing of the GSR particles varies meaning that sometimes the smaller particles work their way further into the material, whereas the larger particles are not able to permeate the outer layer of the material. If the same woollen jumper was shot from further away, the retention rate of GSR would be much lower due to the force decreasing over distance (Dalby, 2010). The lack of force present when contact is made between the jumper and the GSR prevents most of the GSR from being pushed deeper into the fibres. Therefore, the fibres sitting on the outside of the woollen jumper are much more prone to falling off through general use and weather exposure whereas the GSR that is pushed further down into the fibres is much more likely to remain in place, lowering the persistence of GSR evidence. If the victim was wearing a material such a lycra, which is a very smooth fabric, the chance of the GSR getting stuck and pushed deeper into the fibres is considerably reduced in comparison to woollen garments.

Time is also a factor in the persistence of GSR. The longer it takes for the evidence to be collected, the more time the GSR has to fall off. This means that the amount of time between the shooting and the apprehension of the shooter needs to be as minimal as possible to best preserve GSR from the shooting and preventing the loss of evidence. Recovery of GSR from the victim also needs to be completed as quickly as possible to help in the investigation.

A study by Maitre et al. (2018) investigated the persistence of GSR on hands over time. The study consisted of the shooter firstly cleaning their hands; firing three shots then carrying on with their daily routine. The study repeated the test and had evidence recovered from the shooter's hands at different time intervals, increasing by 30 minutes up to a total period of 4 hours. The data was collected through the use of an adhesive stub, with the stub being dabbed until it had lost stickiness. The study

concluded that detection of the three main components (Pb, Ba and Sb), was still detected in over 70% of the samples after 4 hours had elapsed. The study also noted that the most considerable loss of GSR was in the first hour of the shooting (Maitre et al., 2018).

Firearm type can also be a contributing factor in the distribution of GSR. A firearm such as a revolver will deposit much more GSR on the shooter as the weapon is more open with the hammer and pin coming back towards the shooter, whereas a semiautomatic pistol is more enclosed with the empty casing being ejected out the side of the firearm. This, therefore, means that the quantity of GSR that is being shot back towards the shooter from the semiautomatic pistol is more limited compared to the revolver (Blakey, 2017).

This extends to larger firearms such as shotguns, bolt action rifles, assault rifles, machine guns and more. Someone shooting a single shot bolt action rifle is less likely to have as much GSR on them as a person shooting an assault rifle. The higher quantity of shots fired in a short time means that there is more GSR present at a single moment in time when compared to a bolt action rifle. The GSR has time to dissipate while the next round is being chambered. In a semiautomatic or fully automatic firearm, the time between shootable rounds is very short, meaning the quantity of GSR being formed is higher during the firing time.

The hand that is used to open the chamber and cock the rifle for the next shot on the bolt action rifle would be expected to have much more GSR than the opposing arm which is not used. This is purely because the exposure to the GSR is much higher around the chamber after a round has been fired, and due to the other hand maintaining a distance from the chamber the chance of GSR transfer is reduced. The semiautomatic or fully automatic firearms have more GSR coming from the chamber onto the closest arm of the shooter to the chamber, and as aforementioned, the more rounds being fired, the higher the quantity of GSR is expected.

1.3 Analysis

1.3.1 Introduction

There are a range of methods used to determine the presence of GSR. These include presumptive and confirmatory tests. Presumptive tests used for GSR analysis include Sodium Rhodizonate test and Diphenylamine testing (Werner et al., 2020). Confirmatory tests used for GSR analysis include,

Scanning Electron Microscope (SEM), Inductively Coupled Plasma – Optical Emission Spectroscopy (ICP – OES) and Gas Chromatography – Mass Spectrometry (GC – MS).

1.3.2 Methods

Presumptive testing is usually the first type of testing that is carried out on a suspected GSR sample if the investigators are unsure of the presence of GSR. This is done as confirmatory methods are usually costly, therefore ensuring that there is GSR present before making the expense is a crucial part of the sustainability of the respective Police force. A study by Werner et al. (2020) compared three different collection methods for the sodium rhodizonate presumptive test for GSR on hands. Fifteen separate shots were fired by a single shooter, with the shooter's hands being swabbed after every shot. The same fifteen individual shots were repeated with the collection being carried out through the use of a filter paper being rubbed on the shooter's hands for a minimum of one minute. The final GSR collection method was adhesive foil which was firmly pressed against the shooters hands to collect any GSR present. The study concluded that the collection method that gave the best results was the filter paper, which had a higher positive yield than the swab or the adhesive foil (Werner et al., 2020). A disadvantage of presumptive testing is false positives.

Scanning Electron Microscopy (SEM), works by scanning the surface of an object using electrons. This allows for a very high magnification on an object and allows for the researcher to distinguish different components that are present on the object being inspected by both the morphology and elemental analysis. In the case of GSR, the samples are either collected through the use of a swab or a stub. The stub has a sticky surface for sample adhesion allowing for easier collection and preservation of samples on the stub which is particularly important during analysis by SEM as this operates under vacuum. A study by Hinrichs et al. (2017) looked at the estimation of short distance shooting using SEM images of the surroundings of the bullet holes. SEM allowed the researchers to observe the molten and fused polyester fibres in mixed textiles but only at point blank shots. It allowed the researchers to be able to observe the differences within various materials and how these reacted with being shot, which may serve as a distance determinator within an investigation.

GC – MS is an analytical method that utilises the combination of both Gas chromatography (GC) and mass spectrometry (MS) to identify substances within a sample. A study by Goudsmits et al. (2019) utilised GC – MS to analyse organic and inorganic GSR from a single sample. The GSR was collected post shots, using stubs on the hands, with a minimum of fifty dabs per stub. GC – MS was used to scan masses from the samples taken from the shooter's hands. The study found that the generation of a

total chemical profile from a single GSR sample was accomplished through the use of the GC – MS. IGSR was detected in every sample in combination with known propellant stabilisers.

Inductively coupled plasma optical emission spectroscopy (ICP – OES) is a technique used for detection of chemical elements in a sample. A study by Vanini et al. (2015) quantified the amount of GSR deposited post-shot with the aim of predicting the number of shots taken from different firearms. GSR samples were collected from a volunteer's hands post shooting at a ballistic lab. Three different firearms were used, all being different calibres. The samples were prepared in two different ways, with the initial being a dry swab that was mixed into a solution before being analysed by the ICP – OES. The second method was through the use of a microwave digestor which was used to prepare the samples for the ICP – OES (Vanini et al., 2015). The study found that the ICP – OES is an extremely powerful tool for GSR analysis. The sensitivity of the ICP – OES is elevated in comparison to conventional colorimetric tests which rely on the researcher's individual interpretation of colours, and the ICP – OES allowed for identification of the presence of GSR when colorimetric tests gave a negative result, reinforcing the sensitivity of the ICP – OES.

X-rays are another analytical method used in many research projects, allowing researchers to see inside of objects in a non-invasive way. X-rays work by having a beam of focused radiation fired through an object, with some of the radiation interacting with solid material differently to softer materials, which is interpreted into a picture, an example of which can be seen in *figure 1.5*. A study by Lesmana et al (2020), used X-rays to gain insight into the interaction between the bullet and target plates. The study aimed to look at the significance of the jacket on the bullet during penetration and used X-rays as the non-invasive analytical method. The study found that the bullets jacketing provided
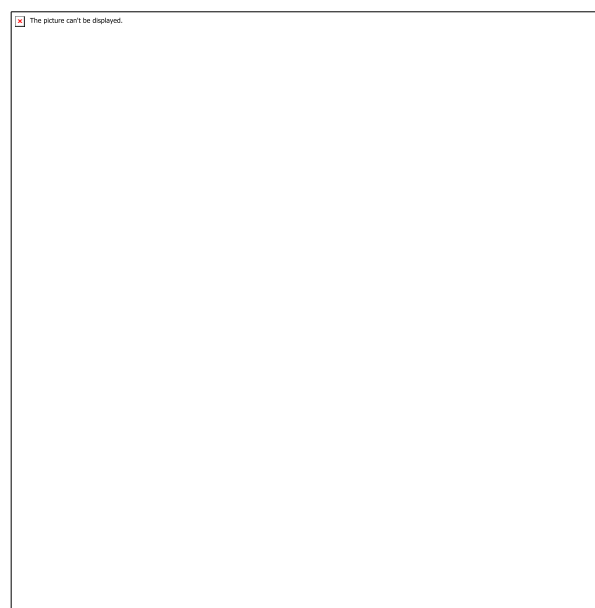
Figure 1.5: X-ray of bullet in lung (Hamidi, 2017).

two main roles, the first of which is absorption during the initial impact allowing the steel core of the bullets, used in this study, to stay relatively intact during entry. Secondly the jacketing around the bullet constrained the steel core.

1.3.3 Application of Methods

While the use of X-rays is widely used across many research fields, the use of X-rays on porcine samples in a ballistic capacity is limited. A study by Jin et al. (2018) utilised a high-speed flash X-ray machine to record images of 60 kg porcine hind limbs and ballistic gelatine as these were shot by a 7.62 mm smoothbore ballistic gun firing steel balls. The study found that the ballistic gelatine reacted in a similar way to the porcine due to the area being shot lacking any bony material (Jin et al., 2018). A limitation of the study is that it only addresses fleshy areas and not any areas which contain bone and other matter that is harder to accurately replicate.

Daghfous et al. (2015) notes and discusses the rise in ballistic related trauma in Brazil, South Africa, Columbia and the USA, and how the rise in Gunshot Wound (GSW) trauma is causing emergency units to adapt to cope with the rise. Due to the rise in GSW and resulting influx of critical patients the use of X-ray's as a non-intrusive method of examination became paramount, with Daghfous et al. (2015) saying, *'X-rays are unavoidable and represent the first line of complementary imaging when confronted with any ballistic trauma'*.

The authors carried out their analysis on a large range of victims who each had different wound types. A weakness of the study is that the victims were all wounded by only one calibre of bullet, the 5.56 x 45 mm NATO round. The large calibre of round means that the study is only applicable to warzones and military forces. Due to the round being highly regulated in the UK, its applicability is highly limited. Another limitation of the study was that only stable patients were used in the study, mostly meaning that the bullet wounds were to their extremities. This is because GSW to the torso are more fatal as opposed to extremities.

1.3.4 Wounding

When a person or soft target such as ballistic gelatine is shot, the transfer of energy from the projectile to the person/object causes permanent and temporary cavitation. Temporary cavitation is caused by a wave of pressure as a result of the bullet impacting, opening a large space pushing the surroundings

out the way as seen in *figure 1.6* (b) (Stefanopoulos, 2015). The elasticity of tissue allows the cavity to bounce back after the pressure has passed, causing the cavitation to disappear, hence the name temporary cavitation. Certain areas of the body cope better with temporary cavitation, more specifically soft organs that can absorb the pressure, such as lungs. Organs that are harder, such as the liver and kidneys do not cope well with the pressure of temporary cavitation, often causing serious injury to the victim (Stefanopoulos, 2015).
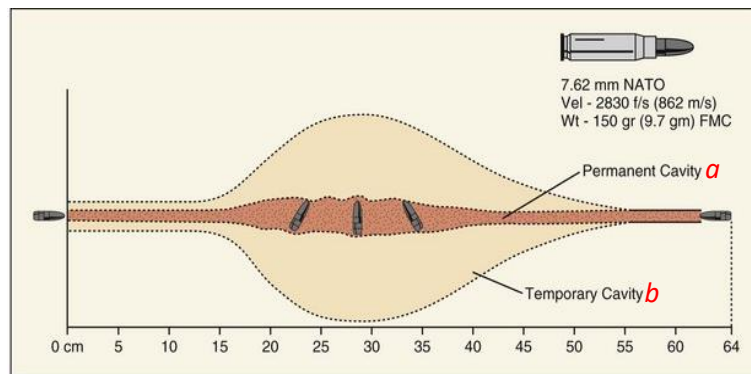
Figure 1.6: Diagram showing (a) permanent and (b) temporary cavitation (Knudsen, 1995).

Permanent cavitation, *figure 1.6 (a),* is the channel caused by the bullet passing through the tissue in a body. Permanent cavitation often causes very serious injury in victims as the cavitation is permanent, meaning there is a channel for blood to escape from the inside of the body (Stefanopoulos, 2015). Often when paired with temporary cavitation injuries, firearms wounds can prove fatal.

A study by Stefanopoulos et al. (2015), focussed upon gunshot wound victims' injuries. The study aimed to investigate different injuries in different parts of the body, specifically maxillofacial injuries. Stefanopoulos et al. (2015) noticed that the victims that were shot by larger calibre firearms, resulting in higher pressure experienced larger cavitation, both temporary and permanent. The injuries sustained through the larger temporary and permanent cavitation proved to be more fatal in the victims the study covered.

Another mechanic in damage caused by a firearm, is the penetration of the bullet. The further the bullet penetrates the victim the potentially worse the injury experienced tends to be. A study by Wen, et al. (2017), investigated the effect of bullet penetration damage caused to humans through the use of ballistic gelatine. This study consisted of shooting a block of ballistic gelatine whilst filming it with two high speed cameras. The cameras filmed the temporary cavitation the bullet caused to the gelatine and allowed for the researchers to analyse the footage to build an understanding of what was happening to the gelatine when initially shot. The ballistic gelatine that was used in the study was an *'elastic-plastic linearly strain hardening material with a polynomial equation of state'*, meaning that

the gelatine was as accurate to human tissue as possible, allowing for more accurate modelling and more applicable results (Wen, 2017). All the information gained through the experiment was computationally interpreted, with penetration depth and cavitation profiles being recorded. The study also found that due to the nature of the gelatine, the permanent cavitation was only small, and the temporary cavitation was well absorbed and diffused by the gelatine's elasticity. Another contributing factors to the bullet's penetration is the powder charge of the bullet. Having a higher powder charge load on a bullet means that there is more propellant inside of the cartridge, so when the bullet is fired, the explosion propelling it down the barrel is larger causing the bullet to have more energy when leaving the barrel (Carlucci, 2018). Conversely, with less propellant inside the cartridge, the bullet will leave the barrel at a slower rate due to there being less force pushing it out of the barrel. With the difference in force propelling the bullet, a difference in penetration is also seen. The bullet penetration increases with the quantity of propellant inside of the bullet.

Studies such as Humphrey et al. (2018), look at the comparison of using biological and gelatine models in ballistic research. The study looked at several different porcine organs and aimed to use ballistic gelatine to model and replicate the consistency of the biological sample. The study found that it is possible to model biological material with a relatively high level of accuracy. Humphrey et al. (2018), discussed the application of the gelatine over biological material, noting limitations to where it can be applied, such as trying to simulate different layers, and of course bony structures. In the case of studying areas that have bony structures, it is possible to use ballistic gelatine, but the difficulty in accurately replicating this is very high, with the disadvantage of high associated cost for the real-world applications. Additionally, the ballistic gelatine does not have an outer coating of skin, with further retracts from the real-world application of the study (Humphrey et al. 2018). Using biological material in some cases is the better option, such as replication of a porcine head is very challenging and expensive, whereas a biological porcine head is much cheaper and can be easily sourced.

1.3.5 Computational Modelling

Computational modelling is fast becoming the expected and preferred method of research within the scientific and forensic fields (Antonov et al. 2018). Computational modelling makes use of computers to model and study the behaviour of complex systems, through the use of mathematics, physics and computer science (Downey, 2018). A computer model that contains numerous variables, that in turn are characterised by the studied system. It is possible to achieve simulations through adjusting each of the variables individually or in unison and observing how the changes impact the outcome. This, therefore, allows for researchers to make predictions about what to expect in the real system, and to

aid in any possible changes to the study (Downey, 2018). Being able to apply and experiment with computational modelling allows researchers to conduct thousands of simulated experiments, to try and identify physical experimental data without the need to physically carry out the experiment (Downey, 2018). This can enable researchers to negate problems in studies being conducted.

One software that allows for computational analysis is called Waikato Environment for Knowledge Analysis (WEKA). WEKA is an open source software that provides tools for data processing, data implementation, learning algorithms and visualisation tools (Srivastava, 2014). This allows for the development of machine learning techniques which can be applied to real world data mining problems, such as many found in scientific fields.

A study by Yacob et al. (2016), used classification techniques such as Pearson correlation coefficient, Principal Component analysis (PCA), before progressing to WEKA. Naïve Bayes Classifier (probabilistic Classifiers) and Decision Tree analysis on the J48 algorithm was used from WEKA. This was due to the software's simplicity, ability for high dimensionality and outperformance compared to other more sophisticated classification software. The study looked at the pin marks left on the back of the bullet casing after firing, as each of the bullet casing acts like a fingerprint for the gun that fired them (Yacob, 2016). The study collected data in the form of images from seven hundred and forty-seven 9 mm cartridges fired from five different pistols and used WEKA to categorise images using a set of known parameters. The study concluded with a 78.4% accuracy of the images being correctly classified, demonstrating the potential of using numerical features and WEKA (Yacob, 2016).

A study by Lee, (2002), looked at the gait pattern for twenty-four test subjects, ten females and fourteen males. Gait refers to the manner of walking which is determined by the persons limb length, posture, weight and footwear, which is combined with a characteristic motion (Lee, 2002). It is possible for gait to be used as a biometric measure to recognise known persons. Gait can also include the clothing worn by a subject, the arm swing of the subject and the period of time the subject stood still.

Data was collected in a controlled indoor environment with the subjects walking perpendicular to a camera. The data was collected from the recordings of the subjects walking in the form of silhouette, with their silhouette being divided into seven individual regions, being the head, arms, torso and legs. The data was computationally modelled using an adaptive background subtraction algorithm which allowed for individual characteristics from each subject's gait pattern to be identified. The study proved successful, being able to identify gender and subject identity from the data library (Lee, 2002). The study concluded that the view and appearance dependent model of gait can also be extended to include and accommodate multiple appearances of a subject (changes in clothing).

A study by Vorburger et al. (2015), looked at topography applications and measurements in tool mark identifications and ballistics. The study makes use of computational modelling, and specifically the learning algorithm, Support Vector Machine (SVM). Computational modelling was chosen due to the possibility of being able to add a numerical value to the data such as tool marks, whilst assessing discriminability. SVM determines efficient decision rules where there is an absence of probability densities. It does this by determining the maximum separation margins between two different objects (Vorburger, 2015). The study found that topography methods when coupled with computational algorithms provide an opportunity to address the uncertainty in tool mark and firearm identification. The algorithms allow for an error rate to be accurately calculated and for exclusion for matching surfaces which are fired from the same firearm.

Changmai et al. (2019) studied the use of machine learning techniques when applied to identifying firearms and other ballistic evidence left at a crime scene. Due to the time-consuming current standards, Changmai et al. (2019) looked to machine learning techniques to automate the laborious process. The study made use of K-Nearest Neighbour (KNN), a machine learning algorithm for classifying data. The data was classified by KNN on how similar the data sample features are to the data used to train the algorithm. The study concluded that while KNN classifiers show promise, the entire data set was divided into 60 % training and 40% testing. This ratio of training to testing yielded an accuracy of 86.67%. The study concluded that automating the identification of firearms will help forensic examiners in the field of ballistics and analysis that would usually take weeks can be performed in a much shorter time frame.

A study conducted by Hare, et al. (2017) focussed on the automatic matching of bullet land impressions. The study aimed to present an automatic matching routine which allowed for an objective assessment of a match between two bullet land impressions. An algorithm the study used to achieve this was Random Forest. Random Forest uses two thirds of the data for fitting with the remaining third being used to evaluate the predictive power and accuracy. This is because the one third is to determine the error rate, which is called Out Of the Bag (OOB). Hare, et al. (2017) presented an algorithm detecting the most prominent but least important structures of bullets. These features were the least important from a firearms identification perspective and were consequently removed by the algorithm. The data was then placed into a random forest model which provided a probabilistic assessment of the match strength and order of the relevance of features. The study concluded that while it was possible to identify sets of bullets, the database required to accurately do this needs to be extensive, and there is no such database in place currently.

Computational based algorithms have also been used in other areas of forensic investigation such as in the use of statistical methods for data analysis and interpretation of paint and glass evidence (Almirall, 2020). Some computational algorithms have the ability to work in conjunction with other algorithms, strengthening the scrutiny of the work. Computational modelling, as mentioned in the aforementioned studies, shows promise within the field of Forensic Science and Investigation, reducing analyst time, clutter and minimising error probability. Computational modelling also has a large applicability to other areas of Forensic Investigation, not only in ballistic studies.

Some studies, such as the one by Park et al. (2019) used learning algorithms to evaluate forensic glass evidence. The study found that the dataset learning process was being dominated by Known Nonmated Fragments (KNM). To negate this issue the decision was made to oversample the dataset using algorithms such as Synthetic Minority Oversampling Technique (SMOTE). The study compared Random Over-Sampling Examples (ROSE) and SMOTE on the dataset and was able to conclude that the best results were as a result from SMOTE (Park, 2019). Due to this the decision was made to continue oversampling using SMOTE. The study concluded that synthetic data created through the use of SMOTE was able to be accurately classified through the use of Random Forest, with the algorithm being able to accurately classify the different glass from two different panes (Park, 2019).

This shows that computational based modelling research has proved vital in the criminal justice system, however forensic investigators must recognise that there are limitations to the current methods employed for the quantitative and qualitative determination of GSR, particularly as there is little research and knowledge related to determining shooter distance.

1.4 Conclusion and Aims

Reconstructing incident scenes is of vital importance within Forensic Investigation. Research has highlighted the possibility of using GSR dispersion as a way of predicting shooter distance, however this has only been achieved at short distances, which is of limited use for real-world applications. This research aims to further explore GSR distribution as a means of determining shooter distance, however this will be coupled to damage caused from Gun Shot Wounds. Radiological information from Gun Shot Wound victims is typically obtained for medical purposes but seldomly used for reconstructing an incident. Therefore, this research aims to begin to understand this unknown, by understanding the elemental distribution of GSR in a scene and combining this with damage caused

to the target. This information will be analysed and modelled computationally in order to understand the benefits of this within forensic investigation.

Chapter 2
Methodology

2.1 Forensic Ballistics

2.1.1 Introduction to Firearms

A firearm by definition according to, The Crown Prosecution Service (2020), is *"a lethal barrelled weapon of any description from which any shot, bullet or other missile can be discharged".* Firearms have begun to increase in popularity with criminal organisations over other weapons, such as knives (Allen, 2020), as it allows for long range attacks as opposed to knives, which requires little distance between the aggressor and the victim.

There are many different types of firearms (GOV.UK, 2020), including;

- Pistols (semi-automatic or single shot)

- Revolvers (Including cylinder loading revolvers)

- Single-shot long firearms (not break action)

- Break action firearms (rifled, smoothbore, combination, rolling/falling block action, short and long firearms)

- Semi-automatic long firearms (smoothbore or rifled)

- Fully automatic firearms (assault rifles, sub machine guns and fully automatic pistols)

- Muzzle loaded firearms

A firearm can be considered to be a device used to propel a projectile at force from a barrel. The force needed to achieve this aim is produced by the creation and expansion of gases caused by the burning of powder charges, known as propellants, from inside of the cartridge (Textbook of small arms, 1929).

The barrel of a firearm is a very important component, as this facilitates the movement of the projectile. Firearms are broadly divided into two different types, according to the internal design of the barrel, these are smooth bore and rifled firearms.

Smooth bore, as seen in *figure 2.1 (a),* is a firearm in which, the bore, i.e. the inside of the barrel, is perfectly smooth from breech to muzzle. If one was to cut through the barrel, a perfectly smooth ring would be observed as seen in *figure 2.1. (a).* An example of smooth bore firearm is a shotgun.

Rifling, as seen in *figure 2.1 (b)* and *figure 2.1 (b'),* is more common on larger firearms with larger calibre rounds. A rifled barrel consists of several raised and depressed portions. The raised portions are known as lands, whereas the depressed portions are known as grooves, as shown in *figure 2.1 (b')* which are machined into the barrel of the firearm. The groves spin the projectile as it travels down the barrel, therefore rifling gives the projectile a gyratory motion (Sun, 2017). This motion continues after the projectile is ejected from the firearm. This gyratory motion or spinning provides two very important effects, which are:

1. Stabilizes bullet flight
2. Decreases air resistance

Stability is improved as the bullet spins upon its longitudinal axis, this causes an increase in accuracy by avoiding sideways movement. Additionally, the gyratory motion minimizes the creation of denser air mass forming as the projectile moves through air, when compared to non-rotating bullets, by continuously moving air throughout its movement. Examples of rifled firearms are hunting rifles and assault rifles.

Smooth Bore Barrel *(a)*
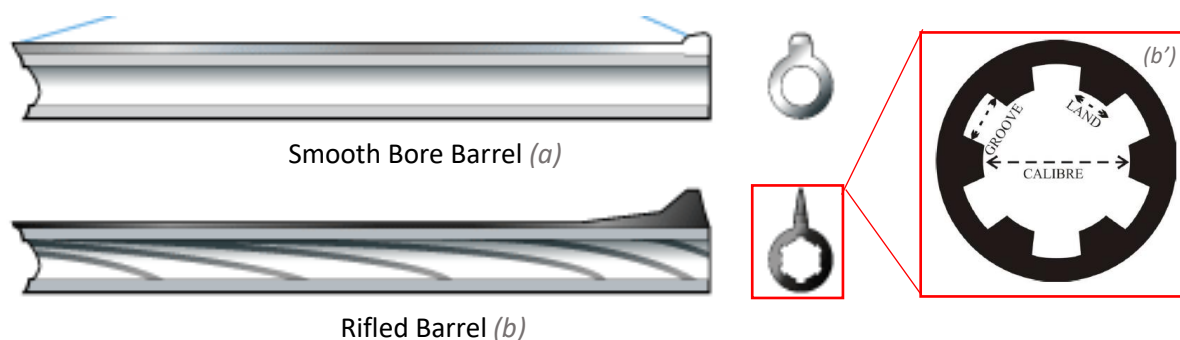
Rifled Barrel *(b)*

Figure 2.1: Labelled firearm barrel cross-sections, where smooth bore and rifled barrels are shown in (a) and (b) respectively. Figure insert (b') shows labelled rifled firearm barrel (howstuffworks, 2005) & (Heard, 2013)

2.1.2 Ballistics

Ballistics is the field of mechanics which studies the projectile in flight. There are four important areas within this area which are: Internal, Intermediate, External and Terminal ballistics.

2.1.2.1 Internal ballistics

Internal ballistics is a large subject including all aspects of the bullet and firearm; however, this area is primarily focussed upon the stage when the bullet is contained within the firearm. When the trigger is pulled on a firearm, the pin strikes a primer found on the base of the bullet (*figure 1.1 (a))*. The priming powder found in the primer explodes violently, causing a rapid rise in temperature. This high temperature flame then passes through a flash hole (*figure 1.1 (c*)) into the main powder propellant charge, causing the ignition of the main powder (fig*ure 1.1 (d)).* The high level of pressure caused by the violent ignition of the main powder charge causes the formation of a high-pressure gas which accelerates the bullet down the barrel, causing this to exit the firearm (Heard, 2013).

Nitrocellulose is commonly added to the main powder charge, and when ignited alone in an open space, will burn gently. If the nitrocellulose is placed into a tightly packed space, the increase of heat and pressure in a combined space, causes the acceleration of combustion (Heard, 2013). In the case of a firearm, the propellant is confined to the capacity of a cartridge case (*figure 1.1 (e)).* The large opening is closed with a bullet which is crimped into place. The complete round of ammunition is enclosed by the firing chamber of the gun (Heard, 2013). Once the aforementioned stages happen and the main propellant charge has been ignited, the pressure increases to a level sufficient to overcome inertia of the bullet, causing the bullet to begin accelerating down the barrel of the firearm (Heard, 2013). However, the heavier the bullet (such as those found in large calibre firearms) the greater the pressure required to overcome the inertia of the bullet. This is usually achieved by having a higher quantity of propellant.

Another factor that affects propellant combustion is the density of the propellant load. The ratio of volume between the cartridge case and propellant powder is a deciding factor in the combustion. The higher the ratio of cartridge case volume to propellant volume, the emptier space in the cartridge case, causing a slower initial rate of combustion, which consequently causes the bullet to have a lower velocity (Heard, 2013).

The internal pressure is caused when the propellant burns, with the majority turning into gas, mostly formed of water vapour and carbon dioxide (Heard, 2013). During initial combustion of the propellant,

the resulting gases are contained within the cartridge case, with an equal application of pressure throughout the cartridge case and bullet base. Once the pressure increases to a level sufficient to begin moving the bullet, the volume occupied by the gases increases, which causes a drop in pressure within the cartridge case.

Once the bullet is travelling down the barrel of the firearm, a resulting force known as to as 'recoil' occurs (Heard, 2013). This is experienced by the shooter, in the case of a pistol/handgun, the grip of the firearm being pressed into the palm of the shooters hand. In the case of rifles, the recoil forces the stock/butt of the firearm into the shoulder of the shooter.

2.1.2.2. Intermediate ballistics

Intermediate ballistics is the initial transition between internal ballistics and external ballistics, taking place at the muzzle of the firearm (Oswatitsch, 1980). The transition commences by the emission of gas from the barrel, both in front of the projectile and the propellant gasses from behind the projectile. The initial motion of the projectile as it exits the barrel of the firearm including the initial barrel and projectile jump as the recoil from the firearm firing and the gas leaving the barrel after the projectile.

2.1.2.3 External ballistics

External ballistics is the study of the projectile in flight, from the moment it leaves the barrel of the firearm to the moment it strikes a target (Heard, 2013). There are two main factors affecting the performance of a bullet upon exiting the barrel of the firearm. These factors are air resistance on the bullet and effects of gravitational pull on the bullet. As a result of these external forces, the bullet will curve downwards over distance as the bullet slows from the air resistance and it pulled down by gravity.

The shape of trajectory can be predetermined by knowing:

- Effects of gravity
- Velocity
- Angle of the barrel upon firing
- Weight of the bullet
- Shape/type of bullet being fired.

The rate of fall can be calculated using the formula;

$$h = \frac{1}{2}gt^2$$

eq. 2.1

Where;

h = drop of projectile (m)

g = Gravity (m/s^2)

t = time (s)

Equation 2.1 shows that the drop is independent of the velocity and mass of the bullet, the rate of fall is only dependent upon time (i.e. time in flight) (Bryce, 2009). A slow-moving bullet will drop the same distance in the same time as a high velocity bullet. The difference is that the high velocity bullet will cover more distance than the slow velocity bullet. Despite this equation, it is widely understood that the bullet does not maintain the same velocity throughout its flight. As a result of air resistance, the bullets velocity decreases as the friction from air slows the bullet.

Ballistic coefficient refers to the density and other factors which affect the loss of velocity due to air resistance of the bullet. The shape and design of the bullet plays a large role in how air resistance affects the bullets velocity. The differences in air resistance within the field of ballistics is referred to as *form factor* and is given the symbol 'i' (Heard, 2013). Knowing this, it is possible to calculate ballistic coefficient using the following equation:

$$C = \frac{w}{id^2}$$

eq. 2.2

Where:

C = ballistic coefficient (kg/m^2)

w = weight of bullet (kg)

i = form factor

d = diameter of the bullet (m)

Projectiles, such as bullets, will have a maximum range when fired. The maximum range of a bullet will be dependent upon several factors, which include but are not limited to, bullet shape, wind, air density, air resistance, gravity, angle of the barrel and propellant charge. In addition to the angle of the barrel, the angle at which a maximum range is obtained is referred to as *"critical angle"* (Heard, 2013). Elevation levels above 35° cause the maximum range of a projectile to begin to decrease (Textbook of small arms, 1929).

Terminal velocity of a projectile is a commonly sought after and valuable piece of information. In cases of experiments being conducted, it is possible to use a chronograph, which will give the velocity of a projectile as it passes through the device. In cases where there is no chronograph present, a calculation can be used to estimate the velocity of the projectile.

This is achieved through the follow equation:

$$M_{m_2 v_2} = M \; x \; \mathrm{g}$$

<div style="float:right; border:1px solid black; padding:4px;">eq. 2.3</div>

Where;

M = mass of object (kg)

m_2 = ballistic coefficient (kg/m^2)

g = gravity (m/s^2)

v = velocity (m/s)

Air resistance experienced by the projectile is dependent upon surface area. Due to these factors, large bullets will drop faster than small bullets when fired (Heard, 2013). This is due to small bullets being unable to maintain their rotation, causing them to tumble whereas larger bullets are able to maintain their rotation leading to a greater stability and increased range.

To compensate for the drop in the bullet when firing, some firearms have adjustable rear sights. The rear sight can be raised to give a sufficient level of elevation to the barrel of the firearm, allowing the bullet to strike a target at greater distances. Small calibre firearms such as shotguns and handguns, are more likely to have fixed sights as these are not intended to shoot far enough for the bullet drop to be too instrumental in the bullet making contract with a target.

When the rear sight is elevated on a firearm such as a rifle, the sights should run parallel with the ground, with only the barrel of the firearm angling upwards above the target. As seen in *figure 2.2*, the line of sight is direct to the target, but the angle of departure is above that of the line of sight.
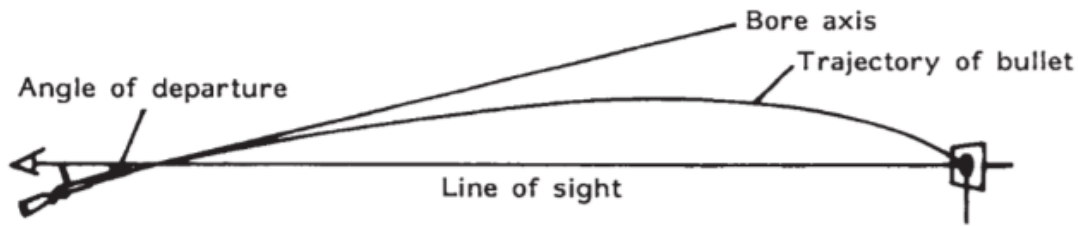
Figure 2.2: Diagram showing bullet flight (Heard, 2013).

While the bullet is traveling to the target, it is exposed to other influencing factors, such as wind. Aside of the air resistance and gravity effects on the projectile, wind can affect the bullets trajectory. An example of this could be the wind blowing from left to right, would cause a sideward motion of the bullet, forcing the bullet to drift to the right of the intended target. Rear facing wind also has an effect on the trajectory of the bullet, causing an increase in velocity as the wind further pushes the bullet forwards. Frontal wind, also referred to as nose wind, can have an opposite effect on the bullet, causing the bullets velocity to decrease quicker than it would in ideal conditions. This if uncompensated can cause a bullet to fall short of a target. If a bullet is experiencing sidewind at 90°, then the bullet drift can be calculated using the following equation (Heard, 2013):

$$D = T \; x \; W$$ eq. 2.4

$$T = \frac{R}{V}$$ eq. 2.5

Where;

D = deflection of bullet due to wind (°)

R = range (m)

V = muzzle velocity (m/s)

T = flight time (s)

W = cross wind speed (m/s)

Rifling can have an effect on the bullet, which is referred to as drift (Heard, 2013). Drift is a result of gyroscopic properties caused by the spinning of the bullet. This is observed with bullets where a right-hand spin on the bullet causes the bullet to drift to the right, and left spin on bullets cause them to drift to the left. Yaw is a similar effect caused by the spinning of the bullet at closer ranges with rifles.

The initial spinning of the bullet as it leaves the barrel of the rifle can cause the bullet to become unstable, as seen in *figure 2.3*. This can result in a loose grouping of bullet impacts on a target. As the range between the firearm and target increases, the effect is lessened and therefore the bullet impact groupings become tighter.
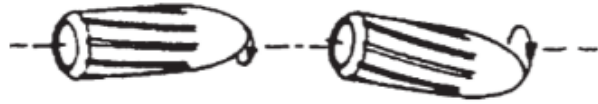
Figure 2.3: Diagram showing bullet yaw (Heard, 2013).

Muzzle energy is a very important factor and property within the field of ballistics. Muzzle energy gives an indication of the power the bullet as it leaves the barrel, and therefore it also gives an indication of the bullets wounding potential (Heard, 2013). Muzzle energy is the potential energy the bullet possess as the bullet passes the muzzle of the firearm and leaves the barrel. This can also be referred to as kinetic energy of the bullet/projectile (Heard, 2013). Most firearms manufacturers and ammunition producers give an indication of the muzzle velocity expected on their products, but nonetheless, it is possible to calculate the muzzle velocity. The equation used for calculating the muzzle velocity of the projectile is:

$$K = \frac{1}{2} MV^2 \qquad \boxed{\text{eq. 2.6}}$$

Where;

K = kinetic energy (J)

M = mass of the bullet/projectile (Kg)

V = velocity of bullet/projectile (m/s)

2.1.2.4 Terminal ballistics

Terminal ballistics, also known as wound ballistics, is a large section of the ballistic field that encompasses the medical field. It is the study of projectile penetration into solids and liquids. Terminal ballistics focuses upon the point at which the projectile reaches and impacts with the target (Terminal ballistics, 2012). Terminal ballistics can be split into two sections;

- Penetration potential

- Wound ballistics

Permanent and temporary cavitation both fall under the title of terminal ballistics. Permanent cavitation is a pathway that is left by the projectile as it passes through the target material. Temporary cavitation is a pressure wave caused by the projectile impacting a target as seen in *figure 1.6.* As a bullet passes through biological tissue, some of the kinetic energy from the bullet is absorbed by the tissue. The transfer of kinetic energy causes the tissue to be pushed away from the bullets path, leaving a temporary cavity wound which is much larger than the bullet *(figure 1.6)* (Fackler, 1985). The elasticity found in biological tissue allows for the tissue pushed away to spring back to its original structure, after the bullet passes and the kinetic energy is dispersed. There is also a permanent cavity which is cut into the tissue by the bullet as this passes through the tissue. It is possible to have several channels of permanent cavitation if the bullet breaks apart upon impact (Heard, 2013).

The temporary cavitation is short in duration before return to a normal structure, but there are also aftershocks experienced, each decreasing in severity. It is possible for the permanent cavitation to be larger than the bullet itself, but this permanent cavitation will still be smaller than the temporary cavitation (Heard, 2013). The sizing of both the permanent and temporary cavitation are dependent upon the weight of the bullet, sizing of the bullet and the velocity of the bullet upon impact. The surrounding structures can also have an effect on the size of permanent and temporary cavitation (Heard, 2013).

When there is a very high velocity bullet, the temporary cavitation is a violent movement due to the higher transfer of kinetic energy when compared to the cavitation caused by the lower velocity bullet. The larger temporary cavitation, caused by the high velocity bullet, can cause more damage to surrounding organs and bony structures (Heard, 2013). Another factor which can contribute to temporary and permanent cavitation sizing is the yaw of the bullet, as aforementioned. This is because the yawing bullet will not impact a surface at 90° causing a larger surface area of the bullet to make impact (Heard, 2013).

When a firearm barrel is placed flush with skin on a victim before being fired, the resulting entry wound can be larger than the exit wound. This is because the gases following the bullet down the barrel have no other area to dissipate other than forward and so entering the target. The gases expand at a higher rate than what the bullet travels through the tissue, and with nowhere to go the gases burst back out of the entry wound, causing a large wound (Heard, 2013). Another indication of a contact wound is the powder burn from the gunshot residue, and heat from the barrel as seen in *figure 1.4.*

2.1.3. Ammunition

Ammunition is important in relation to firearm and ammunition identification. While the firearms themselves are built to last, the ammunition is a consumable used by the firearm.

Cartridge designs depend upon the intended calibre of the firearm. The different calibres have different size cartridges to house the propellant and bullet (*figure 1.1*). The cartridge case is left after the firearm has been fired and can be used to determine the calibre of firearm. Other evidence which can be obtained from cartridge cases are the country of origin, manufacturer, year of production and make of the ammunition itself. This information can be found by inspecting the cartridge and checking the headstamp.

Different cartridges are produced to fulfil different roles, each having different characteristics such as shape and weight. Functionality of different types of cartridge cases are produced, mostly for different calibres of firearms (Carlucci, 2018). In some cases, the cartridge is left without a projectile, and the end is crimped closed. This is called a blank and has many different uses, including training purposes and starter guns for racing events.

Most projectiles are coated in a thin covering of metal which is referred to as a jacket, or jacketing. The different jackets found on different projectiles depends upon their intended use. Some examples of different types of jacketing are; full metal jacket, grain jacketed soft point, hollow point and tracer rounds as seen in *figure 2.4*.
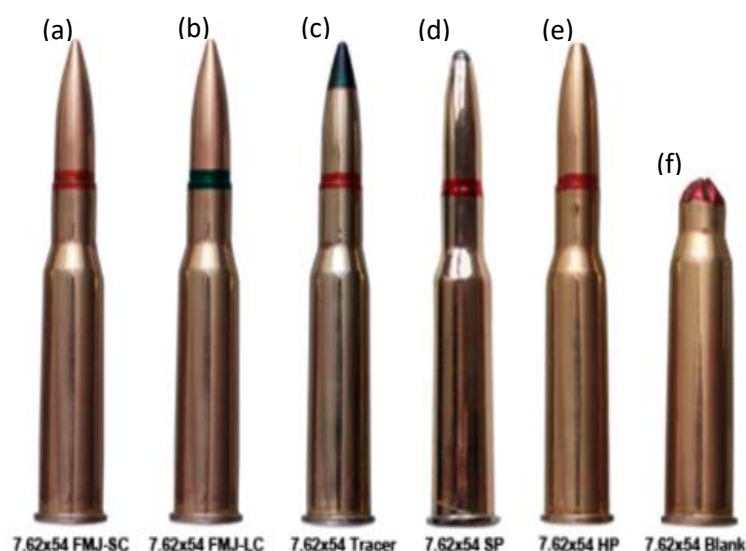
Figure 2.4: Different types of jacketed bullets where (a) Full Metal Jacket – Steel Core (FMJ-SC), (b) Full Metal Jacket – Lead Core (FMJ-LC), (c) Tracer, (d) Soft Point, (e) Hollow Point and (f) Blank (Arsenal, 2020).

The maximum effective range of small calibre firearms is a widely disputed topic (Carlucci, 2018). The amount of energy required for a projectile to be effective is difficult to quantify. The maximum effective distance of small calibre firearms is difficult to quantify due to a large number of variables including but not limited to, bullet design, velocity, bullet weight, bullet placement, bullet diameter and weapon accuracy. Due to this, the maximum effective range is usually referred to as the maximum range a firearm can accurately hit a target and inflict damage (Heard, 2013).

2.1.4. Porcine Head

Porcine samples are used widely in within the field of science, especially within the field of forensic investigation. This is due to the similarities within the anatomy of porcine samples when compared to human anatomy. Due to these similarities, porcine samples are used to simulate a human, and provide the researchers with a method of analysing a biological sample.

The porcine head, as seen in *figure 2.5,* is surrounded by skin, which is formed of the epidermis, dermis and hypodermis (aka. Subcutaneous layer) (Fails, 2018). There are many functions of the skin, such as to protection from the environment. The skin also has many other functions including but not limited to, temperature regulation and excursion of waste products, lubrication and immunity.
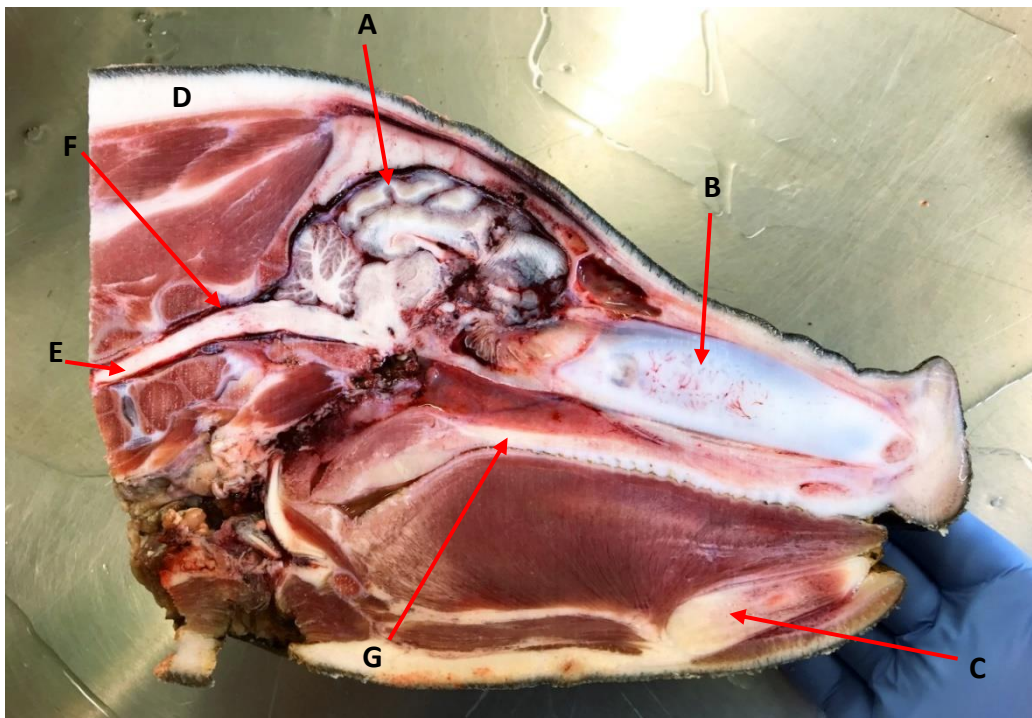
Figure 2.5: Cross section of pig head, left hand side (Atterholt, 2018), where (A) brain, (B) Nasal Cavity, (C) Mandible, (D) Skin and fatty tissue, (E) Spinal cord, (F) Vertebrae and (G) Teeth

The epidermis, as seen in *figure 2.6 (a),* is the outermost of the three layers of skin. The main functions of the epidermis are to provide a barrier against infection and to regulate the release of
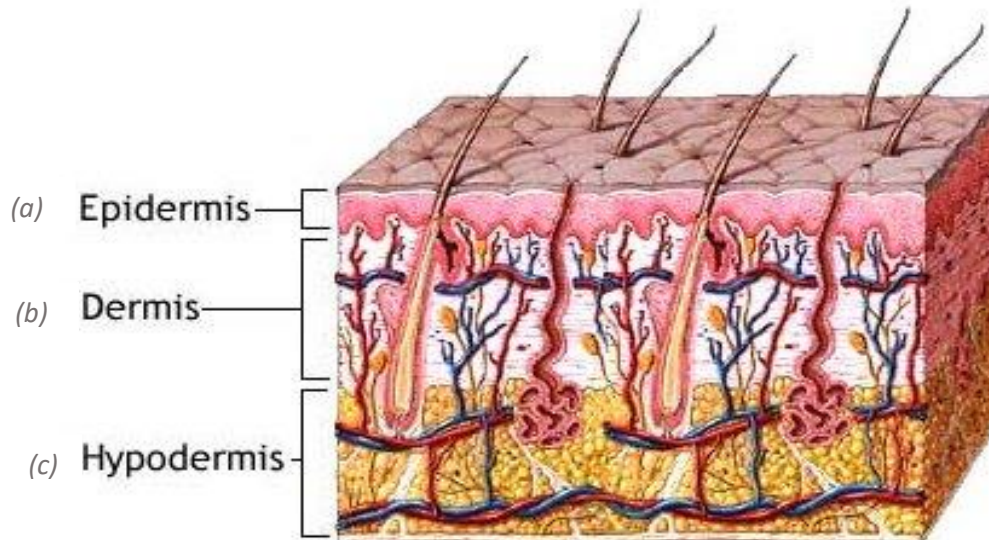
Figure 2.6: Diagram of skin layers (Darling, 2016).

water. This layer is composed of multiple layers of flattened cells (Fails, 2018).

The dermis lies between the subcutaneous layer and the epidermis as seen in *figure 2.6 (b)* (Fails, 2018). Commonly referred to as the middle layer of skin, the dermis contains connective tissue which is mostly formed from collagen and elastin. The dermis is rich in blood vessels due to the collagen and elastin Lastly, the Hypodermis, also known as the subcutaneous layer, as seen in *figure 2.6 (c).* The hypodermis contains macrophages, fibroblasts and adipose cells. Macrophages are a type of white blood cells of the immune system (Fails, 2018). Fibroblasts cells control the production of synthesis of collagen. Lastly adipose tissue, also known as fat cells, is primarily composed of fat cells which specialise in the storage of energy for a later use and protection.

There are three different types of muscles, smooth muscles, skeletal muscles and cardiac muscles. Although all three of the different types of muscles share properties, they all differ from each other at a microscopic level (Tortora, 2009).

Skeletal muscle is named as such due to its purpose, moving the skeleton frame. The skeletal muscles attach to anchor points on the bony structures of the skeleton and when contracting the striated tissue, causes the muscle to shorten (contract) causing movement. Skeletal muscle works in a voluntary manner, being consciously controlled through the use of neurons. Some skeletal muscles are different and are consequently subconsciously controlled, such as the diaphragm. (Tortora, 2009).

Skeletal muscles are surrounded by connective tissue called the fascia, protecting the muscular tissue. The subcutaneous layer of the skin, *figure 2.6 (c),* separates muscle from skin. The fascia surrounding skeletal muscles has three different layers of connective tissue separate from it around the muscles. These are called the epimysium, perimysium and endomysium and all aid in strengthening the fascia around the muscle (Tortora, 2009).

Smooth muscle is found inside of blood vessels, airways and other hollow internal structures (Tortora, 2009). Smooth muscle can also be found within the skin, attached to hair follicles. Unlike the skeletal muscle, there are no striations found on the muscle. Smooth muscle is involuntary controlled muscle, with no conscious thought able to control it.

The porcine cranium can be considered to be the next layer, this is formed from the following bony structures: Parietal Bones, Temporal Bone, Occipital bone (squama Occipitalis), Zygomatic Bone, Frontal Bones, Nasal bones, Maxilla, Incisive bones, Mandible and Lacrimal Bone, as seen in *figure 2.7*.

a – Parietal Bones

b – Occipital bone (squama Occipitalis)

c – Temporal Bone

d – Lacrimal Bone

e – Zygomatic Bone

f – Maxilla

g – Frontal Bones

h – Nasal bones

i – Incisive bones

J – External Auditory Meatus

k – Mandible

l – Nuchal Crest
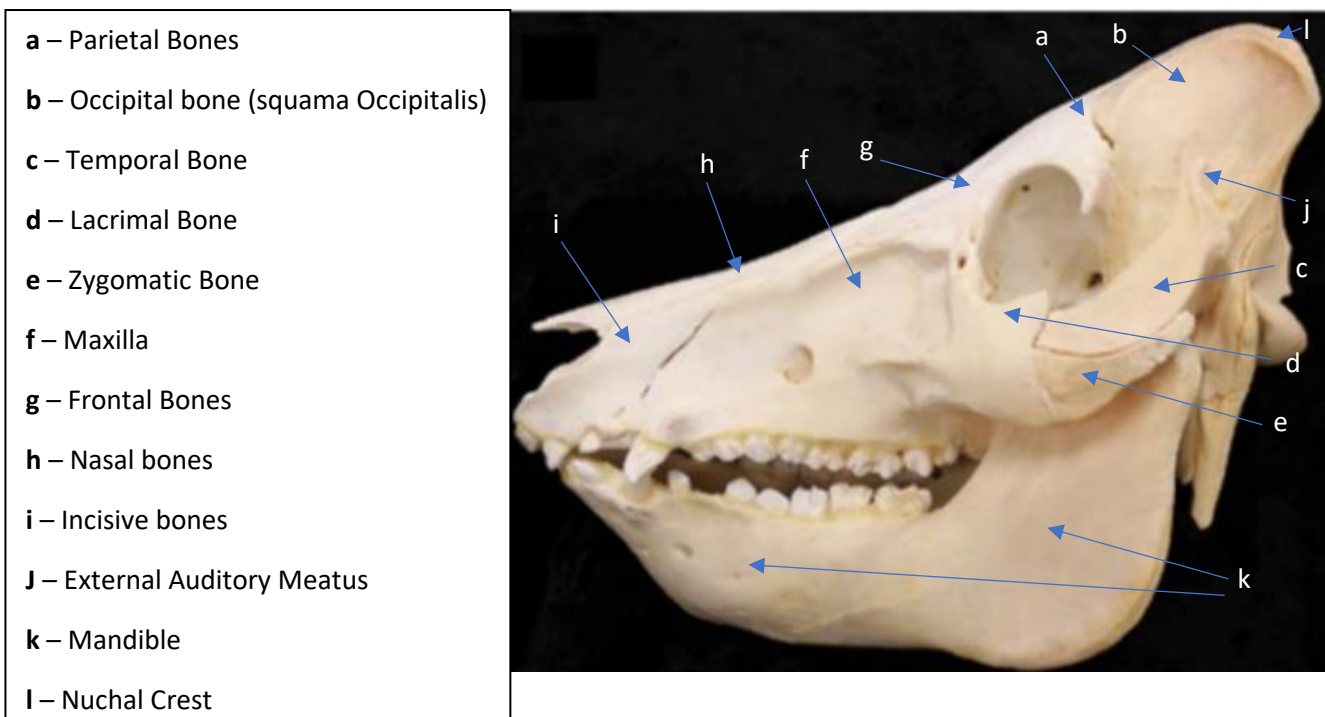
Figure 2.7: Image of a porcine cranium (Fails and Magee, 2018).

2.2 Experimental Setup for Ballistic Analysis

2.2.1. Venue for Experiment

The firearms range that was chosen to host the experiment was the Police firearms range in Maidstone, located within the Police headquarters. The firearms range is a detached building with an indoors firearms range. Due to this, extractors are located at the end of the firearms range aiding in air circulation and preventing a build-up of Gun Shot Residue (GSR) in the air. The firearms range had not been cleaned prior to the experiment being conducted. The lack of cleaning of the range before conducting the experiment meant for extra precautions being taken to prevent any cross contamination from the firearms range to the porcine heads, as discussed within this chapter.

2.2.2 Firearm and Ammunition Used in Project

The firearm that was chosen for the study is a Heckler & Koch MP5 as seen in *figure 2.8*. This firearm was chosen as it fires a common round used by handguns, the 9 mm bullet. The MP5 uses a smooth bore barrel, like handheld firearms, meaning that the bullet is not spun when traveling down the barrel of the firearm. This is important as most handguns are smooth bore and lack any kind of rifling. The MP5 was also chosen as it has a longer barrel making it more accurate, enabling the shooter to consistently hit marks, meaning that the rounds hit in a tighter grouping.

The ammunition calibre that was chosen for the experiment is the 9 mm bullet. This round was chosen as it is one of the most common rounds used in handguns, which are commonly linked to crime (Allen, and Audickas, 2020). The bullets were provided by Kent and Essex firearms Police.

Figure 2.8: Image of Heckler & Kock MP5 (heckler & koch, 2020).

2.2.3 Experimental Setup at Range

Porcine heads were supported using a specially designed stand. The design was created using AutoCAD, a computer-aided design, which allowed for accurate drawings to be produced, *figure 2.9*. This design was presented and agreed upon by the Chief Firearms officer at Kent Police.

The stand was manufactured using wood and glue, to comply with health and safety considerations on the range. As shown in *figure 2.9*, the stand is a 'V' shaped design on a base plate which is in place to support the porcine heads.
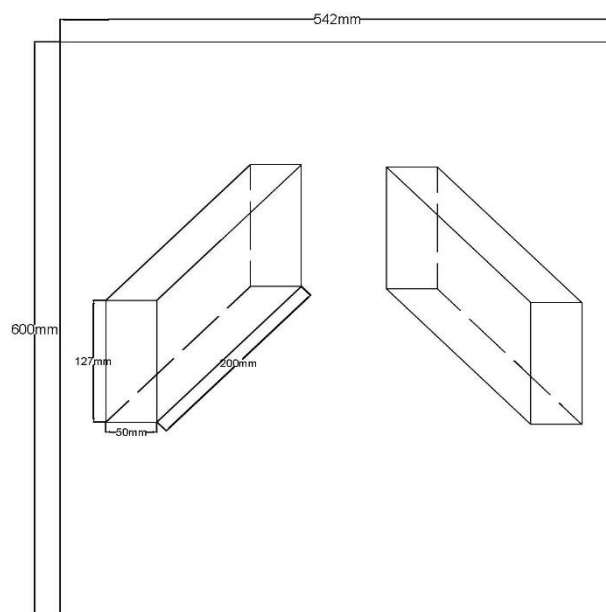
Figure 2.9: AutoCAD drawing of porcine head stand.

An enclosure for the stand was also created, as seen in *figure 2.10.* This was created in order to prevent any of the biological material from the porcine head contaminating the firearms range. This enclosure consisted of a small table, fitted with timbers erected vertically in each corner. A tarpaulin was then attached, creating a hollow box with one side open to allow for the porcine heads to be placed on the stand and then shot by the firearms officer.

Once this was in place, the stand was covered with a sterile plastic sheet prior to the porcine head placement, in order to minimise cross-contamination of GSR from the firearms range to the porcine head. A second sterile plastic sheet was placed over the first plastic sheet to prevent cross contamination between the porcine heads once on the stand and shot. The second plastic sheet was removed post shot and sealed in an evidence bag, preventing any contamination from the firearms range, as well as between any of the porcine heads. The second sterile plastic sheeting was replaced

for every porcine head, with the first plastic sheet staying in place through the entire duration at the firearms range.
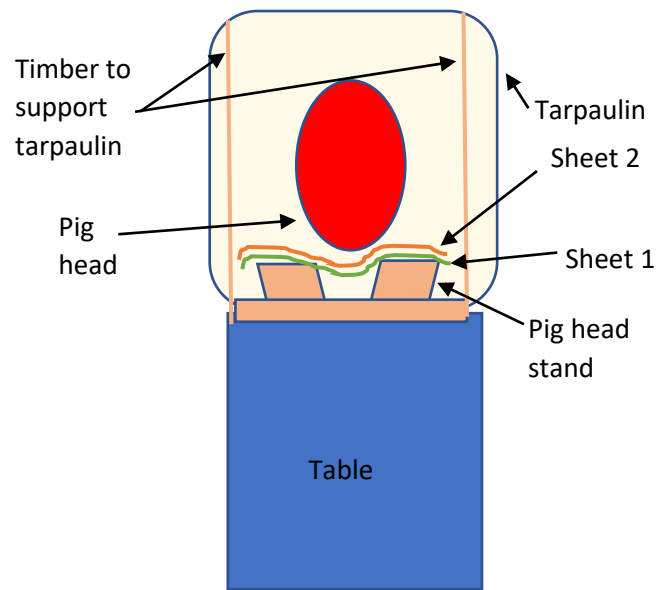
Figure 2.10: Diagram of experimental setup at firearms range.

2.2.4 Exhibit Setup

The porcine head was placed with the back of the head, i.e. the open wound base, facing to the left from the shooters perspective and the snout facing to the right side of the porcine head stand as seen in *figure 2.11*. This allowed for the firearms officer to shoot the side of the porcine head while it was supported by the stand. A black adhesive dot was placed onto the head to assist the shooter with the desired bullet entry location, as seen in *figure 2.11*.

Shooter distances were measured out from the stand using a tape measure. The tape measure was wheeled out keeping as true a line as possible with the desired shot measurements being marked on the floor using masking tape. The masking tape acted as a point of reference for the firearms officer, where the barrel of the firearm was placed on the marked distance. The distances of 0 m, 15 m and 30 m were measured out and marked. The firearms officer ranged through three different body positions to remain accurate during shooting, including standing (0 metres), kneeling (15 metres) and prone (30 metres).

Figure 2.11: Still image of porcine head during experiment

The camera used to capture the footage of the shots was placed on a tripod in front and slightly to the right of the porcine head. This enabled the camera to have the porcine head in frame. It also enabled the shooter to safely conduct the shot. This was decided as the best location after conversations with the shooter and range master to comply with health and safety.

2.3 Analysis

2.3.1. Porcine heads used in the project

Porcine heads were used for this experiment. Literature has shown (Carter, 2001) that human and porcine heads possess similar anatomy and therefore deform similarly. For this reason, porcine heads were used to understand ballistic injury. All procedures were approved by the Ethics committee at Canterbury Christ Church University.

Three porcine heads were used for the experiment, examples of which can be seen in *figure 2.12*. The porcine heads used in the experiment were purchased from a butcher at Worgans Farm Shop, Bishopsbourne. The weight of each porcine head was approximately 4.5 Kg. These porcine heads were stored in a blacked-out storage box within a temperature-controlled room at 5°C.

Figure 2.12: Sample of porcine heads images from laboratory.

The porcine heads were brought into the laboratory for initial analysis of the wounds, and for elemental GSR collection from the surface of the porcine heads. The worktop was cleaned following a decontamination Standard Operating Procedure (SOP) (as summarised in appendix A). Once the worktop was fully decontaminated, sterile plastic sheeting was placed onto the surface. With the sterile plastic sheeting in place, the porcine head was placed onto the plastic as seen in *figure 2.13*. The heads were checked for damage initially, with the aim of identifying any damage caused by the bullet, such as entry and exit wounds.

The porcine heads were swabbed by rotating a cotton tip swab, four times over the sample area. Swabs were taken from three different locations on the porcine head, as represented by circles seen on *figure 2.13*. Swab circle 1 is the entry wound of the bullet itself, and is the smallest area swabbed. Swab circle 2 corresponded to the medium sized area, followed by circle 3, the largest sized area, as seen in *figure 2.13*.
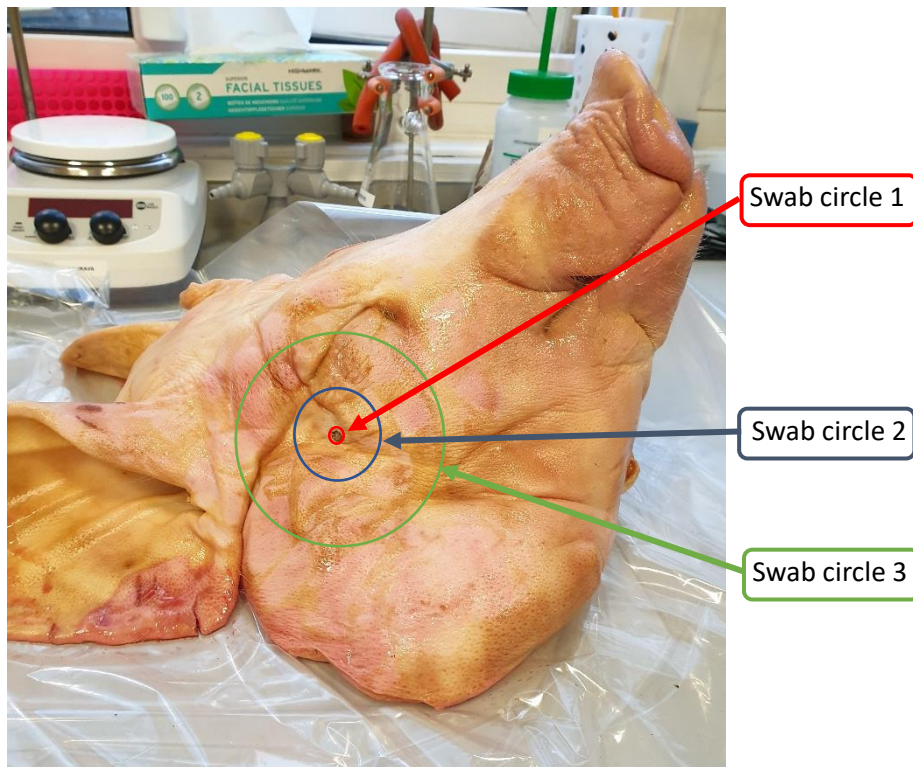
Figure 2.13: Image of porcine head on laboratory bench.

Once this was completed each porcine head was placed into a thick plastic bag, with the opening of the bag being swan necked and then zip tied shut. The swan necked and zip tied bag containing the porcine head, was subsequently placed into another thick plastic bag which was also swan necked and zip tied, leaving the porcine head double bagged and properly sealed. The double bagged porcine head was then placed back into the blacked-out transportation box. The worktop was then fully decontaminated following the decontamination SOP (appendix A). This process was repeated for all porcine heads.

2.3.2 X – ray Analysis

Originally discovered by Wilhelm Conrad Röentgen in 1895, X-ray's revolutionised the fields of science and medicine (Russo, 2017). Röentgen made the discovery after observing a fluorescent glow caused by crystals near a high voltage cathode ray tube. After some further research, Roentgen showed that X-rays could penetrate soft tissue, but not the bony structures (Reeves, 2012).

X-rays are part of the electromagnetic spectrum (Dowsett, 2006). Visible light is a small part of a large range of waves that form the electromagnetic spectrum, as seen in *figure 2.14*. Waves that are located above the visible spectrum are split into infrared and radio waves. Ultraviolet, x-rays and gamma rays are found below the visible range. The reason behind the differences within the spectrum is a difference in wavelengths (Dowsett, 2006). The differences in the wavelengths cause some of the properties to change and differ. For example, ultraviolet light is invisible to the human eye, but can cause burns and kill bacteria. With a slightly longer wavelength, the visible light spectrum is observed.
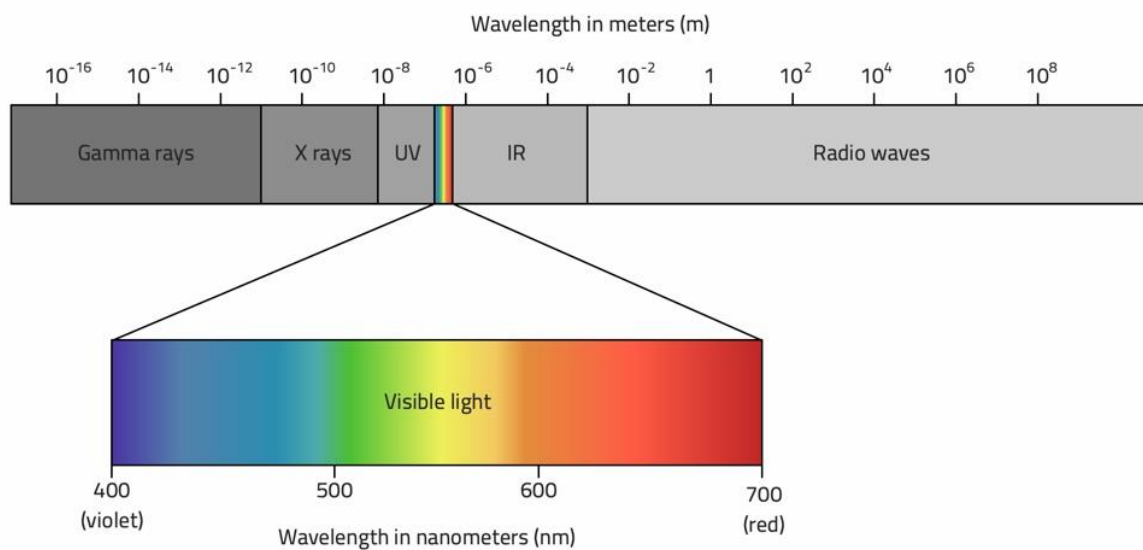
Figure 2.14: Diagram showing different wavelengths (Dowsett, 2006)

In modern society, X-rays are commonly used in the medical fields through the use of specialist equipment, composing of an X-ray generator and X-ray detector. In these machines, the anode and cathode are both contained within a vacuum, which supports electrical conduction, as seen in *figure 2.15*. The vacuum is usually formed inside of an envelope around the anode and cathode, with the envelope being made from glass (Maltz, 2009). X-rays are formed by accelerating electrons and forcing them to collide with a focal point on the anode which is usually made from a metal (e.g. molybdenum, copper, tungsten or graphite).

The deceleration upon collision with the focal point causes the release of radiation referred to as braking radiation or bremsstrahlung radiation (Maltz, 2009). The collision causes electrons, from low energy levels to be expelled. This vacancy is filled by higher energy electrons dropping down to fill said vacancy, which causes the emission of X-ray photons with precise energy levels. These X-ray photons are referred to as characteristic X-rays (Maltz, 2009). X-ray tubes function as an energy converter,

using electrical energy and converting this into x-ray radiation and heat. The heat is considered a bi-product (Maltz, 2009).
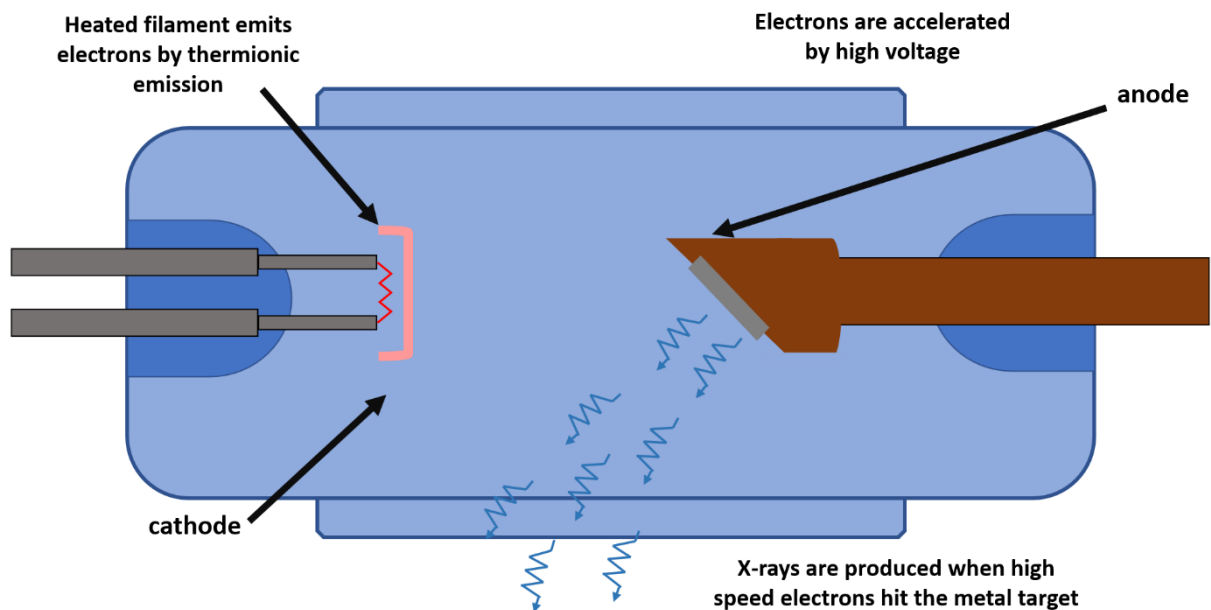
Figure 2.15: Diagram showing components of an X-ray tube (Maltz, 2009).

When an electron passes closely to an atomic nucleus, the direction of motion will be changed (Plaats, 1980). When the direction of motion is changed, there is a low probability that the electron loses energy, which is in the form of a photon. The lost photons are referred to as bremsstrahlung photons, as seen in *figure 2.16* and form the main part of the X-rays being used during diagnostic imaging X-rays (Maltz, 2009).

Characteristic X-rays, *figure 2.16*, are emitted when there is a space in an electron K shell, which is filled with an electron from the outer shell of the atom. The energy emitted by the higher energy electron to drop down into the lower energy space, equals the difference in binding energy of the electron in the two different energy levels. The empty spaces in the K shell can be caused by accelerated electrons causing ionisation, or photoelectric absorption from bremsstrahlung photons.
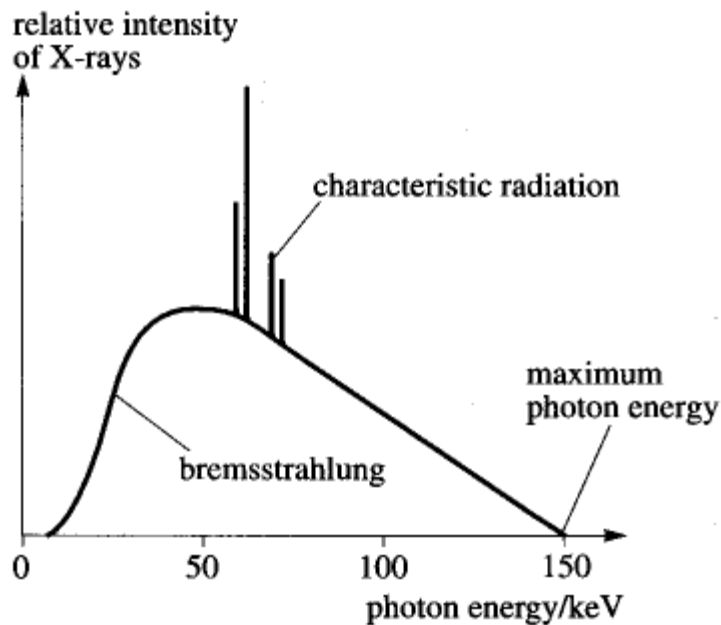
Figure 2.16: Graph showing relative intensity of X-rays and photon energy (PhysicsOpenLab, 2017).

The penetrating power of an X-ray beam is adjusted and controlled through the voltage of the X-ray tube. When the voltage is set higher, the X-ray is more penetrating and energetic, allowing for visualisations of different tissues (Sookaromdee, 2017). The different density levels, seen as light and dark areas, are defined as contrast. This is known by the terms lucency and opacity, where lucency refers to the 'blackness' and opacity refers to the 'whiteness' seen on radiographs.

The dosage of the X-ray beam is controlled by the voltage and exposure timer. The higher the voltage or exposure time, the more X-ray photons are produced, causing a higher density of photons on the X-ray film. The dosage of X-ray photons is referred to as milliampere (mA) and milliampere seconds (mAs) (Sookaromdee, 2017). The focal size of the X-ray tube is adjusted to keep the main focal points in frame. Having a small focal point allows for a more accurate representation of the imaged area, but it will also be harder to use a higher mAs. Another method that can be applied when taking X-rays is called X-ray grid. The X-ray grid looks like a metal plate which is flat in appearance and contains narrow lead strips (Sookaromdee, 2017). The grid is used to reduce the scatter of radiation away from the item being X-rayed, increasing the image quality.

Once the right settings have been confirmed and input into the X-ray machine, the beam alignment needs to be correctly set (Sookaromdee, 2017). The X-ray beam must be properly aligned with the X-ray film for a high-quality image to be obtained. To help achieve the best image possible, the imaged

person/item needs to be as close as possible to the table. This is to prevent any shadows being formed on the X-rays as these are a 2D image of a 3D object (Sookaromdee, 2017).

When an X-ray image is taken, different organs and structures within the body or item being captured, appears differently in the image depending upon the density (Myer, 1977). Gas such as that found in lungs, appear black in X-ray imaging as the number of molecules that can stop or resist the X-ray beam as it passes through is minimal, darkening the film as seen in *figure 2.17 (a)* (Myer, 1977). Fat appears a few shades lighter than gas when captured on an X-ray image, appearing as a dark grey as seen in *figure 2.17 (b).* Water which is retained within a body will also appear when X-rayed, as seen in *figure 2.17 (c).* The water which makes up around 70% of a human body, will appear slightly lighter compared to fat, and although water levels differ between organs, it is universally well recognised (Myer, 1977).

Bones appear as a much brighter representation as the density of bone allows for the blockage of X-rays, causing a bright spot in the X-ray film, as seen in *figure 2.17 (d)* (Myer, 1977). This is due to the X-rays not being able to pass through the bone and darken the film underneath. Lastly, metal will give the brightest signal when captured in an X-ray image (Myer, 1977). The density of the metal prevents almost all of the X-rays from passing through and being able to darken the X-ray film behind the item, as seen in *figure 2.17 (e)* (Myer, 1977).
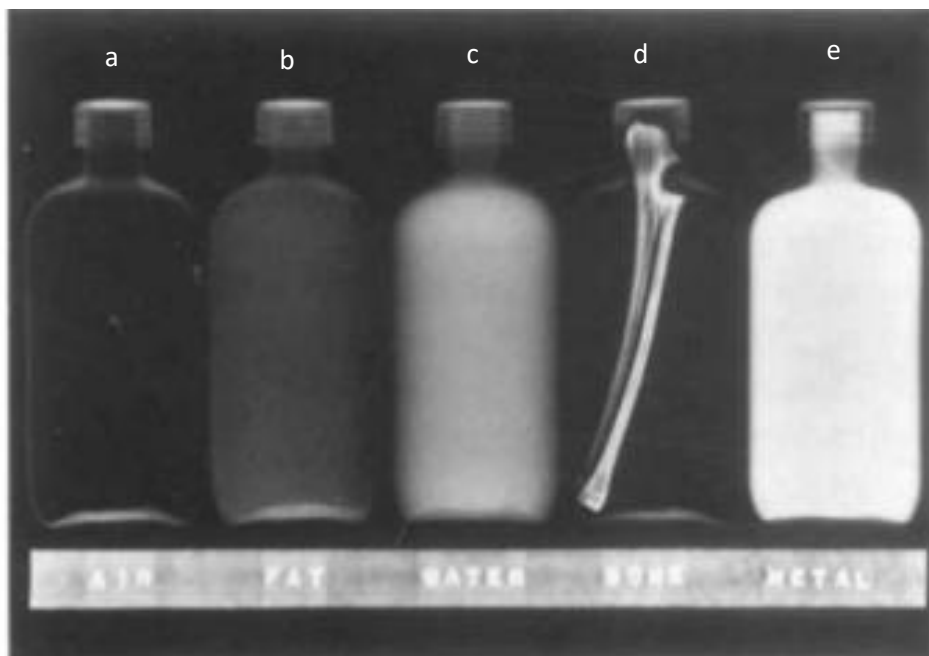
Figure 2.17: Radiographic captures of densities where, (a) Air, (b) Fat, (c) Water, (d) Bone and (e) Metal (Myer, 1977)

2.3.2.1 X – ray Experimental Details

The porcine heads were analysed on the Canterbury Christ Church University campus, within the Johnson building which contains the X-ray equipment. The X-ray table was cleaned and prepared ready for the porcine head samples. The samples themselves were double bagged in clear polyester bags with the top of the bags zip-tied shut. The porcine heads inside of the bags were one by one placed onto the table and positioned in different orientations being supported in place through the use of angled foam supports and small sandbags.

The porcine heads were adjusted after initial X-raying to make sure that the alignment of the heads was correct and to prevent any distortion in the images. This was achieved through trial and error, with adjustments being made and X-rays being repeated until the desired images were produced.

The porcine heads were X-rayed both pre- and post-shoot, giving a before and after image of the heads. This was done as it allows for direct comparison. X-ray images were obtained using a Multix Top Unit X-ray instrument fitted with an Afga digital radiography detector. Analysis of the resulting images was carried out using RadiAnt DICOM viewer (RadiAnt DICOM viewer, 2020). Due to the lack of literature available for pig X-ray analysis, the experiment setup is explained in greater detail within chapter 3.

2.3.3 Atomic Absorption Spectroscopy (AAS)

Atomic Absorption Spectroscopy (AAS) is the absorption of electromagnetic radiation by atoms (Van Loon, 2012). Electrons orbiting atoms are characterised by azimuthal quantum numbers and major numbers respectively. AAS detects elements in either a liquid or solid sample through the characteristic wavelengths of electromagnetic radiation from a source of light. Individual elements found within the sample will absorb wavelengths differently and the absorbances are measured against known standards enabling each element present to be identified (Van Loon, 2012).

The sample is turned into a gaseous form through the use of a nebuliser (*figure 2.19 (a))* which then enters into an energy source, such as a flame seen in *figure 2.19 (b).* The energy in the form of heat from the flame causes the atoms to enter an excited state due to the increase in energy (Van Loon, 2012). The excited atoms in the sample absorb electromagnetic radiation at specific wavelengths which is produced from a hollow lamp cathode *(figure 2.19 (c)).* The electromagnetic radiation is directed into the sample (Van Loon, 2012). This is absorbed by the sample, excites the atoms of the

elements in the sample, causing the electrons to become excited, promoting these to higher energy states as seen in *figure 2.18*. The amount of electromagnetic radiation absorbed gives information about the sample (Van Loon, 2012).
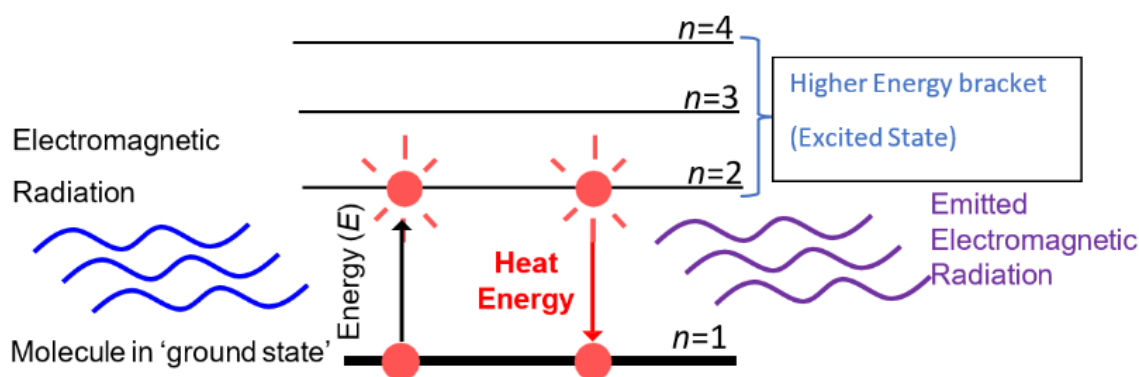
Figure 2.18: Diagram showing electromagnetic radiation exciting an electron.

Electrons only remain in these excited states for a few nanoseconds (Analytical Methods for Atomic Absorption Spectroscopy, 1996) before dropping back down to the ground state. The electron does this by releasing energy which is called quanta as seen in *figure 2.18*. The quanta enter a monochromator as seen in *figure 2.19 (d)* (Van Loon, 2012). The monochromator is an optical device which separates the different quanta and amplifies them using either optical dispersion or a prism, before exiting the monochromator. Once the focussed and amplified quanta exit the monochromator, the quanta enter a detector as seen on *figure 2.19 (e).* The detector is highly sensitive and can distinguish the different concentrations of each specific element found within the sample (Van Loon, 2012). This then allows the analyst to read the data via a computer.
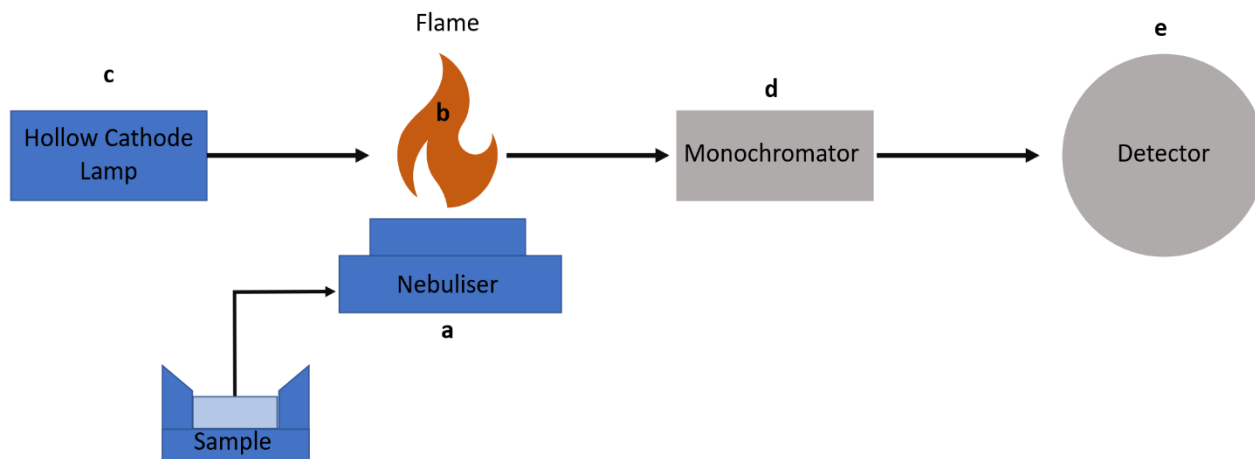
Figure 2.19: Diagram showing components of an Atomic Absorption Spectrometer (Van Loon, 2012).

2.3.3.1 Atomic Absorption Spectroscopy (AAS) Experimental Section

Within analytical chemistry, calibration graphs are vital. These are used to determine the concentration of an unknown substance, by using a known concentration to make the calibration curve, which the unknown sample is compared against (Farrukh, 2012). Typically, a large standard concentration range is used, this is to gain an approximation of the concentration. Once this is determined, a second calibration graph is produced, with a narrow concentration range to improve accuracy.

The calibration curve method involves preparing standard solutions of a minimum of three concentrations, which are run through the AAS and the absorbance is recorded (Farrukh, 2012). The recorded values are used to create the calibration curve, which enables the analyst to be able to make the appropriate changes to the concentration and run another calibration in a narrower measurable range. With the narrowed scope of the second calibration graph it is then possible to determine the concentration of the unknown elements (Farrukh, 2012).

When forming a calibration curve, knowing the concentration of the calibration sample is vital. Knowing the calibration sample concentration, allows for the unknown sample concentration to be determined (Johnson, 2003). In order to do this, stock sample solution is typically used which is diluted to obtain the desired concentration range which is typically achieved using serial dilution.

Serial dilution is a process in which a series of progressive dilutions are carried out at regular increments, where the subsequent dilution is less concentrated than the proceeding, by a constant amount (Johnson, 2003). Serial dilution is only applied to a sample when the initial concentration is

large, and the final desired concentration is small. To be able to ensure that the serial dilutions follow the same constant increments, a mathematical equation is applied, as seen in equation 2.7.

$$c_1 \times v_1 = c_2 \times v_2$$

Where:

- c_1 = Initial concentration of solution

- v_1 = Initial volume of solution

- c_2 = Final concentration solution

- v_2 = Final volume of solution

A series of standards were prepared, ranging from a 0.5 ppm to 4 ppm. The reason for the relatively low range was due to previous studies such as the one completed by Sahu et al. (2018), which looked at GSR concentrations. From the previous studies it was apparent that the concentrations of GSR found is relatively low. This allowed for the concentrations prepared for this study to be made to an appropriate level. Using equation 2.7, the standard concentrations were made as seen in *table 2.1.* All samples were analysed using a PerkinElmer 800 atomic absorption spectrometer.

Table 2.1: Table showing serial dilutions steps

Starting Concentration (ppm)	End Concentration (ppm)	Equation	Quantity Taken from solution (ml)
1000 ppm	500 ppm	$v_1 = \dfrac{500 \times 10}{1000}$	$v_1 = 5$ ml
500 ppm	250 ppm	$v_1 = \dfrac{250 \times 10}{500}$	$v_1 = 5$ ml
250 ppm	125 ppm	$v_1 = \dfrac{125 \times 10}{250}$	$v_1 = 5$ ml
125 ppm	50 ppm	$v_1 = \dfrac{50 \times 20}{125}$	$v_1 = 8$ ml
50 ppm	30 ppm	$v_1 = \dfrac{30 \times 20}{50}$	$v_1 = 12$ ml
30 ppm	20 ppm	$v_1 = \dfrac{20 \times 20}{30}$	$v_1 = 13.3$ ml
20 ppm	10 ppm	$v_1 = \dfrac{10 \times 20}{20}$	$v_1 = 10$ ml
10 ppm	5 ppm	$v_1 = \dfrac{5 \times 20}{10}$	$v_1 = 10$ ml
5 ppm	1 ppm	$v_1 = \dfrac{1 \times 20}{5}$	$v_1 = 4\ ml$

2.3.4 Microwave Digestor

Commonly used in elemental science, microwave digestion is used to dissolve heavy metals in the presence of organic molecules. This is done to change sample state from solid to liquid. This is important and valuable as liquid samples can be analysed through the use of sensitive equipment such as Inductively Coupled Plasma – Optical Emissions Spectrometry (ICP-OES).

The change in the samples state is achieved through the use of a strong acid, such as Nitric acid (65%), which is placed into a vessel with the sample. The vessel with the sample and acid inside, as seen in *figure 2.20 (A*), has a small plastic cap placed over the opening, tightly sealing the vessel, as seen in *figure 2.20 (B).* Once the small plastic cap has been placed onto the vessel, a small metal disc (known as a rupture disc) is placed on top of the cap, as seen in *figure 2.20 (C).* This is to prevent any possible rupture or explosion of the vessel if there is a large build-up of gas. The rupture disc (*figure 2.20 (C)*) acts as a blast cap, with the metal cap giving way and releasing the build-up of gasses, avoiding a more serious explosion. Once all of the aforementioned components are set up, the lid of the vessel is screwed into place, as seen in *figure 2.20 (D).*
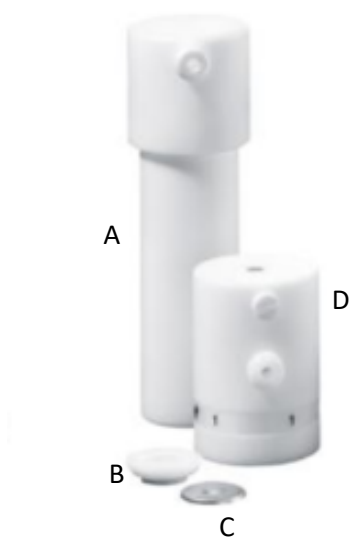
Figure 2.20: Microwave Digestor vessels, where (A) Vessel, (B) Plastic cap, (C) Rupture disc and (D) Vessel lid (BERGHOF, 2020)

The sample sealed properly inside of the vessel is placed into a microwave digestor as seen in *figure 2.21*. Once the samples are secured in place, the microwave digestor has the lid closed and locked,

and a pre-programmed run in activated. The heat inside the vessels rises, as does the pressure, causing the sample contained within the begin the break-down process at an accelerated rate.

The samples stay sealed inside of the microwave digestor once the run is complete and the samples are digested. This is to allow for the samples to adequately cool before being handled by the operator. Due to the samples being hot, care is needed by the operator that is unloading the machine. Also, due to the increase in pressure and temperature, it is possible for nitric acid gas to build up inside of the vessels during digestion. The operator must be mindful of the potential acidic gasses within the vessel and take appropriate precautions, such as making sure the nozzle as seen on *figure 2.20 (D)* is facing away from their body in case of nitric gas release.

Upon removal from the microwave digestor, the vessels need to be directly placed into a fume hood in case of nitric gas leakage. Once the samples are inside of the fume hood, decanting of the sample can commence (Berghof, 2020). Appropriate Personal Protective Equipment (PPE) must be worn whist the decanting process is taking place.

Figure 2.21: Speedwave Xpert Microwave Digestor with vessels (CHEMEUROPE, 2020)

2.3.4.1 Microwave Digestor Experimental Details

The microwave digestor used: *Speedwave Xpert*

The pre-prepared cotton swab tips were in eppendorf tubes and individually labelled prior to commencing the microwave digestion. The cotton swab tips were placed into individual vessels of which there was 12 vessels available for each run of the microwave digestor. Once the 12 vessels had a sample in each, 7 ml of nitric acid (65%) was added to each vessel.

The plastic caps, as seen in *figure 2.20 (B),* had the sealing edges rolled out to allow for a tighter seal with the vessels. Once each of the plastic caps had the sides rolled out and was adequately sealing the vessels shut, a metal rupture disc, as seen in *figure 2.20 (C),* was placed onto the plastic cap. With the rupture disc in place, the lid *(figure 2.20 (D))* was placed on and screwed tight, sealing the vessel with the sample in. This was repeated for every sample and vessel.

With the prepared vessels ready, the vessels were carefully placed into the microwave digestor with the nozzle facing into the centre, matching up with their respective attachment point. The vessel nozzles were then screwed into the appropriate receptors, locking the vessels in place. With all the vessels in place, the lid of the microwave digestor was closed shut, self-locking. The correct run plan was selected on the accompanying touch screen connected to the microwave digestor. The setting used for the Microwave digestor for the digestion of cotton swab tips, is as follows;

Table 2.2: Microwave Digestor Settings (BERGHOF, 2020)

Temperature Program	Step	Temperature (°C)	Pressure (bar)	Ta (Minute)	Time (Minute)	Power (%)
	1	140	80	2	5	80
	2	200	80	5	10	90
	3	50	60	1	20	0
	4	0	0	0	0	0
	5	0	0	0	0	0

Once the samples had fully run through the program, the lid was opened on the microwave digestor. The samples were taken one at a time and placed into a fume hood which was closely located to the microwave digestor. The vessels had the lid removed, ensuring that the nozzle was facing to the back of the fume hood, away from the operator in case of leaking nitric acid gas. The samples now in liquid

form were decanted into volumetric flasks using a funnel and filter paper. The vessel then was rinsed through three times with distilled water which also passed through the filter paper and funnel.

With the vessel adequately cleaned, the filter paper was removed and placed into a bin contained within the fume hood. The funnel was rinsed using distilled water which also enters the volumetric flask. Once the funnel was clean, the volumetric flask was then filled to the marker with distilled water and decanted into a falcon tube for storage. This is repeated for each of the vessels with clean volumetric flasks for each sample. The only equipment used in all samples is the funnel, which is cleaned at the end of each use to prevent any cross contamination between samples.

2.4 Predictive Analysis

Predictive analysis encompasses different statistical techniques such as machine learning, data mining and predictive modelling (McCue, 2015). The purpose of predictive analysis is to use already known data to make predictions about unknown data. In science, predictive analysis is used to enquire into the possibility and likely outcome of an experiment where possible. Being able to do this allows for scientist to make decisions on the direction to take studies and experiments (McCue, 2015). The accuracy of predictive analysis depends on the quality and quantity of existing data (McCue, 2015). Algorithms are used to be able to make sense of the information and to be able to classify the dataset and results into the representative classifications.

2.4.1. Algorithm

The type of algorithm used is an important consideration when modelling data computationally. The purpose of an algorithm is to make sure that the data adheres to a set of rules, with the aim of solving a question posed. Due to this, the steps that an algorithm takes need to be in the correct order to ensure that the data follows the correct rules during simulations.

The list of commands and rules that form an algorithm have to be written by a programmer for computational application. Writing an algorithm can be time consuming, and the time required is dependent upon the complexity of the proposed algorithm. A strength possessed by algorithms is that once written and programmed, they are completed and can be distributed. Due to this, researchers are able to apply different algorithms to their datasets, picking and choosing the most applicable. Being able to pick and choose the best algorithm allows for researchers to be able to try many different algorithms on their datasets until they find the best algorithm for the task. There are different types of algorithms which can be assigned depending upon the task. A few examples are classifying algorithms are K Nearest Neighbour (KNN), Random Forest and Naïve Bayes. Some image processing

algorithms are Simple Colour Histogram, Gabor Filter and Edge Histogram Filter. A few other examples of algorithms are SMOTE, Resample and Kernel Filter. There are many different types of algorithms that server to achieve different aims and answer different questions (Arndt, 2010).

2.4.1.2. Gabor Filter Algorithm

A Gabor filter algorithm is an image processing algorithm used to analyse textures within an image. Within an image, texture refers to the features describing the occupied space distribution of grey levels, corresponding to the pixels within a specific region (Stentiford, 2004). Multiple points need to be used to represent texture. Therefore, texture is characterised by spatial distribution of energy levels, and consequently cannot be defined for one particular point.
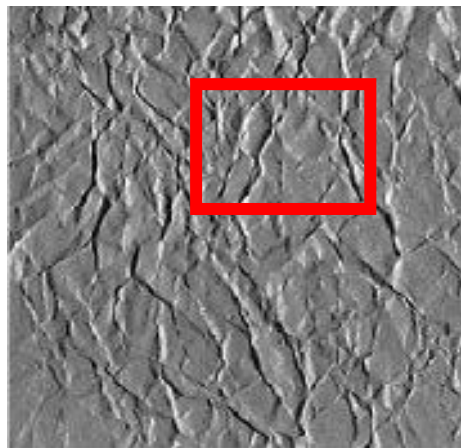
Figure 2.22: Image showing a textured surface where, highlighted area shows different grey pixels. The variation in intensities of these pixels are used to define texture (Stentiford, 2004)

The Gabor filter analyses if there are any specific frequencies contained within an image, which allows for the textures to be localised. If the textures are not localised within an image, the filter will detect the direction of texture travel. The Gabor filter is specifically designed and suited for texture identifications and not for different colour identifications. This algorithm type determines the difference between images based from the textures that are present or missing between images. The Gabor filter is formed from a Gaussian kernel modulated by a sinusoidal plane wave.

A gaussian filter can be used to generate a kernel for computational modelling. A kernel is a computer program that is found at the core of the operating system used by the computer. The kernel has complete control over the computer and operating system (Yang, 2011). When the gaussian filter is applied as a kernel, the filter can interact with an image and give values to different peaks identified within the image.

The values that are created by a gaussian filter are normal in distribution, with the centre having the highest value (as seen in *figure 2.23*). The highest intensity is found at the peak of a gaussian, with the lowest frequencies being found at either side of the peak, being closest to 0, as seen in *figure 2.23*. Once a gaussian filter kernel has been created it can be applied to an image. The gaussian filter gives a higher value to the pixel at the centre of the kernel. The higher value kernel is applied to an edge within a chosen image (Du, 2015).
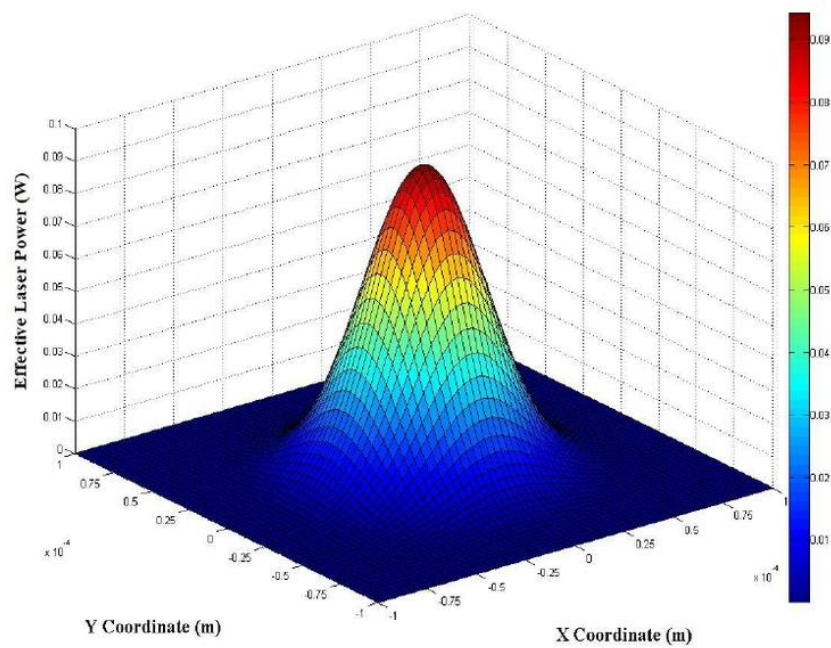
Figure 2.23: Image showing a 3D gaussian filter (Du, 2015)

A sinusoidal model is a series of wavelengths that used to look at different elevations on imaging. The wavelengths can be implemented at different angles over an image allowing for an accurate account of peaks to be identified.

2.4.1.3. Simple Colour Histogram Algorithm

A colour histogram is based on certain colours in space, for example Red, Green, Blue (RGB). Images are composed of pixels which contain different colour and shades, each of these are defined by an RGB triplet. The RGB triplet represents the three-dimension coordinate of a specific point. Each colour is represented by a different point and the combination of the numbers within the triplet will define the colour (Munisami, 2015). The colour histogram can be built for different colour spaces, for example RGB colour histograms.

Colour histograms focus upon the proportion of different colours found within an image. The values of the colour histogram are recorded as numerical values for each of the RGB colours. Algorithms such as the Simple Colour Histogram Algorithm used through WEKA has a database of 64 different RGB combinations. When selected as an image processing algorithm, the image is checked for matches to each of the 64 RGB values, which are shown as numerical values on WEKA.

2.4.1.4. K Nearest Neighbour (KNN) Algorithm

K Nearest Neighbour (KNN) is a non-parametric algorithm method of classification. KNN requires training examples from a presented dataset, which is then used for testing to classify the remaining data from within the dataset. It is an instance-based learning algorithm, also known as *lazy learning*, with the function approximated locally, since the algorithm relies on the distance between data points for classification. This algorithm is able to classify unknown samples within a dataset by using either a single neighbouring sample as seen in *figure 2.24 (a),* or an unknown sample through several different neighbouring samples as seen in *figure 2.24 (b). Figure 2.24 (b)* shows that there are more red squares close to the unknown sample than green triangles. As there are more of the red squares neighbouring the unknown sample, the unknown sample would be classified as a red square and not a green triangle. It is therefore apparent, that when the algorithm is able to classify an unknown from more than one neighbouring sample, a higher accuracy is achieved. Due to this the amount of training samples is very important for the accuracy of results.
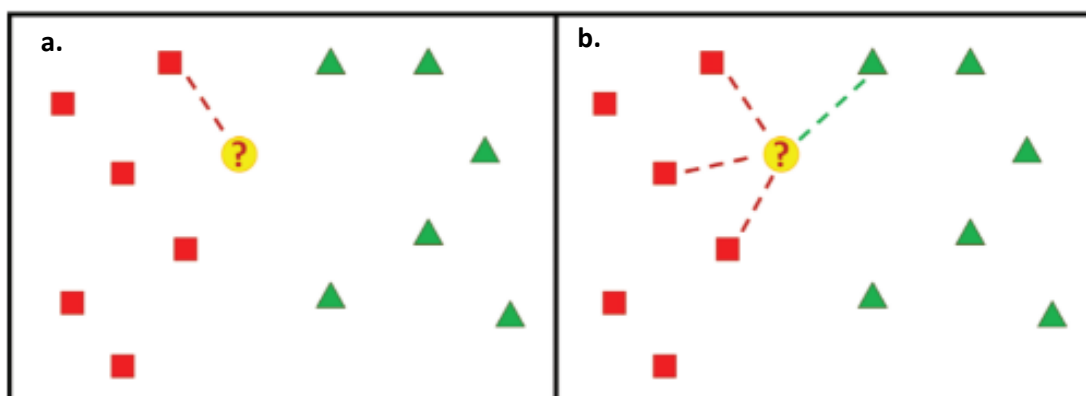
Figure 2.24: K Nearest Neighbour Diagram (Imandoust, 2013)

2.4.1.5 Naïve Bayes Algorithm

Naïve Bayes is a simple probabilistic classifier based on Bayes theory. Bayes theory is a mathematical formula applied for calculating conditional probabilities, equation 2.8.

$$P(A|B) = \frac{P(B|A)\,P(A)}{P(B)}$$

eq. 2.8

Where:

P = Probability

A and *B* = Independent events

Bayes theorem uses already known datasets or events. It uses these to form a mathematical calculation of an event. All of the considered factors within the aforementioned equation can be seen in *table 2.3.*

Table 2.3: Table of information for Bayes Theory equation

Equations	Definition
$A\ \&\ B$	Represent events.
$P(A|B)$	The probability of event *A* will occur given that *B* happened.
$P(B|A)$	The probability of event *B* will happen given that *A* happened.
$P(B)\ \&\ P(A)$	Unconditional probability of *A* and *B,* respectively happening.

Naïve Bayes is a powerful algorithm, based on the Bayes theorem, which uses assumption of independence of the predictor data. Naïve Bayes assumes that a specific feature within a dataset is unrelated or independent to other features from within the same set of data (Ranganathan, 2018). The assumption remains valid even if the features are linked to one another. It is for this reason that the algorithm is named as Naïve, due to it assuming all the contributing factors act independently to the probability (Ranganathan, 2018).

A presented dataset will contain *n* instances, x_i where *i* = 1,..n. Each of the instance contain a set of attributes, *p*, ($x_i = x_{i1}$, … x_{ip}). Naïve Bayes assumes that each of the instances belongs to one class only, $y = (y_1, y_2, … y_c)$. The machine learning algorithm makes reference to the probabilistic model, Bayes. It does this by assigning a posterior class probability to an instance. For example, *P (Y = y_j| X = x_i),* which then uses the aforementioned probabilities to assign an instance to each of the classes, as seen in equation 2.9 (Ranganathan, 2018).

$$P(y_j|x_i) = \frac{P(x_i|y_j)P(y_j)}{P(x_i)}$$

eq. 2.9

Where:

P (y$_j$| x$_i$) = Posterior probability or likelihood of the hypothesis

P (x$_i$ | y$_j$) = Conditional probability or likelihood of the hypothesis

P (y$_j$) = Class prior probability of the hypothesis

P (x$_i$) = Probability of observing the data, irrespective of hypothesis

Therefore, Naïve Bayes is a technique used for constructing classifying models, which assign class labels to instances. Naïve Bayes classifiers can be effectively trained through the use of training sets within a data set, in a supervised learning setting.

2.4.1.6 Random Forest Algorithm

Random Forest is a fully automatic, powerful machine learning technique. It requires minimal data for preparation, and still achieves effective results and models. Random Forest is constructed from other decision trees that all work together to produce predictions and provide deeper insights into data structure. Decision trees work like a flowchart, with each node representing an attribute test. Each of the branches represent the outcome of the test on the attributes. Each of the leaf nodes represents a labelled class (Biau, 2016).

Random Forest being made from several different decision trees works by creating many different weak decision trees with a few features. Decision tree's such as the one seen in *figure 2.25*, are formed from three main components; 1. The node *(figure 2.25(a))* which represents an attribute or feature. 2. A branch leading from the above node as seen in figure *2.25 (b).* The branch leading from the node represents the outcome and leads onto either another node where it will split into subsequent branches or leads into the leaves. 3. The leaves of the tree are where the final decision is located and made, as seen in *figure 2.25 (c).*
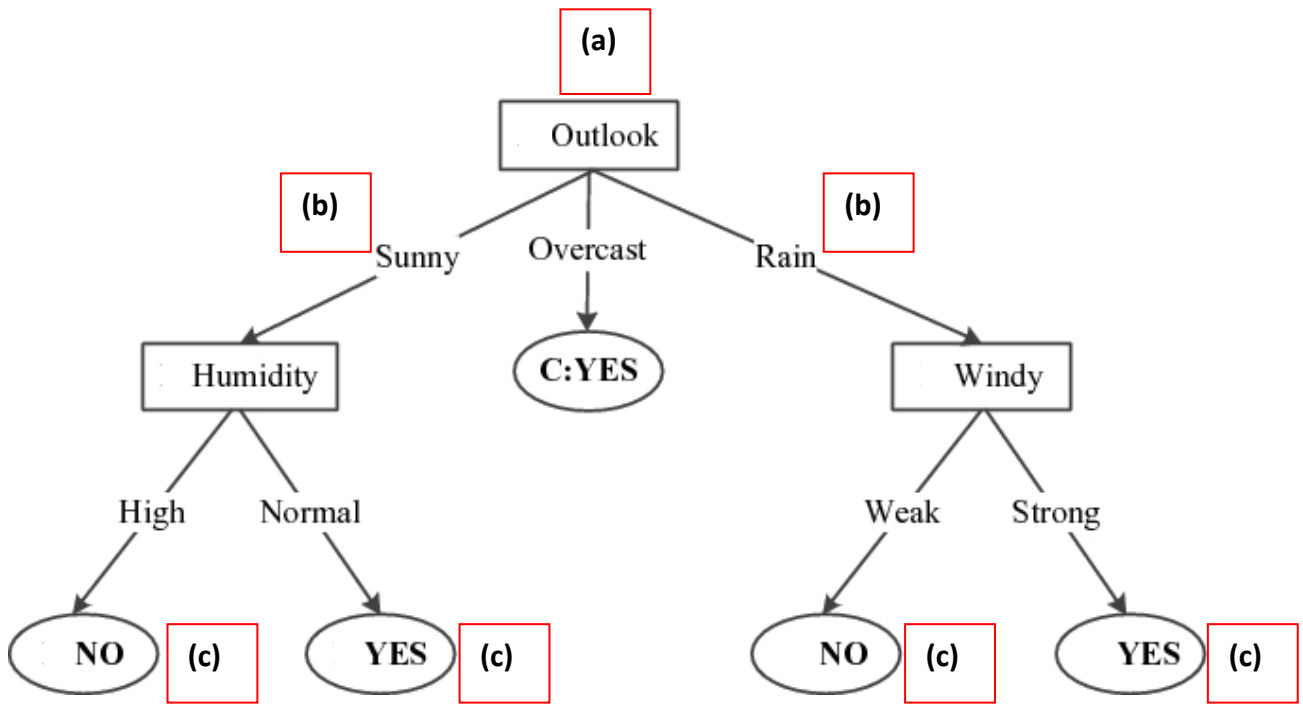
Figure 2.25: Decision tree machine learning weather (Decision Tree Tutorials & Notes | Machine Learning | HackerEarth, 2020).

Once multiple weak decision trees have been tested, they are all combined into a single strong learner, and classified by either the average or majority. The majority/ average from these decision trees is the final result. Random Forest is able to run multiple trees at the same time and complete the aforementioned steps in minimal time, allowing for quick computational results.

Chapter 3
Radiography

3.1 Radiography

3.1.1 Introduction

Radiography is a type of imagining technique which uses X-rays (Chan, 2013). X-rays are directed through an object and allow for an internal view of the object and are often used in the field of medicine for diagnostic purposes (Chan, 2013). These are also used in various other fields such as material chemistry and forensic investigation, particularly for research purposes. A few examples in which radiography is applied within forensic investigation are post-mortem imaging, Forensic Anthropology and Forensic Archaeology (Thali, 2011 and Hughes, 1997).

In relation to Forensic Ballistics it is important to accurately reconstruct an incident. However, on occasions there is minimal evidence available to the investigator. Post-mortems can provide insightful information regarding the victim's death, such as bullet calibre and shot direction. However, the link between damage and distance is not fully understood (Hinrichs, 2017), as research has primarily focussed upon shots at short distance which has limitations for real world applications (Bresson, 2009).

Radiography is a technique that is commonly used within the medical field, particularly in cases of Gun Shot Wounds (GSW). When a GSW victim has a radiological image taken, there is a plethora of information gathered through the use radiological imaging, however this data is only utilized by medical personnel. This chapter aims to gain an understanding of the use and value of radiological information within Forensic Investigation, particularly to determine its applicability to reconstructing incidents.

3.2 Experimental Setup

3.2.1 Limitations within the Literature

As summarised within chapters 1 and 2, there is little literature focussed upon porcine radiography. An understanding of porcine anatomy has been reported within the literature (Carter et al., 2001); however, this was from various different porcine breeds, ages and other variables. This highlights a gap in knowledge within veterinary medicine. Therefore, before commencing on the original research question, additional research needed to be focused upon developing a radiographic technique/standard operating procedure (SOP) for consistent X-ray imaging of the porcine heads.

3.2.2 Experimental Setup

Once the porcine heads had been brought to the radiology suite, the first objective was to develop a radiographic technique through experimentation. A porcine head was placed onto the X-ray table, the bag which was used during the transportation process (section 2.3.2.1) remained in place throughout the procedure to allow for safe handling and to prevent cross-contamination.

During the development of the radiography technique, the decision was made to image the porcine heads from both the superior-inferior and lateral views using a standard lateral skull setting (72 kV). To ensure that the porcine heads remained stable throughout the imaging process, foam blocks were used for support, as seen in *figure 3.1*. The foam supports were radiolucent, and therefore have minimal visualisation in the resultant images.
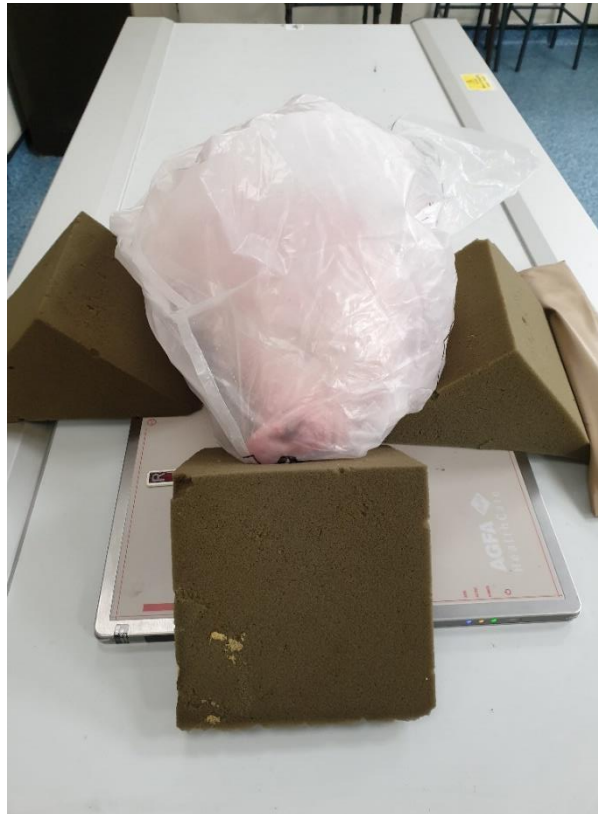
Figure 3.1: Image of double bagged porcine head supported by foam blocks on a digital detector. X-ray tube located above the porcine head.

During the radiographic process, images were taken one at a time through a trial and error method to establish a repeatable radiographic technique. One useful indicator of correct positioning was teeth alignment. Superimposition of the teeth confirmed a true lateral view of the porcine head.

During the radiographic imaging process, it is important that the item being imaged is parallel to imaging equipment and X-ray table. If the imaging equipment, X-ray table and item being imaged are not all parallel, then the image will be geometrically unsharp (Doi, 1974), which would limit the accuracy of radiographic measurements.

Figure 3.2 (a) shows imaging equipment being properly aligned with the X-ray table and the object being imaged. As a result of the proper alignment, the image produced is not distorted and gives an accurate representation of the object. If there is misalignment of the imaging equipment, X-ray table or object being imaged, such as seen in *figure 3.2 (b),* then the resulting image is distorted and not an accurate representation. If there is a distortion such as seen in *figure 3.2 (b),* the resulting image can mislead research findings such as inaccuracies in measurements and misrepresentations of anatomy and trauma.
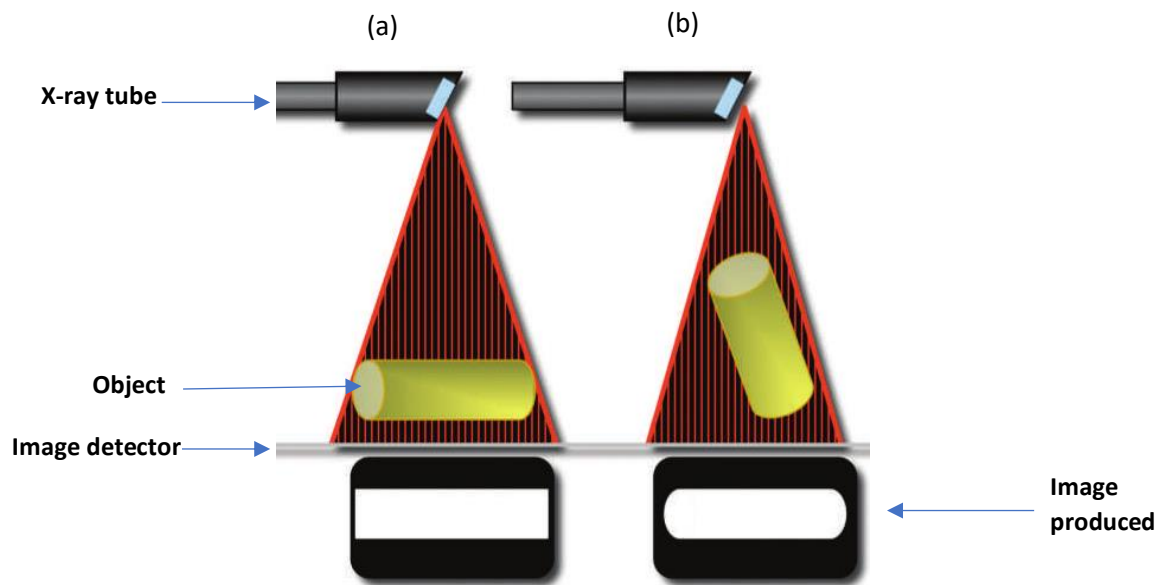
Figure 3.2: Diagram showing (a) accurate alignment of imaging equipment, object being imaged and X-ray table and (b) incorrect alignment of the object imaged causing distortion (Gribel et al., 2011).

Teeth alignment was therefore important to allow accurate representation of the anatomy on a radiograph. In order to achieve this the teeth were aligned by manipulating the pigs jaw externally. Upon obtaining the X-ray image, it was apparent that a satisfactory alignment was not achieved, as seen in *figure 3.3 (a). Figure 3.3 (a')* shows an amplification of this area where an outline of three sides of the teeth are observed, where one row corresponds to the opposing side of the head, as highlighted by the arrow *(figure 3.3 (a')),* thereby indicating that alignment was not correct.
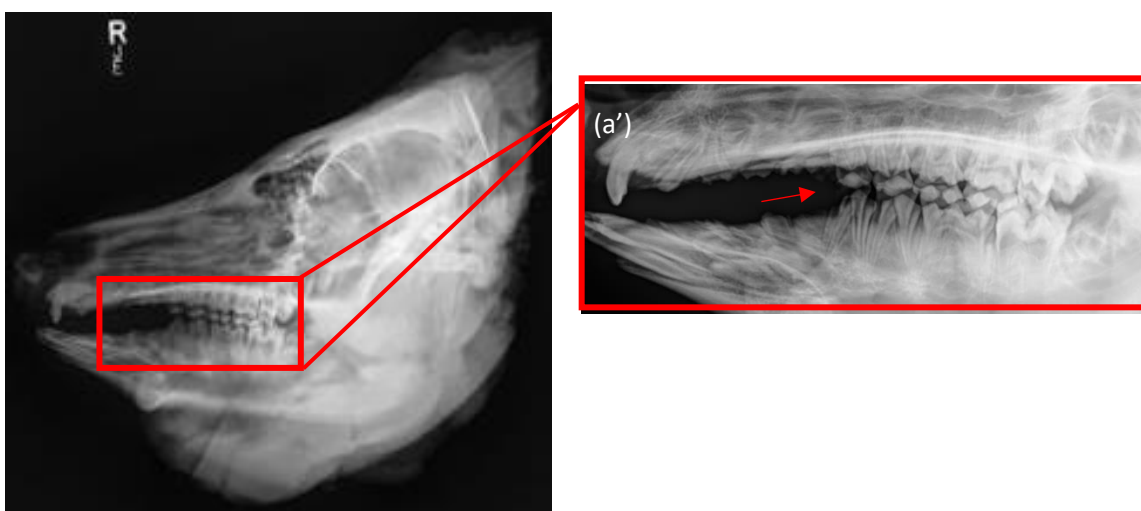
Figure 3.3: X-ray image of porcine head with slight misalignment seen in the teeth, where (a') shows an amplification of this area.

Further trial and error allowed for the teeth to be aligned by the researcher inserting the middle and index fingers into the porcine heads nasal passage. This allowed for minute corrections to the positioning of the jaw thus allowing for correct alignment as seen in *figure 3.4.*

Figure 3.4: X-ray image of porcine head with correct teeth alignment.

Additionally, nostrils alignment was also found to be important when changing the positioning of the head, where this process differed in relation to imaging angles.

- *Superior to inferior view*: Nostrils were aligned with each other and in parallel with the X-ray table.
- *Lateral view*: Nostrils aligned with each other and at 90° with respect to the X-ray table.

Once the method for teeth alignment was determined to a satisfactory standard, the next step was to improve the image quality. This was achieved by considering a series of factors such as sharpness, resolution, density and contrast (Doi, 1974).

Early X-ray images, such as that seen in *figure 3.5 (a),* showed a high degree of background noise where a lack of detail, particularly around the snout area of the porcine head and other areas of soft tissue, is observed. In order to remedy this, a scatter removal grid (100 cm focus-film-distance) was used in order to improve the signal to noise ratio and therefore the image quality. The grid is a part of the X-ray equipment that filters out deflected radiation, reducing image blur (Chan, 2013). This showed a marked improvement as can be seen in *figure 3.5 (b),* where it is possible to see the snout of the pig, as well as the ears and other soft tissue which is not visible in *figure 3.5 (a).* Additionally, greater detail is seen within the teeth. The reason that the visibility is greater on the tissue is due to a lower mAs value (approx. 5 mAs) used as well as a reduction in scatter radiation.

Automatic Exposure Control (AEC) chambers within the X-ray table were used to control the exposure values. This is usually important for reducing the radiation dose within medicine but allowed for reproducibility by preventing overexposure and allowing for visualisation of the soft tissues (Kereiakes, 2019). Originally the detector was placed directly under the porcine head, as seen in *figure 3.1,* but a satisfactory standard was not achieved until the detector was placed back into the X-ray table. The detector positioning allowed for a reduction in scatter radiation and preventing overexposure which led to an improved image quality. Therefore, these parameters were used for imaging all of the exhibits.
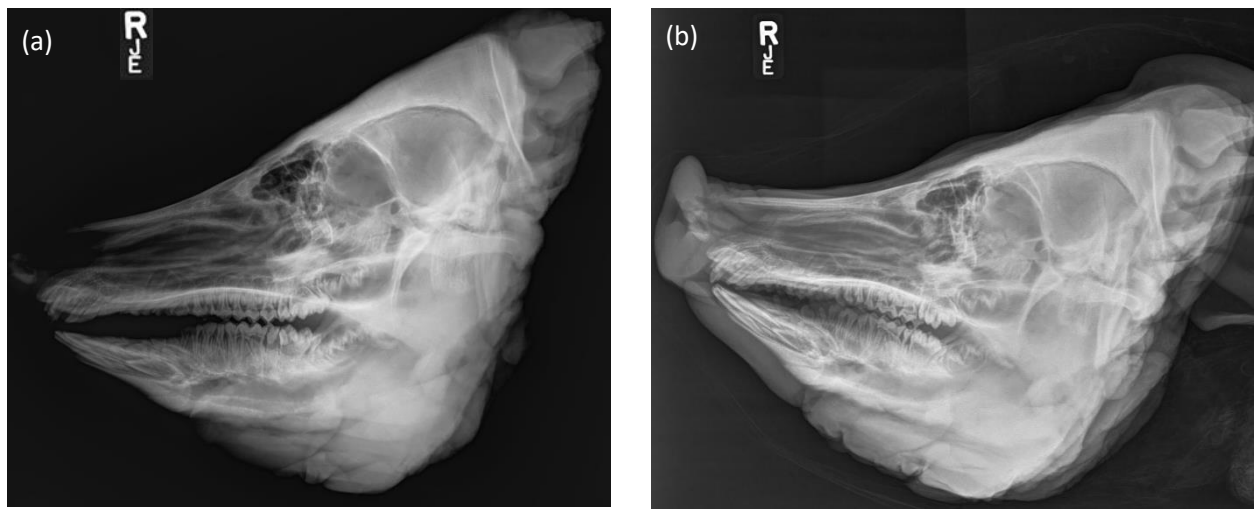
Figure 3.5: X-ray images of porcine heads where (a) shows early image of porcine head three without the use of a grid and (b) preferred imaging method of porcine head three using a grid.

3.3 Pre-Shot Data

3.3.1 Analysis

Some damage to the forehead of the porcine heads was observed during the initial visual inspection, as seen in *figure 3.6*. This damage was incurred during the butchering process, prior to purchase. Each head showed scoring along the midline, which was light and therefore primarily constrained to the skin on the cranium.

Figure 3.6: Porcine head with butcher damage

Prior to commencing the experiment, the porcine heads were analysed using a systematic approach for assessing radiographs (section 2.3.1.1). Firstly, a comparison was made to the work done by Kyllar et al. (2013), which investigated the craniofacial structures in pigs. The study collected different images of porcine heads, such as the one seen in *figure 3.7 (a)*. When using *figure 3.7 (a)* to compare to *figure 3.7 (b),* it can be seen that there are differences in lucency and opacity particularly along the length of the snout in some sections, one of these areas is highlighted in *figure 3.7 (b).* This shows an area of lucency which is considered to be due to a variation in morphologies between different breeds of pigs, however this variation is thought to be minimal. Therefore, the work by Kyllar (2013) was used as a reference for comparison in this research.
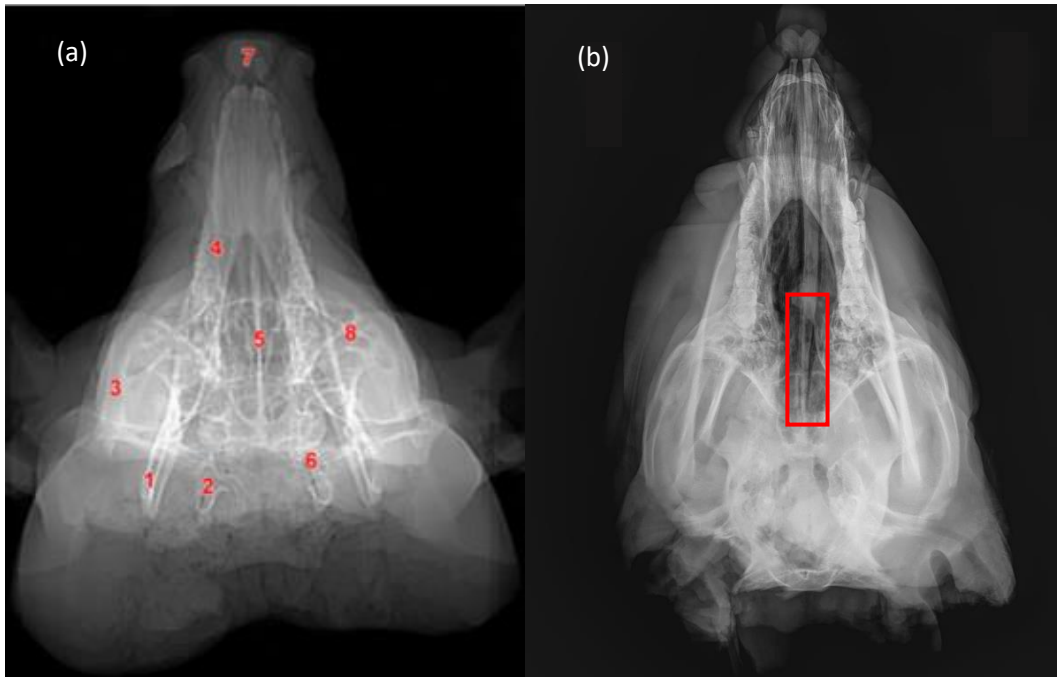
Figure 3.7: (a) Radiograph of Porcine head (Kyllar et al., 2013) and (b) Radiograph of porcine head with butcher inflicted damage used for the experiment.

The limited literature available was used to understand the normal radiographic anatomy of the porcine head. However, it was not possible to include anatomical variations.

In this study, alignment and cartilage were considered due to the mandible requiring a suitable alignment with the maxilla. The only other joint requiring consideration was the C1 vertebrae however, due to the decapitation process, this was not considered to be cartilage for the purpose of this study. An accurate alignment was achieved using the experimental set up described above.

X-ray images do not show any sudden stops or sharp edges, equally there are no inconsistencies or aspects that are different between the left and right sides of the skull, thereby indicating no damage to the bony structures.

As per standard radiological procedures, these X-ray images were reviewed by a second radiographer. This report can be found in appendix B.

3.4 Post-Shot Data

3.4.1 Physical Analysis

Once shot, the porcine heads were taken back to the Christ Church University Campus. Once back on site the porcine heads were taken for initial physical data collection in the laboratory. Upon initial visual inspection, bullet entry wounds were clearly visible as seen in *figure 3.8.*

Porcine head number two shot at 0 metres (point blank) can be seen in *figure 3.8 (a).* The figure shows the small entry wound with a blackening around this area. The blackening is GSR dispensed from the firearm and observed due to the short distance from the barrel to the porcine head. *Figure 3.8 (b)* shows porcine head one that was shot at 15 metres, where the bullet entry wound is clearly visible with minimal blackening present on the surface due to the increased distance of the shot, which allowed for a higher dispersion rate of GSR. *Figure 3.8 (c)* shows porcine head three which was shot at 30 metres. The entry wound is small in size as observed in the previous wounds with minimal blackening around the entry wound.
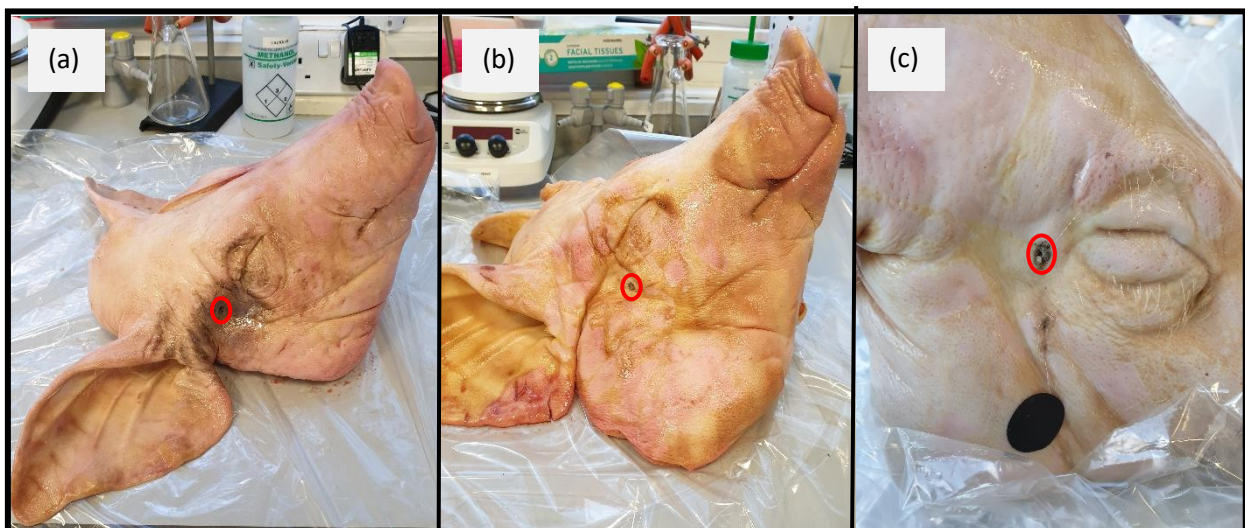
Figure 3.8: Porcine heads shot at (a) 0 metres, (b) 15 metres and (c) 30 metres.

One of the issues encountered with the experiment was the differences in impact points between all of the porcine heads. As discussed in section 2.2.4, the shooter used black stickers as a reference target point. Due to human error, there was a low probability of hitting the target at the same point on each head. The shooter was able to achieve a high level of accuracy as seen in *figure 3.8*, therefore the shots were considered to be of a satisfactory standard for the purpose of the experiment.

The entry wounds on the porcine heads (a) and (c) as seen in *figure 3.8* are similar, whereas (b) is slightly below of the eye socket. Due to the difference in the entry location, the analysis will be affected as the bullet may have the potential of travelling through thicker or thinner bone.

With regards to finding an exit wound, none was identified on any of the porcine heads. It is apparent that a linear bullet trajectory did not occur for any of the shots, as the bullet exit wound would have been observed on the opposite side of the bullet entry point. It is possible that bullets exited through the large wound left from decapitation. This indicates bullet deviation and therefore X-ray analysis was considered important to determine this.

3.4.2 X-ray Analysis

Once the post-shot porcine heads had been imaged in the same way as pre-shot, the radiological images were collected for a comparison.

Figure 3.9: Porcine head number two (0 metres) (a) Pre-shot lateral image, (b) Pre-shot superior image, (c) Post-shot lateral image and (d) Post-shot superior image.

Figure 3.9 shows X-ray images of porcine head number two which was shot point blank (0 metres). The lateral X-ray taken of head pre-shot when compared to post-shot shows soft tissue damage indicated by the yellow arrow in *figure 3.9 (c).* Arrowhead one shows what appears to be a fracture in the Parietal bone. The second arrowhead identified as two, shows what appears to be a fracture of the Lacrimal bone.

Figure 3.9 (d) shows the superior view of porcine head number two post-shot. When compared to the pre-shot X-ray image, it is observed that damage has occurred. The arrowhead shows a fracture on the Nuchal crest which is located within the proximity of the permanent cavitation caused by the bullet. The yellow arrow points towards soft tissue damage, which is located around the temporal fossa, however it must be noted that this area of lucency may be due to gas build up due to post-mortem changes.

Due to there being no identifiable exit wounds, the bullet must have deviated during penetration and excited through the back of the porcine head. A possible reason for this is the high kinetic energy from the bullet as the distance between the barrel of the firearm was placed flush to the porcine head. *Figure 3.9 (c – d)* shows some areas of opacity in the area surrounding the head. This is due to the double bagging of the head as described in section 2.3.2.1. This does not deduct from the quality of the radiological images and was therefore an amendment to the procedure was not required.

Figure 3.10: Porcine head number one (15 metres) (a) Pre-shot lateral image, (b) Pre-shot superior image, (c) Post-shot lateral image and (d) Post-shot superior image.

Porcine head number one (15 metres) post-shot X-ray can be seen in *figure 3.10 (c).* When comparing the lateral X-rays for pre- and post- shot there appears to be soft tissue damage, as marked by the

yellow arrow. The soft tissue damage appears to run between the back of the Temporal Fossa and the Nuchal crest. When a comparison is made between the superior view of porcine head number one, pre-shot and post-shot, more differences can be observed. The soft tissue damage can be identified on the porcine head in *figure 3.10 (d).* Indicated by the yellow arrow, the porcine head shows what appears to be soft tissue damage running the porcine head in the image.

The red arrow heads on *figure 3.10 (d)* indicate the location of potential damage to the boney structures. The red arrow head indicated as (1) shows a fracture on the back of the external auditory meatus bone of the porcine skull. The red arrow head indicated as (2) shows what appreares to be fracture to the Lacrimal bone and is found within the proximity of the permanent cavitaiton, where the bullet entered the procine head.

The bullets permanent cavitation can be observed relatively clearly in the soft tissue damage to the porcine head. Originating on the left side of *figure 3.10 (d),* a trail of soft tissue damage can be observed which is further indicated by the yellow arrow. There is no bullet retention in the porcine head, and there was also a lack of obvious exit wound caused by the bullet. When trying to follow the permanent cavitation path to find the possible exit location of the bullet, the path becomes very difficult to follow. Therefore it is apparent that bullet path deviation occurred, causing the bullet to direct to the back of the porcine head, where the open wound was located. One of the possible reasons for this was that the kinetic energy of the bullet is very high due to the firearm not being very far from the porcine head, only 15 metres.
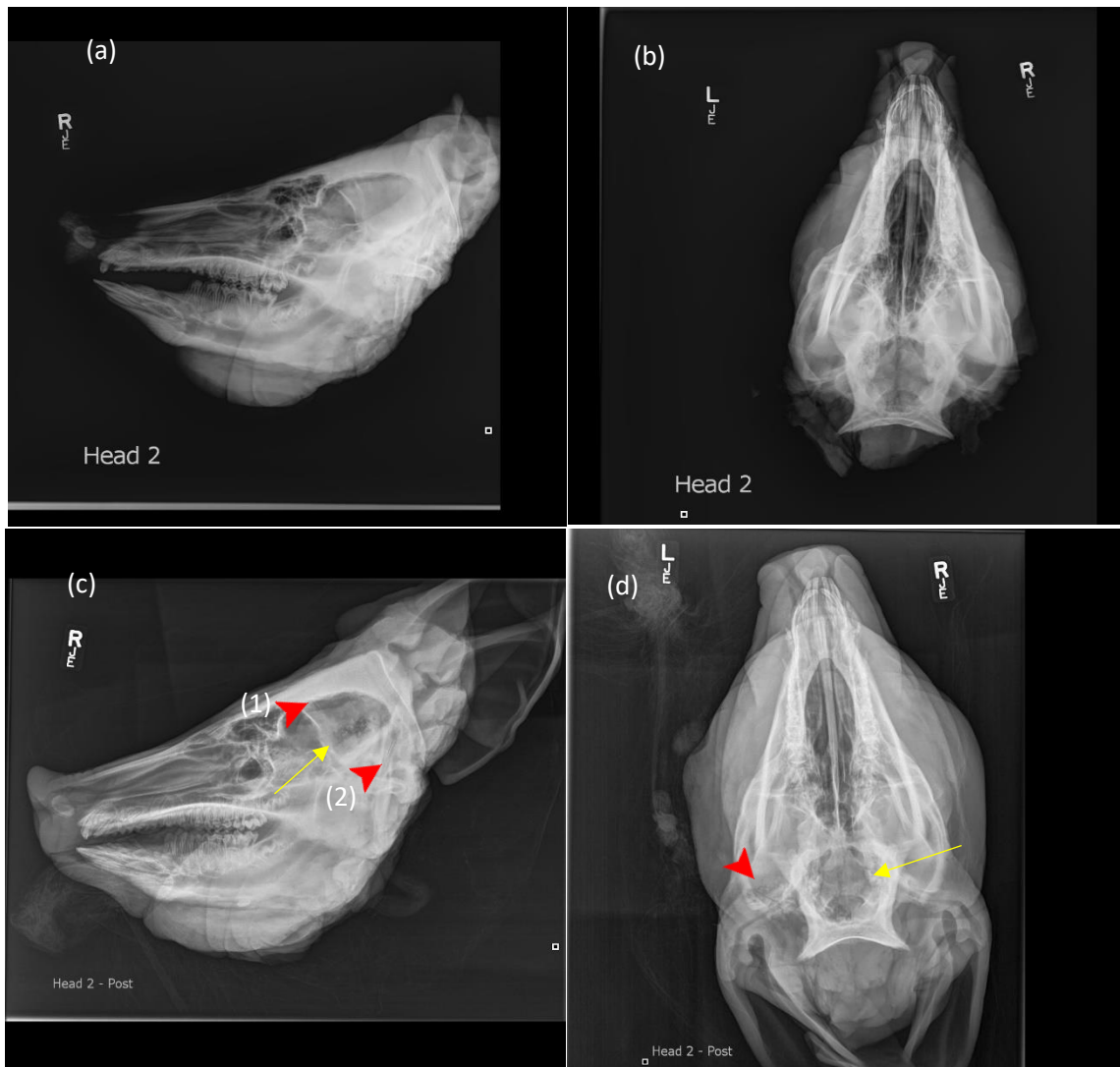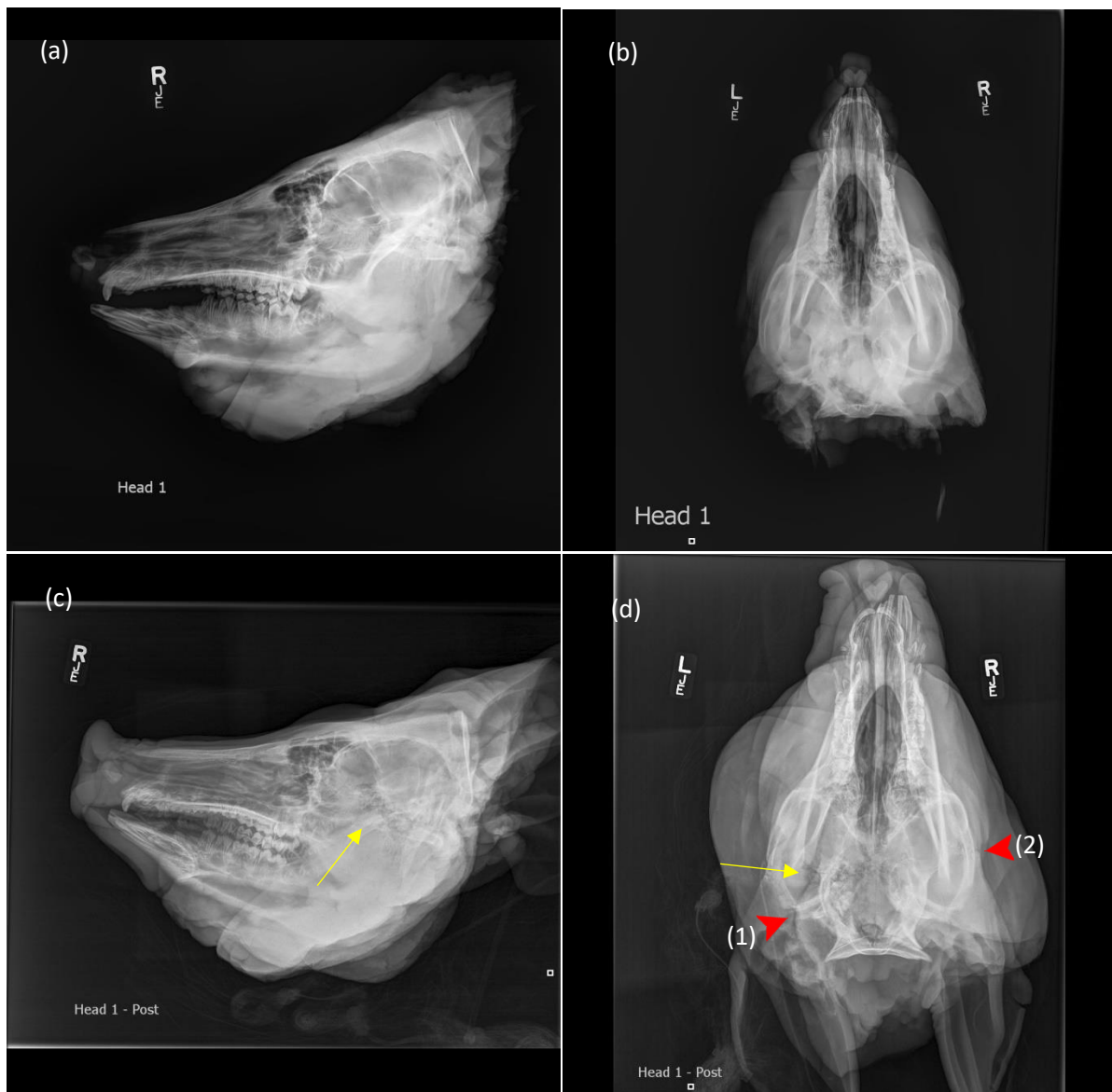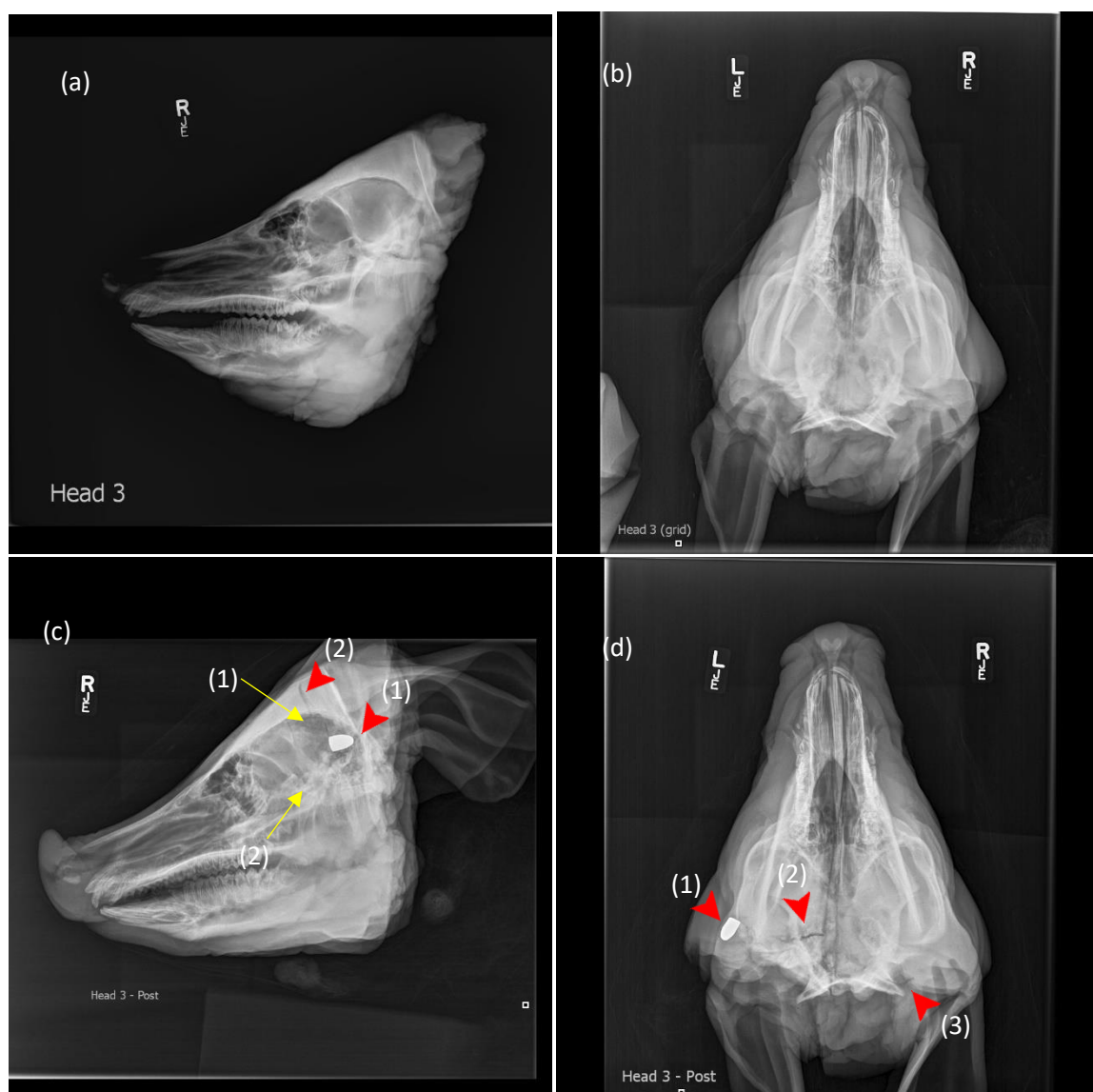
Figure 3.11: Porcine head number three (30 metres) (a) Pre-shot lateral image, (b) Pre-shot superior image, (c) Post-shot lateral image and (d) Post-shot superior image.

Figure 3.11 shows the pre- and post-shot X-ray images collected for porcine head number three which was shot at 30 metres, where damage in post-shot images is clearly visible. One of the most apparent differences between these X-ray images is the retention of the bullet. The retained bullet is indicated by the red arrow head one in *figure 3.11 (c).* The retained bullet is not the only identifiable difference in the X-ray images. The arrow head indicated as number two, indicates the presence of a fracture which appears to cross the pariteal bones. There is also soft tissue damage indicated by the yellow arrows. The yellow arrow labelled as one shows an area of lucency which may be due to a build of decomposition gases. The yellow arrow labelled as two is pointing to the soft tissue damage which is most likely as a result of the bullet entry wound.

Figure 3.11 (d) shows the post-shot superior X-ray image of porcine head three. When a comparison is made between *figure 3.11 (b)* and *figure 3.11 (d),* the damage which is as a result of the bullet becomes apparent. In *figure 3.11 (d)* the retained bullet is still highly visable and is indicated with red arrow head number one. Arrow head number two indicates the location of a fracture on the nuchal crest, which is on the same path the bullet is located. Arrow head number three shows a small potential fracture located on the Occipital bone. The soft tissue damage is located in the same line as the fracture fractrue (arrow head two) and as the retained bullet (arrow head one), indicating that these damages are as a direct result of the bullets permanent cavitation.

A number of external forces affect projectile motion (section 2.1.2.3), the bullets exposure time to these factors increases with distance or time in flight, with Kinetic energy being one of these affected factors. As head number three was shot at the largest distance (30 m), this would have experienced the greatest effects of external forces. It is possible that a terminal bullet velocity was reached which would signify lower kinetic energy upon impact, thereby causing bullet retention.

As per previously mentioned, a second radiographers report was completed which can be found in appendix B. The second radiographers report confirms and supports the previously made points regarding the porcine heads conditions and key points of interest.

A limitation of this method is that the bullet entry points are slightly different on each of the porcine heads. This is down to human error as it is not achieveable for the firearms officer to hit the exact same point on each of the heads consistently at the increasing distances. Another limitation was the number of porcine heads which were shot. While more heads were planned to be shot, this was not achieveable due to the COVID-19 restrictions.

In conclusion, although only one pig head the retained bullet it is possible to see the path of the bullets in the other heads. The permanent cavitation in the soft tissue is evidence of bullet passage. Whilst these changes are easily observed using radiographs, it is possible that some of these soft tissue changes are due to decomposition.

Future work should consider regular radiographic imaging of the heads to track post-mortem changes. Additionally, there was difficulty when considering breaks and fractures occurring as a direct result of ballistic impact. Therefore, it was only possible to identify a few of these fractures as specified above.

3.5 Conclusion

Radiological images have potential importance in the field of forensic investigation. In current practice, radiological images are not used during the reconstruction of an incident despite the plethra of information they contain. The limited use of X-ray imaging within this field may be due in part to the lack of standard operating procedures (SOP). Therefore, SOP development for radiolological imaging of the porcine heads was a key part of the study as it allows for reproducible images to be obtained and for these to be admitted as evidence in a criminal investigation.

As well as SOP development, the quality of radiological images that were captured through the use of the developed SOP proved to be to a much higher standard than reported in previous literature.

From the radiological images obtained in this study it is possible to draw some conclusions. Bullet retention is affected by the distance between the shooter and the target. It was observed that the closer the shooter was to the target, the less bullet retention was experienced. A difficulty was encountered when trying to differentiate between decomposition changes and bullet damage as these factors are represented in a similar way within the radiological images. Whilst this was difficult to process by eye, the use of computational modelling may prove benefical for the determination of shot distance.

While there were some limitations that were encountered during the testing and data collection, this does not deduct from the importance and value of the study. While having more data would be benifical to the study, the three porcine heads allowed or preliminary data analysis and provides promise for future testing and further investigation.

Chapter 4
GSR distribution with distance

4.0 Introduction

This chapter will focus upon the interpretation and evaluation of gunshot residue spread at increasing distances. Atomic Absorption Spectroscopy (AAS) was the method used for the quantification of GSR present in the cotton swabs used for the sample collection as specified in section 2.3.3. A series of graphical and tabular data sets are used in order to achieve this aim.

4.1 Results

4.1.1 Calibration

Firstly, it is important to establish a method for determining an instruments accuracy as the uncertainty cannot be established without recalibration. Additionally, it is important to identify how the intensity relates to concentration, this was achieved using calibration graphs, as seen in *figure 4.1.* Data used for these calibration graphs can also be seen in *table 4.1.*
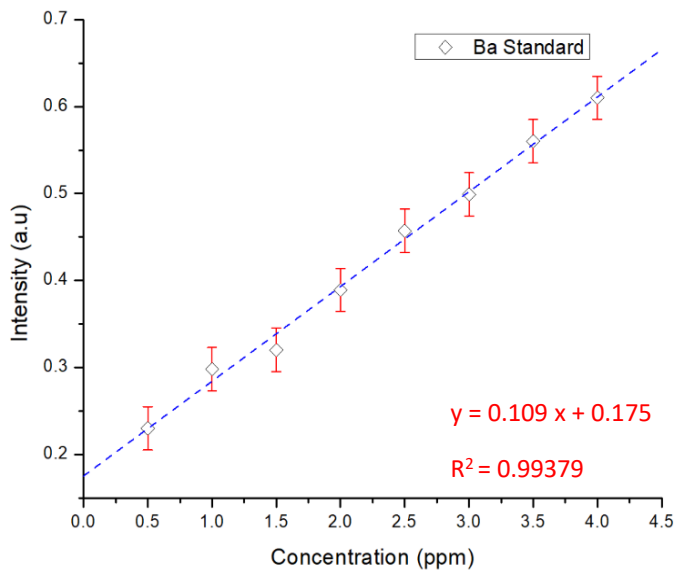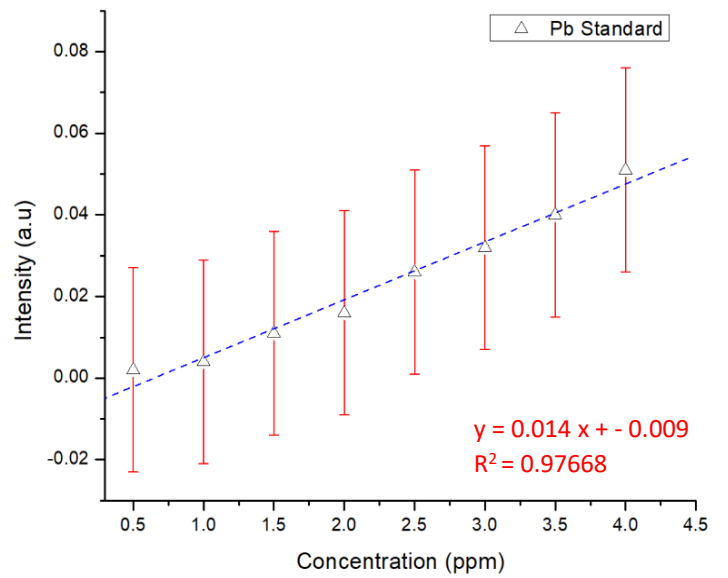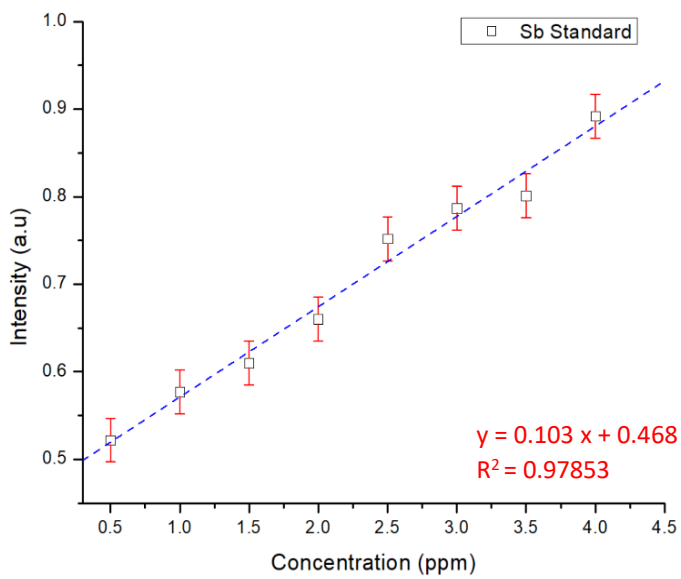
Figure 4.1: Graphs showing calibrations graphs for barium, antimony and lead.

Table 4.1: Data used for calibrations of lead, barium and antimony.

Lead (Pb)								
Conc. (ppm)	0.5	1	1.5	2	2.5	3	3.5	4
Intensity (a.u)	0.002	0.004	0.011	0.016	0.026	0.032	0.040	0.051
Error	0.025	0.025	0.025	0.025	0.025	0.025	0.025	0.025
Antimony (Sb)								
Conc. (ppm)	0.5	1	1.5	2	2.5	3	3.5	4
Intensity (a.u)	0.522	0.577	0.610	0.660	0.752	0.787	0.801	0.892
Error	0.025	0.025	0.025	0.025	0.025	0.025	0.025	0.025
Barium (Ba)								
Conc. (ppm)	0.5	1	1.5	2	2.5	3	3.5	4
Intensity (a.u)	0.230	0.298	0.320	0.389	0.457	0.499	0.560	0.610
Error	0.025	0.025	0.025	0.025	0.025	0.025	0.025	0.025

As can be seen above, three calibration standards were chosen which were lead (Pb), antimony (Sb) and barium (Ba). A series of these standards were prepared within the concentration range of $0.5 \geq x \leq 4$ ppm. This range was paramount to ensuring Pb, Sb and Ba concentrations of the analyte fall within a range of standards. The method used for the preparation of these standards is specified in, section 2.3.3.1.

Figure 4.1 shows that concentration values increase linearly with intensity, this data can therefore be graphed using the equation of line:

$$y = mx + C$$

eq. 4.1

Where:

m = slope/gradient

C = intercept

The equations for each aforementioned elements are detailed in *figure 4.1* along with the R^2 values. R^2 is important as it is a statistical measure of how close the datapoints are to the line of best fit, also known as regression. An R^2 value of 1, indicates that the data fits the model precisely, therefore the closer the R^2 value is to 1, the stronger the indication that the model explains the variability of the data. The calculated R^2 values (*figure 4.1*) indicate that the methods and instrument are sufficiently

accurate. Therefore, these calibration graphs support the accuracy and validity of the results discussed within this section.

4.1.2 Experimental Results

Figure 4.2 shows the variation in GSR concentration with distance. Predetermined shooter distances were selected, as mentioned in section 2.2.4. Data used for these graphs can also be seen in *table 4.2.*
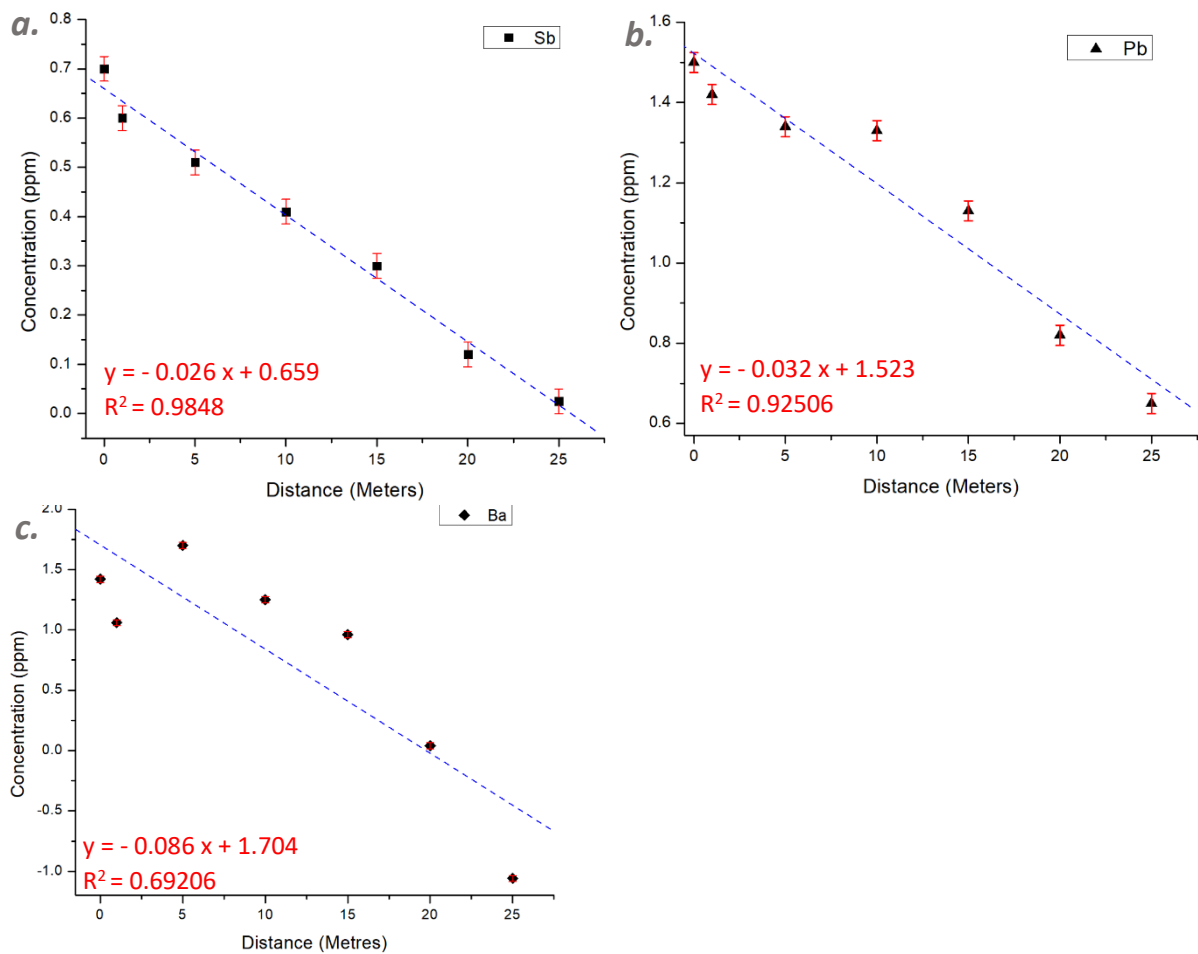
Figure 4.2: Graphs showing variation in barium, antimony and lead concentration over distance.

Table 4.2. Experimental data obtained for lead, barium and antimony distribution with distance.

Lead (Pb)							
Conc. (ppm)	1.50	1.42	1.34	1.33	1.13	0.82	0.65
Distance (m)	0	1	5	10	15	20	25
Error	0.025	0.025	0.025	0.025	0.025	0.025	0.025
Antimony (Sb)							
Conc. (ppm)	0.70	0.60	0.51	0.41	0.30	0.12	0.025
Distance (m)	0	1	5	10	15	20	25
Error	0.025	0.025	0.025	0.025	0.025	0.025	0.025
Barium (Ba)							
Conc. (ppm)	1.42	1.06	1.70	1.25	0.96	0.04	-1.06
Distance (m)	0	1	5	10	15	20	25
Error	0.025	0.025	0.025	0.025	0.025	0.025	0.025

Figure 4.2. shows a general decrease with increasing distance. This observation is consistent with what would be expected from gunshot residue spread and that which has been reported previously by other authors (Caldwell, 2019). Therefore, the data indicates that the closer the source is to the target, the higher amount of GSR deposition occurs. This is consistent with the physical spread of GSR with distance as seen in *figure 4.3,* where GSR spread increases over distance, showing that GSR particles have a higher suspension in air at shorter distances.
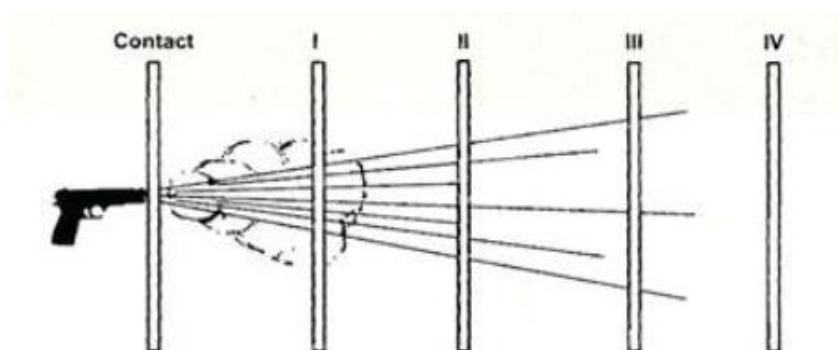
Figure 4.3: Diagram of GSR dispersion at increasing distances (Phillips, 2011).

Figure 4.2 (a) shows the concentration of Antimony (Sb) over distance. The datapoints indicate that as the distance from the source and target increased, the concentration of Sb decreased in a linear fashion. With the calculated error present on the graph, it is possible to identify that all datum points

can all be placed onto the line of best fit. The R^2 value for Sb variation with distance is 0.9848, as seen in *figure 4.2 (a)* is indicating that the data points are close to the line of best fit, and therefore show a consistent trend.

Figure 4.2 (b) shows the concentration of lead (Pb) distribution over distance. The data indicates, as with *figure 4.2.(a),* that as the distance between shooter and target increased, the concentration of lead decreased in a linear fashion. A deviation to this linear decrease is observed at 10 m, where a similar concentration to that observed at 5 m was obtained, possible reasons for this is discussed within this chapter. This is reflected in the R^2 value of 0.92506 *(figure 4.2.(b)).*

Figure 4.2. (c) shows the concentration of the GSR element Barium (Ba) over distance. Unlike the data obtained for lead *(Figure 4. b)* and antimony *(Figure 4. a),* the data obtained for the barium distribution shows greater variation at the shorter distances. The first three shots provide considerable differences in the deposition of Barium on the target, with the 3rd shot (5 m) having the highest elemental deposition. Typically, the first would be expected to have the largest concentration of elemental GSR as the element has the least distance to travel from the barrel of the firearm to the target area, as discussed above and shown in *figure 4.3*.

a.

y = - 0.086 x + 1.704
R^2 = 0.69206

b.

y = - 0.105 x + 2.305
R^2 = 0.91211
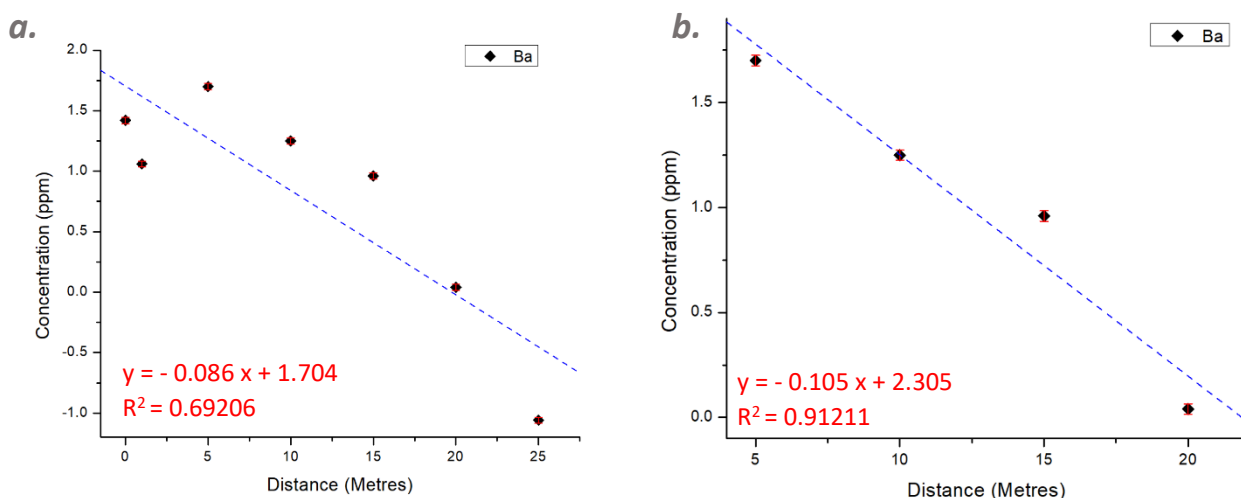
Figure 4.4: Graphs showing variation in barium over distance where (a) includes outlining data points and (b) with outliers removed.

As seen in *figure 4.4*, the data points at 0 m, 1 m and 25 m are outliers. These are considered to be outliers as the rest of the data points form a linear trend. The data points for 0 m and 1 m are identified as outliers as the next datapoint, 5 m, is a higher concentration than both previous data points. The data from all three GSR elements indicates that there is a linear decrease in concentration over

distance, which is identified in Ba from 5 m. The data point for 25 m is also an outlier due to the negative value obtained for concentration which may be due to the concentration of the barium present on the target was at a concentration below the limit of detection of the instrument, and therefore not detectable using AAS.

When a line of best fit is applied to *figure 4.4. (b*) using the data points, which are not outliers, a linear decrease in concentration over distance is observed. The linear decrease in concentration is in keeping with expectations and observations from *figure 4.2. (a)* and *(b),* as well as with existing literature (Caldwell, 2019).

The confidence intervals, for example the 95% confidence interval, could not be determined. The accumulation of data was limited to one set, due to current pandemic (covid-19) considerations.

4.2 Discussion

The data presented in *figure 4.2* gives a strong indication that the concentration of GSR decreases with increasing distance. The decrease in concentration of GSR elements as the distance between the source and the target increases, is also seen in *figure 4.3*. Both antimony and lead have R^2 values, which further supports this finding.

As discussed, there are some inconsistencies in this trend, particularly in relation to Barium concentrations. This is particularly interesting as both Barium and Antimony possess similar atomic weights (137.33 amu Vs 121.76 amu). This discrepancy might be due to differences within particle morphology. A study by Brożek-Mucha, (2007), researched the morphology of GSR. The study used Scanning Electron Microscopy (SEM) with the aim of identifying differences in the morphology between airborne GSR and GSR present within the cartridge case. The study found that GSR elements have different cooling times and consequently their morphology can change (Brożek-Mucha, 2007). Brożek-Mucha, (2007), also found that the morphology of GSR can be dependent upon the brand of ammunition being fired. The authors also discovered that soft metals found within GSR, such as lead that have low melting points, are prone to chemical and physical interactions within the internal ballistics phase (i.e. prior to the bullet leaving the barrel). These changes with GSR morphology could explain the outlaying data points within the Barium graph, *figure 4.4.(a).* To conclusively determine this further work would be required, such as SEM analysis of the exhibits in order to allow for the morphology to be determined.

The vast majority of research has focused upon the analysis of GSR spread at short distances (Caldwell, 2018, Campbell, 2018 and Ditrich, 2012). Very little work has been aimed at investigating this distribution at distances above 15 m (Gerard et al., 2011). This a limitation within ballistics research as the real-world applicability is minimal. The results of this study show that it is possible to detect lead and traces of antimony at distances up to and including 25 m.

The detection of GSR at these increased distances may be due to the experimental set up (section 2.2.3) One of the considerations of the GSR deposition and suspension in air was the extractor fans present at the firearms range. Extraction fans and air inlets are required by law for health and safety considerations (control of hazardous substances in indoor ranges, 2020). The desired laminar airflow is achieved through a negative pressure downrange, achieved using an extraction system rated 10% greater than the air inlet. The location of the extractor was the bottom end of the firearms range, where the targets are placed for shooting. The location of air inlets, which allow for air flow through the firearms range, are not known. This raises issues, as it can cause some of the GSR particles to have a higher air suspension time at certain points within the range. Thereby causing the GSR to travel further than typically expected, thus causing outliers in the data. It can also cause outlaying data, if there is an inlet source placed further downrange from the GSR source. This is because, as GSR particles travel after expulsion from the GSR source, a number of inherent factors will affect GSR spread such has air temperature and barrel length, as this can cause GSR plume drawback (Ditrich, 2012). These factors coupled to the air inlet considerations can cause GSR particles to have a higher degree of airborne retention time. Additionally, due to the negative pressure caused between an inlet and extractor, it can also carry the GSR particles further.

Another factor of the air inlets and extractors is laminar air flow. Laminar air flow is when the air flows evenly, spanning from the ceiling of the room to the floor, with minimal turbulence from an inlet point to an extractor (Phillips, 2020). This airflow is affected by shooter position, as the body of the shooter creates a void in the air movement. The void created by the shooter can cause a patch of stale air that does not move. The size of the void in front of the source can be influenced by the positioning of the shooter. If the shooter is standing, then the size of the void will be larger due to their body blocking a larger area. This affects GSR travel due to the void but the GSR will also be much higher from the ground, increasing the time it takes before the GSR lands on surfaces when dispensed from the source. If the shooter is kneeling, then the size of the void created is much smaller than when the shooter is standing. The drawback is that the GSR source is closer to the surface, decreasing the time before the GSR will settle. Lastly, if the shooter is prone (laying), the void created is the smallest. The issue with this is that the barrel of the GSR source is very close to the surface, and consequently is much more likely to cause the GSR to settle earlier.

Trying to find a best position for the shooter is a difficult process of compromise. The shooter needs to remain accurate for the target, while remaining comfortable, and position themselves to try and reduce the laminar airflow. The main objective is to maintain health and safety during the shooting process. During the experiment, the shooter ranged through all three body positions to maintain their accuracy and safety (as summarized in section 2.2.4).

The air flow through the firearms range could explain why GSR was present at further distances, such as at 25 m. Due to having a negative air pressure at the end of the range (close to the targets), could have caused the GSR to travel further than what would be experienced and expected in a real-world scenario.

Despite the air flow of the indoors firearm range, it does not detract from the value of the experiment and study, as all of the data was gathered in the same environment. Due to the experimental shots being carried out in the same environment, it allows for comparison between datasets collected from the target. All of the GSR experienced the same environmental factors caused by the extractor system. Thereby highlighting the significance of the questions posed within this research.

Additionally, a study carried out by Gerard et al. (2011), looked at long range deposition of GSR and the mechanisms of its transportation. The study ranged from 4.5 m, 9 m, 13.5 m and 18 m, looking at the deposition of GSR. The study found that GSR was present at all distances, including 18 m. The GSR present was then split into one of three categories being, small (0 to 2.9 μm), medium (3 to 7.9 μm) and large (8 μm or greater) particle size. For the 18 m GSR samples, a large percentage of the GSR present fell into the medium sized particle category. The study theorises that the lack of large GSR particles at further distances was most likely due to the bullet spinning off the larger GSR particles during travel, further highlighting the need to link distance and particle morphology as discussed above.

Swabbing is a commonly used method of evidence and sample collection within the field of ballistics and Forensic Investigation. The swab is a cheaply acquired collective tool, and as a result is often a preferred method of collection (You et al., 2019). A limitation of swabs is that it is possible for some of the sample to fall of the swab during transportation and also during the collection process, as some of the GSR sample can be left on the target, which is particularly applicable to GSR exhibits.

Another collection method within the field is through the use of a stub (Taudte et al., 2016). A stub is a small circular plate of metal. The plate is a receptacle for a carbon-based adhesive which allows for the desired sample to be collected. The adhesive layer allows for a high level of sample collection from a target, as the sample adheres to the adhesive pad on the stub. This allows for a higher percentage

of sample collection over the swabbing method discussed previously. It can also allow for the collection of samples which may be stuck to other materials such as the target. The stub being adhesive also means that the sample can be transported without any loss as the adhesive holds everything in place.

This does not come without a few draw backs. The stub having an adhesive, causes there to be other elements present during analysis but in the case of GSR, there is not much of a problem as the elements being looked for are inorganic whereas the carbon-based adhesive is organic. The adhesive of the stub can also cause there to be collection of other material, for example the collection of bullet fragments from the target. This can cause irregularities within the data sets, particularly if distance determination is required. The cost of a stub is much higher than the cost of a swab which is a factor to be considered, as many real-world applications would make use of swabs due to their ease of use and much cheaper purchase price. This is seen as many police forces make use of swabs due to the aforementioned factors.

Although, the stub could potentially be the preferred method of sample collection, the limitations including cost and training greatly outweigh the advantages. Therefore, future work should continue to focus upon the use of swabs.

One of the limitations of the study was that there was a lack of replicated shots. This means that a comparison of data was not possible. If there was a higher number of replicated shots it would be possible to try and identify a pattern for each specific distance in order to determine the reproducibility of these findings. Also, due to the lack of replicated shots, the confidence interval could not be determined. Additionally, the velocity of the bullet was unknown as there was no chronograph at the firearms range. Due to this it is impossible to know the velocity of each of the bullets as they impacted with the target. Knowing the velocity of bullet impact at each of the distances could enable a possible pattern between velocity and GSR dispersion to be identified. A study by Botello et al., (2013), researched the velocity on distance determination with GSR. The study found that velocity has a weak correlation to larger distances, with propellant burn rate and charge being more predominant. Though the correlation is weak, the more data obtained the more concessive the study can be, making the most informed conclusion.

Another limitation of the experiment was the propellant charge in each round was unknown. It is possible for some of the rounds to have either a higher or lower propellant charge than what was indicated (section 2.1.2). The use of a chronograph would give an indication as to if there was a higher load or lower propellant load in the bullet casing. This is because if there is a higher propellant charge then the bullet would have a higher velocity due to the extra pressure from the higher level of

propellant. If there was a lower level of propellant in the bullet casing, then the bullet would have a lower velocity and not impact with as much kinetic energy transfer.

It is possible to have other sources of contamination for the main three GSR elements, Lead, Barium and Antimony. The contamination sources come from everyday items such as brake pads in cars (Tucker et al., 2017), which can give a false positive in testing. This can be a problem within real life application due to people such as car mechanics and members of the public who are able to complete maintenance on their own vehicles giving false positives to testing. Although, during the control samples there was no other contaminations found.

4.3 Conclusion

The results presented within this chapter, show that Gun Shot residue follows a linear trend, where concentration decreases with increasing distance. This is a factor which has been considered previous authors. However, this research shows that it is possible to detect the presence of lead and antimony at distances up to and including 25 m. Despite understanding limitations within the experiment and data collection method, consistency throughout the experiment has allowed for data interpretation, as all data and shots were subject to the same environmental conditions, thereby reinforcing the value of these findings.

Careful consideration was given both prior and post experiment to the sample collection method. Although stubs provide great potential, these have a series of limitations as discussed previously. Therefore, it is considered that any future work should continue to use swabs as the predominant sample collection method. This is reinforced by the widespread use of swabs within the Forensic Investigation field.

If the study was to be replicated some further consideration should be given to GSR airborne retention time and how extractor systems can impact data. Furthermore, careful consideration to gunshot residue morphology should be considered.

Chapter 5
Computational Modelling

5.0 Introduction

Computational modelling makes use of computers to study and simulate systems, often complex, using physics, computer science and mathematics (Computational Modelling, 2020). Numerous variables are found within a computational model, which help to characterise the system being studied. Simulations are achieved through adjusting variables, either in combination with other variables, or alone, and observing the results. Due to the nature of computational modelling, it allows for the conduction of multiple simultaneous simulated experiments. Allowing for scientists to narrow down their scope to the more likely results of the experiment (Computational Modelling, 2020). This can often save the scientist a high amount of time as the computational modelling simulations do not require a physical experiment to be conducted. Not having to conduct many experiments to try and understand the possible outcomes, allows for scientist to make the necessary adaptations and adjustments to the experiment, prior to this being conducted (Computational Modelling, 2020).

Several different modelling algorithms can be used alone or in combination with each other. For example, it is possible to use unsupervised learning algorithms to perform complex processing tasks, allowing for the model to identify patterns in the data. If a pattern is identified, then it is possible to use a supervised learning technique to fully understand the applicability.

There are many instances within Forensic Investigation where a direct visual comparison of exhibits is required, such as handwriting and fingerprint comparison. These visual comparisons require the examiner to recognise patterns and use this, in combination with their experience, to determine if a match is obtained. Pattern identification within an image is achievable using computational modelling, specifically using image processing algorithms. One particular type of image processing algorithm widely used within Forensic Investigation is Gabor filter. Research has shown a wide range of applications such as within fingerprint and handwriting analysis. A study by Lee et al. (1999), used a Gabor filter to extract fingerprint features from grey-level images. This research found that the Gabor

filter is highly applicable and efficient at fingerprint recognition, with a recognition rate of 97.2% (Lee, 1999). Additionally, a study by Hamamoto et al. (1998), applied the Gabor filter as a method of analysis on numerical character recognition. The study managed to successfully apply the Gabor filter to handwritten numerical datasets. The study concluded, that out of the 7,000 datasets tested, an error rate of 2.34% was found, highlighting the applicability of Gabor filter to Forensic handwriting analysis (Hamamoto et al., 1998).

A study by Singh et al. (2010) made use of Gabor filter and a Red, Green, Blue (RGB) colour histogram for content retrieval from X-ray images. The study found that the RGB colour histogram was able to extract content from the X-ray images, although it was identified that the applicability to large datasets was not efficient. Due to this, the integration of a texture detection algorithm increases the efficiency of content extraction where the RGB colour histogram began to fail (Singh, 2010).

This research highlights the importance of computational modelling within Forensic Investigation, as it can process large datasets in a relatively short period of time. However, due to the complexity of the datasets it is often necessary to use multiple different processing and classifying algorithms to accurately define the data. Interestingly, the applicability of computational modelling, in particular image processing algorithms, has not been applied to gunshot residue and damage analysis within a Forensic Ballistic setting. The aims of this chapter are to determine the applicability of computational modelling when applied to GSR and damage analysis.

5.1 Pig Image Distance

5.1.1 Pig Images

Images of the porcine heads were obtained, as discussed in Chapter 3. X-ray images were taken of the three porcine heads, from two planes both before and after the shooting. This was done to allow for a direct comparison of the heads with and without the ballistic damage, thereby gaining an understanding of the damage caused. Some examples of the porcine head images that were collected can be observed in *table 5.1.*

Table 5.1: Pre- and Post- shot X-ray images of Porcine Heads used for the study

Shot Distance	Pre-Shot Porcine Heads	Post- Shot Porcine Heads
0 Metres		
15 Metres		
30 Metres		

5.1.2 Image Manipulation

As discussed previously, due to the covid-19 global pandemic, it was not possible to collect a large number of datasets. Therefore, image manipulation was required to build more data. This process is known as data augmentation (Mikołajczyk, 2018).

A problem commonly experienced within the field of machine learning is an inability to obtain enough or uneven datasets. This lack of data for machine learning, causes problems for the training process.

This problem is overcome using data augmentation. In image processing, data augmentation is common and widely accepted within the field (Wong, 2016 and Mikołajczyk, 2018). Data augmentation allows for the creation of additional datasets, for image analysis. There are multiple methods used in order to achieve this task, such as classical image transformations (e.g. rotating, cropping and zooming), as well as data-space transformations (e.g. data warping and synthetic over-sampling) examples (Mikołajczyk, 2018).

Within this study, data augmentation was carried out using classical image transformations, where images were either flipped vertically (fv) or the number of pixels within the image was reduced (r). This allowed for the creation of multiple copies of the original image for training. Augmenting data for image analysis does not deduct from the validity and value of the experiment. This is because although some of the data is synthetic, it is formed from actual data that has been collected with small changes made, such as reduced image size.

5.1.3 Pig Image Distance Algorithm

When trying to make the use of algorithms for distance detection there are several important considerations. One of the most important considerations is the number of folds used for cross-validation. A model is constructed on the basis of one set of data and is then tested against the previously unseen data. Cross-validation ensures that a model has captured the true characteristics of the system being studied without overestimating external characteristics such as experimental noise. Cross validation is nonbiased, as it allows for every dataset to be observed and tested as well as that used for the training (Bolouri, 2008).

Due to there being 18 images presented for the data, the decision was made that 6 folds would be most suitable. This is because each fold would contain 3 images (i.e. 18/6 = 3). This allows for the machine learning algorithm to use 15 images for training and the 3 remaining images for analysis. Giving the machine learning algorithm a good amount of data images to train enables the best accuracy when running the analysis. Once the first set of folds has been tested, the original 3 images are changed to be used for the training, and 3 of the original training images are tested. This is completed every time that the algorithm and classification is run.

Initially the images were tested using the algorithm Gabor filter (section 2.4.1.2), with the classifying algorithms being changed to build an understanding of what works best for the images when trying to understand the distance. The classifying algorithms used for the Gabor filter can be found in *table 5.2.*

Table 5.2: Gabor Image processing algorithm, Classifying algorithm and accuracy

Image Processing Algorithm	Classifying Algorithm	Correctly Classified Instances	Incorrectly Classified Instances	Correctly Classified Instances (%)	Confusion Matrix Classifications			
Gabor Filter	Random Forest	11	7	61%	Short	Mid	Far	
					4	2	0	Short
					2	4	0	Mid
					0	3	3	Far
Gabor Filter	K Nearest Neighbour	13	5	72%	Short	Mid	Far	
					4	1	1	Short
					1	4	1	Mid
					0	1	5	Far
Gabor Filter	Naïve Bayes	11	7	61%	Short	Mid	Far	
					5	1	0	Short
					1	5	0	Mid
					2	3	1	Far

Further information regarding the classifying algorithms Random Forest, K Nearest Neighbour (KNN) and Naïve Bayes can be found in section 2.4.

From the classifying algorithms tested, the best accuracy was found to be K Nearest Neighbour (KNN) as this showed a clear ability to classify the data (*table 5.2*). To determine if there were any further improvements, two different image processing algorithms, that specialise in edge and texture detection, were chosen to be tested. These are shown in *table 5.3*.

Table 5.3: Edge and Texture algorithms results

Image Processing Algorithm	Classifying Algorithm	Correctly Classified Instances	Incorrectly Classified Instances	Correctly Classified Instances (%)	Confusion Matrix Classifications			
Binary Pattern Pyramid Filter	K Nearest Neighbour	8	10	44%	Short	Mid	Far	
					4	1	1	Short
					3	2	1	Mid
					3	1	2	Far
Edge Histogram Filter	K Nearest Neighbour	6	12	33%	Short	Mid	Far	
					2	2	2	Short
					2	2	2	Mid
					2	2	2	Far

Tables 5.2 and *5.3* show that the most accurate image processing algorithm was Gabor filter with KNN as the classifying algorithm. However, texture analysis did not provide sufficient accuracy to determine distance, therefore a different approach was carried out. Testing different algorithms on data sets to determine the most applicable is commonly done within computational modelling (Chauhan et al., 2016) (Zhang and Sejdić, 2019). This process is repeated until a satisfactory level of correctly classified instances is achieved.
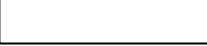
Due to this, the algorithm type changed from texture and edge detection to a colour histogram algorithm. Colour histogram algorithms detect the differences in colours within a presented image. The algorithm uses a set of 64 RGB (Red Green Blue) colours, and searches the image, noting the matches of detected colours. The image processing algorithm and classification algorithm chosen are shown in *table 5.4*.

Table 5.4: Simple Colour Histogram Accuracy

Image Processing Algorithm	Classifying Algorithm	Correctly Classified Instances	Incorrectly Classified Instances	Correctly Classified Instances (%)	Confusion Matrix Classifications			
Simple Colour Histogram	Random Forest	18	0	100%	Short	Mid	Far	
					6	0	0	Short
					0	6	0	Mid
					0	0	6	Far
Simple Colour Histogram	Naïve Bayes	18	0	100%	Short	Mid	Far	
					6	0	0	Short
					0	6	0	Mid
					0	0	6	Far
Simple Colour Histogram	K Nearest Neighbour	18	0	100%	Short	Mid	Far	
					6	0	0	Short
					0	6	0	Mid
					0	0	6	Far

Table 5.4 shows that the accuracy of classified instances when the Simple Colour Histogram was used in conjunction with the classifying algorithms was 100%. Therefore, the decision was made to not run further testing as a maximum accuracy had been achieved. To further understand how the Simple Colour Histogram and classifying algorithm was able to conclude with 100% accuracy the selected attributes were looked at in further detail. A ranker was used on WEKA's selected attributes tab, which allowed for the most important attributing points to be highlighted. These were RGB colour histograms 63, 21, 42 and 0. JAVA script (SimpleColorHistogram.java example, 2020), was used to determine the colour palette of each of these histograms, the results of which are summarized in *table 5.5.*

Table 5.5: RGB Colour Histogram Values

RGB Histogram Number	RGB Coordinate Value	Colour
0	0, 0, 0	
21	85, 85, 85	
42	170, 170, 170	
63	255, 255, 255	

The colours RGB 63 (255, 255, 255), RGB 21 (85, 85, 85), RGB 42 (170, 170, 170) and RGB 0 (0, 0, 0) were identified as the only contributing attributes. This is because X-ray images have no colour, and when all the RGB values are checked, these all show shades of grey, black and white. The other RGB values were removed from the algorithm with the aforementioned being the only RGB values left. The algorithms were run again, with a Simple Colour Histogram classified by Random Forest with a correctly classified instance of 100%. This further highlights that the aforementioned RGB values are the only important ones when classifying the X-ray images for distance.

The findings from the computational modelling are significant. This method of computational modelling application, being novel and never tried in this way before, shows promise. There are some limitations, such as while a strong detection accuracy for the distances was able to be concluded by the algorithms working in conjunction when detecting the colour, it is not possible to conclude that it would work all the time with a 100% accuracy. This is because the data pool was too small to be able to draw a full conclusion. To be able to give a more definitive answer, a higher number of data images would need to be collected and applied to the algorithms. From what was observed and conducted, it is possible to indicate that the colour histogram is much more important when classifying the distance compared to a texture or edge histogram. This is observed by the accuracy of texture algorithms ranging from 33% to 72%, whereas the Simple Colour Histogram was able to detect with 100% accuracy.

This also highlights the applicability of potential use in the case of human injuries, and therefore the importance of further work in this area. Being able to retrieve information from X-ray images through the use of texture and colour filters has great potential in Forensic Investigation.

5.1.4 Pig Pre- and Post- Shot

The image data that was used for pre-shot and post-shot determination was less than the 18 images used for the distance. Each of the heads had a total of 4 X-rays taken, 2 pre-shot and 2 post-shot. This meant that for all of the heads a total dataset of 12 images was obtained and used for the testing and training. As discussed previously, data augmentation was required in order to determine the most appropriate algorithms to use for the analysis. However, further data augmentation was not required within this phase of analysis, as this previously unknown has already been determined (section 5.1.2).

Expanding upon the knowledge gained through distance detection with the porcine head X-rays, the decision to continue using 6-fold cross-validation was made. This meant that each fold had a total of 2 images present (12/6 = 2).

The image processing algorithm Simple Colour Histogram was tested first due to the success with classifying distance, as discussed in section 5.1.3. The classifying algorithm chosen to work in conjunction with the image processing algorithm was Random Forest. This combination of algorithms only managed to correctly classify 50% of the images. Therefore, subsequent testing was carried out as shown in *table 5.6*.

Table 5.6: Colour histogram filters used in determining Pre- or Post-shot porcine heads.

Image Processing Algorithm	Classifying Algorithm	Correctly Classified Instances	Incorrectly Classified Instances	Correctly Classified Instances (%)	Confusion Matrix Classifiers		
Simple Colour Histogram	Random Forest	6	6	50%	Pre	Post	
					4	2	Pre
					4	2	Post
Simple Colour Histogram	Naïve Bayes	7	5	58%	Pre	Post	
					4	2	Pre
					3	3	Post
Simple Colour Histogram	K Nearest Neighbour	6	6	50%	Pre	Post	
					4	2	Pre
					4	2	Post
Edge Histogram filter	Random Forest	8	4	66%	Pre	Post	
					2	4	Pre
					4	2	Post
Edge Histogram filter	Naïve Bayes	8	4	66%	Pre	Post	
					2	4	Pre
					4	2	Post
Edge Histogram filter	K Nearest Neighbour	6	6	50%	Pre	Post	
					4	2	Pre
					4	2	Post

Due to the lack of accuracy obtained through the use of the simple colour histogram, a different type of image processing algorithm was chosen. The Gabor filter algorithm was chosen as the image processing algorithm, with a series of classifying algorithms tested as seen in *table 5.7*.

Table 5.7: Gabor filter in determining Pre- or Post-shot porcine heads.

Image Processing Algorithm	Classifying Algorithm	Correctly Classified Instances	Incorrectly Classified Instances	Correctly Classified Instances (%)	Confusion Matrix Classifiers		
Gabor Filter	Random Forest	10	2	83%	Pre	Post	
					5	1	Pre
					1	5	Post
Gabor Filter	Naïve Bayes	6	6	50%	Pre	Post	
					3	3	Pre
					3	3	Post
Gabor Filter	K Nearest Neighbour	11	1	91%	Pre	Post	
					6	0	Pre
					1	5	Post

The classifying algorithm K Nearest Neighbour achieved the highest accuracy of 91% with only one image being incorrectly classified. This shows that K Nearest Neighbour was the best option for classifying the data detected by the Gabor filter.

From what is observed in *table 5.7*, it is possible to see that the results obtained had a much higher accuracy than when the same image dataset was tested through the use of a colour histogram algorithm, as seen in *table 5.6*. A critical evaluation of the X-ray data set was discussed within chapter 3. This showed that only small differences were observed visually between pre- and post-shot X-rays. Therefore, it is possible that these minute changes in shades were not detectable using colour filter. A 64 RGB palette was used in the JAVA script (SimpleColorHistogram.java example, 2020), this therefore limits the amount of detectable colour shades. It is possible that increasing the number of RGB colours would lead to an increased accuracy in colour detection. These results, therefore, indicate that texture is very important when trying to determine if the image is from before or after the porcine head has been shot. As discussed previously in chapter 3, some visual soft tissue damage was observed in the path taken by the bullet. This was visualized by a change in texture within the skull cavity when compared to the pre-shot image, however it is possible that some textural differences found within the porcine skulls could be a result of decomposition, as discussed previously. These textural differences can accurately be exploited for pre- or post- injury determination.

5.2 GSR Data Distribution

5.2.1 Data

Data that was collected for the GSR concentration at different distances for each element as previously discussed can be seen in *table 5.8*. The data was recorded in an Excel format, which needed to be converted to an '.arff' file for use on WEKA. Initially the Excel file was saved as a '.CSV' file before conversion to an '.arff' file via a website (Convert CSV to ARFF online, 2020). This then allowed for input into WEKA.

Table 5.8: GSR Distribution Data at different Distances

Distance (m)	Sb Concentration (ppm)	Pb Concentration (ppm)	Ba Concentration (ppm)	Class
0	0.7	1.5	1.42	Short
1	0.6	1.42	1.06	Short
5	0.51	1.34	1.7	Short
10	0.41	1.33	1.25	Mid
15	0.3	1.13	0.96	Mid
20	0.12	0.82	0.04	Far
25	0.025	0.65	0	Far

Barium (Ba) concentration at 25 m is shown as 0 in the *table 5.8*. It was observed in *table 4.2* that the value obtained from AAS analysis was -1.06 ppm. This is due to the concentration of Ba being lower than the limit of detection of the equipment. This, therefore, means that Ba was not present at 25 m. Consequently, a value of 0 was input into the table to allow for computational analysis.

Once the data was opened on WEKA is was apparent that the dataset had unequal distances with 2 values for both far and mid, and 3 for short. To compensate for this the decision was made to create synthetic data through the use of the algorithm Synthetic Minority Over-sampling Technique (SMOTE). SMOTE is a method of oversampling a dataset being classified when there is a lack of data in the dataset. This is commonly done in computational analysis when the dataset is not large enough to give the machine learning algorithm enough data to classify properly (Wong, 2016). When the machine learning algorithm does not have enough training data, a very low accuracy is achieved.

When a lack of data is experienced during a study where the acquisition of more data is not possible, it is common and widely accepted to use algorithms such as SMOTE to create synthetic data from current data (Park, 2019 and Saad Hussein, 2019). SMOTE does this by taking a sample from the dataset and looking at its KNN (section 2.4.1.4). The synthetic datapoint is then created from the vector between one of the K neighbours and a current datapoint.

Due to the low amount of values within the dataset, the decision was made to use percentage split. This is the split in the datasets used for training the machine learning algorithm. For example, if there are 10 values in a dataset, 10% percentage split would use 1 value for training and the remaining 9 values for testing. Percentage slit for each classifying algorithm is detailed in *table 5.9*.

Once SMOTE had been used on the GSR datasets, the synthetic data applied enabled there to be 3 counts for short, mid and far as opposed to the original 3 short, 2 mid and 2 far. With the dataset made equal, the dataset was then tested. A summary of these results can be seen in *table 5.9*.

Table 5.9: Different percentage splits within dataset and corresponding accuracy

Classifying Algorithm	Percentage Split (%)	Correctly Classified Instances	Incorrectly Classified Instances	Total Tested Instances	Correctly Classified Instances (%)
Naïve Bayes	10 %	1	7	8	12.5 %
Naïve Bayes	20 %	4	3	7	57 %
Naïve Bayes	30 %	5	1	6	83 %
Naïve Bayes	40 %	4	1	5	80%
Naïve Bayes	50 %	3	1	4	75%
Naïve Bayes	70 %	1	2	3	33%
Naïve Bayes	80 %	2	0	2	100%

From what is observed in *table 5.9*, it was apparent that Naïve Bayes was not able to classify the dataset well. The best result came when 80% of the dataset was used for training, leaving on 2 values from the dataset for testing. Due to the small quantity of values for testing this cannot be accepted. With the lack of applicable accuracy from Naïve Bayes, the decision was made to try a different classify algorithm, KNN. The result from KNN can be seen in *table 5.10*.

Table 5.10: Different percentage splits classified by KNN (K Nearest Neighbour)

Classifying Algorithm	Percentage Split (%)	Correctly Classified Instances	Incorrectly Classified Instances	Total Tested Instances	Correctly Classified Instances (%)
KNN	20 %	4	3	7	57 %
KNN	30 %	6	0	6	100 %
KNN	50 %	4	0	4	100 %
KNN	80 %	2	0	2	100 %

From what is observed in *table 5.10,* it is possible to see that KNN was much more applicable to the presented GSR dataset. The classifying algorithm was able to correctly classify all of the presented instances for 80%, 50% and 30% percentage splits in the training to testing data. The increased accuracy at lower percentage splits shows promise and highlights the applicability of KNN when compared to results from Naïve Bayes, as seen in *table 5.9.*

5.3 Conclusion

The findings from this chapter highlight the applicability and potential for computational modelling to be applied to ballistic studies, specifically GSR dispersion and X-ray imaging. In relation to damage analysis, the results of this chapter found that, within computational modelling, colour differences are not significant enough in order to allow for correct classification. However, colour histograms proved to be an important consideration as an indicator for distance. Conversely, texture proved to be an important factor for damage analysis, as this was able to conclusively classify pre-shot from post-shot X-ray images. Additionally, elemental analysis of GSR spread shows potential for predicting Ba, Pb and Sb concentrations within an incident scene.

While the findings provide insight into the substantial potential of this research, a higher number of datasets would be required before making any final conclusions. Further research is required to understand the full potential and applicability of computational modelling withing Forensic Ballistics.

Chapter 6
Conclusion

A review of the Forensic Ballistics literature revealed that limited research has been carried out in the determination of Gun Shot Residue spread at large distances. Research has primarily focussed upon the understanding of spread at short distances, which is of limited use within Forensic Investigation. Equally, some research had focussed upon Gun Shot Wound damage, but this had been largely limited to military applications. This research aimed to contribute to knowledge in this area by further understanding GSR spread at larger distances and understanding the link between ballistic damage and how this varies over distance.

In order to investigate this potential, a series of practical based experiments were conducted in various scientific fields. However, the volume of data gained limited its applicability to real world scenarios which highlighted the potential value of computational modelling. Computational modelling has been rapidly increasing within various scientific fields, but forensic investigation has been largely left behind. Being able to apply computational modelling to forensic investigation is important and could carry great benefits.

A focal point throughout this research was its applicability for real world applications, therefore, careful consideration was given to the medium. Porcine heads were ideal as these are known to have similar anatomical structures to humans. Equally consideration was given to the ammunition used, where a 9 mm round was chosen as this is a common round in easily concealed firearms.

Upon conduction of the radiological imaging of the porcine heads, it became apparent that there was no procedure in place for imaging this type of medium. Therefore, a procedure was developed which has the potential for conversion into a standard operating procedure (SOP). Once radiographs had been obtained, the interpretation proved to be very difficult.

Any exit wounds from the bullets were not observed due to the large open wound caused by the decapitation process. However, it was apparent that bullet deviation was occurring as bullet exit wounds were not in track with the bullet entry wound, for which radiography proved vital.

Radiological imaging allowed for the visualisation of bony structure and soft tissue damage. However, an issue encountered during the radiological imaging of the porcine heads related to areas of lucency where this may be due to either soft tissue damage, gas build up due to decomposition gases, or both. This made it difficult to differentiate between the damage caused by the bullet and from the decomposition of the porcine head.

In the future it may be beneficial to gain an understanding of decomposition changes to the permanent cavitation by taking radiographical images at regular intervals. Additionally, future work should focus upon resolving the issues encountered with the decapitation wound, where replicating the skin through either attaching a layer of latex or porcine skin would be beneficial for the observation of bullet exit wounds.

In elemental analysis it was found that GSR concentrations of elements generally decreased with increasing distance which was consistent with that observed by other authors. There was inconsistencies within the barium concentrations, which could be due to several different factors such swabbing technique or negative pressure. It is also possible that the location of the extractors could have had an effect on the barium concentrations. Future work should consider further understanding the effects that the firearms range extractors have on GSR air retention time and deposition time.

The practical work that was done for the radiography and elemental chapter was combined to understand if the data could be applied to computational modelling. Various different algorithms were tested, but k-nearest neighbour (KNN) was found to provide the highest accuracy and be able to effectively classify short, mid and far shots. KNN found that colour was most important when classifying distance, but that the texture was most important when classify damage.

When looking at the radiological images of the porcine heads, it was difficult to identify the damage, however this was quickly achieved through the use of computational modelling. Despite this, the data must always be reviewed by a radiographer. Data manipulation was required due to the lower number of datasets. Future work will aim to gather additional data to understand the variability and fully determine the applicability of this method within forensic investigation.

In summary, it is envisioned that this work will serve as a starting point for future development and applicability of new methods for reconstructing firearm related incidents.

Appendix A

Decontamination SOP

Principle of the Method

In order to prevent contamination of exhibits and to demonstrate that the integrity of the exhibit has been maintained throughout your examination it is important that you follow strict decontamination procedures. The following procedures must be completed before & after the examination of each exhibit.

Equipment and materials required

• Personal Protective Equipment (PPE)

• Cleaning Detergent

• Distilled water

• Tissue paper

• Bench roll

• Tape lift or sellotape

• Acetate sheet

BEFORE ANALYSIS

4.1. Put on a laboratory coat & a new pair of disposable gloves.

4.2. Spray the bench using detergent solution & wipe the bench using a clean piece of tissue paper.

4.3. Spray the bench using distilled water & wipe the bench using a clean piece of tissue paper.

4.4. If appropriate for your examination (e.g. if you are required to recovery hair and fibres or particulates) using a tape lift or sellotape, tape lift your decontaminated examination bench and stick tape lift/sellotape on to an acetate sheet. If you are not required to collect Bench Blanks proceed on to step 4.7.

4.5. Label the tape lift as 'Bench Blank' ensure that you include information such as the exhibit number, police reference number, FSP reference number, your name, date, lab and bench.

4.6. Briefly visually examine the tape lift for any obvious contaminants. If there are any contaminants present repeat steps 4.1-4.6. Once you have obtained a clean Bench Blank proceed on to step 4.7.

4.7. Obtain a piece of bench roll that is approximately twice the size of the exhibit & place it onto the bench close to the edge of the bench. Secure the four corners of the bench roll to the bench using small pieces of sellotape.

AFTER ANALYSIS

4.8. After repackaging the exhibit, remove the bench roll from the bench & place into the bin.

4.9. Spray the bench using detergent solution & wipe the bench using a clean piece of tissue paper.

Reference: *CCCU Forensic Toolkit*

Appendix B

Radiography interpretation:

James Elliott –
Diagnostic radiographer, senior radiographer (Maidstone Hospital) and lecturer (Canterbury Christ Church University). Masters in Forensic Radiography. I do not have experience with viewing or reporting porcine radiographs.

Method of image viewing –
RadiAnt DICOM Viewer 2020.2 (64-bit)
Radiographs were viewed on a standard (non-medical) computer screen.
Radiographs were not inverted, meaning that bones were depicted as white and air showed as black.
Two views were made of each head
      Superior/inferior view – Meaning the x-rays passed through the top of the head and exited the bottom to hit the x-ray detector.
      Right lateral view - Meaning the x-rays passed through the left side of the head and exited the right side to hit the x-ray detector.
Radiographic measurements of the skull were based upon those depicted in Choudhary et al (2017). Measurements have an accuracy of +/- 0.1cm.

Interpretation language –
Radiolucent / radiolucency = 'blackness' seen on the radiograph (x-ray). Can be shortened to lucent/lucency.

Radiopaque / opaque / opacity = 'whiteness' seen on the radiography.

Midline / medial = towards the centre of the anatomy, i.e. in the middle.

Distally = furthest from the middle or start of a part of anatomy. For example distal portion of a finger.

Midpoint / mid = in the middle, normally referring to a single bone or anatomy, for example the mid shaft of the femur.

Bilateral = both sides, for example bilateral knee osteoarthritis means involving both knees.

Contralateral = the opposite side, for example the contralateral knee would be *the other* knee.

Anterior = the 'front' of the anatomy.

Posterior = the 'back of the anatomy.

Patchy = not uniform, showing irregularity.

Linear = a straight line.

Interpretation syntax –

A system of description is used to formalise the observations and interpretation of the radiographs. Where necessary, commentary has been provided using these key points.

A – Anatomy, **A** – Alignment, **B** – Bone damage, **C** – Cartilage (i.e. joint involvement), **S** – Soft tissue damage and foreign bodies.
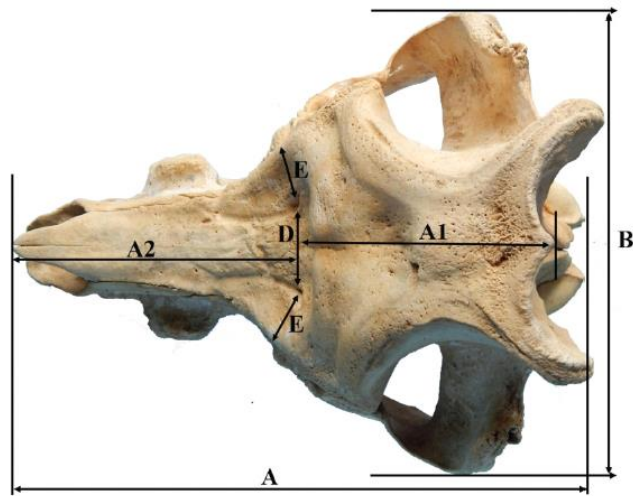
Fig. 1: Measurements of the skull of Indian wild pig showing skull length (A), cranial length (A1), nasal length (A2), skull width (B), distance between supraorbital foramina (D) and distance between orbital rim to supraorbital foramina (E)
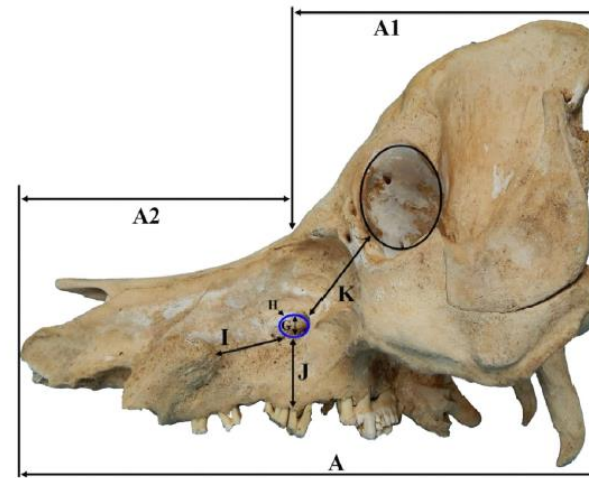
Fig. 2: Measurements of the skull of Indian wild pig showing skull length (A), cranial length (A1), nasal length (A2), skull width (B), diameter of the infraorbital foramina (G), circumference of the infraorbital foramina (H), distance from process of alveolar socket of canine tooth to the infraorbital canal (I), Infra-orbital foramina to the root of fourth premolar alveolar tooth (J), infraorbital foramina to the orbital rim (K)

A. Skull Length; from the dorsal lateral nasal cartilages to the external occipital protuberance; sub-divided into cranial length (A1) and nasal length (A2).

B. Skull width; maximum distance between two zygomatic arches.

|	Radiographic image	Pre-gunshot observations	Post gunshot interpretation
Pig head 1	Superior/inferior view	An area of lucency can be seen within the nasal region, located in the midline distal to the cranium. This would be akin to the sinus anatomy. Linear opaque anatomy can also be seen within the sinuses, running proximally to distally to the tip of the snout. The outline of teeth can be seen within the jaw, but it is difficult to determine whether these are on the maxilla or mandible, with a degree of superimposition occurring. Soft tissue appears unremarkable, although the site of head removal shows irregularities in texture due to the ragged severance of tissues. No discernible damage can be seen to bony anatomy, with soft tissues of the brain demonstrating only very minor patches of lucency (which may be accounted for in underlying anatomy, such as the trachea or oesophagus). There are no sharp breaks in bone continuity seen within this view. The alignment of the teeth (maxilla and mandible) and zygomatic arches afford a high degree of accurate representation of the anatomy. Soft tissues of the cheeks and ears are seen bilaterally. There is no discernible artefact by the plastic bag. Laterality markers are noted. Radiographic measurements: Skull length – 26.0 cm Skull width – 14.9 cm Cranial length – 10.5 cm Nasal length – 15.4 cm	The teeth of the maxilla and mandible are not aligned, as shown by the malposition of the front incisors. This has not affected the interpretation of the imaging as the molars and zygomatic arches still appear equal both sides. The soft tissues of the left cheek appears much greater than the right. It also demonstrates an increase in lucency, albeit patchy. The changes in radiodensity may be due to positioning (i.e. more flesh has been placed upon the left) or decomposition changes. The right side shows these lucencies less. A linear patchy line of lucency can be seen extending across the mid cranium, more prominently on the left side. Radiographic measurements put this at 1.7 cm in length and 16.0 cm in width. With the bullet entry point being the right side of the head, a small irregular patchy lucency can be seen at the midpoint of the right zygomatic arche. This not the point of entry (as this is shown to be higher, more superiorly, within the photographs), but it may demonstrate the entry point of the bullet in above structures. The left zygomatic arch appears to have an interruption to its lateral border. There are overlying densities from soft tissue and the lucencies mentioned earlier. With a lack of exit wound seen on this head it is plausible that the bullet exited posteriorly at this point, through the open wound. No bullet or other high-density object can be seen. Laterality marker is seen. Surrounding bags cannot be visualised.

| | Lateral view | The nasal region is easier to see on the lateral view, with an area of increased lucency proximally along the superior aspect which presumably would be the frontal sinus (or equivalent).

A circle of greater opacity can be seen within the cranium, which appears to be the brain cavity is located. The top of the cranium shows a smooth lucent line which extends through the full thickness of the skull. This shares similar appearance to 'growth plates' within human radiography.

The maxilla and mandible are clearly visualised on the lateral, with superimposition of teeth.

As with the superior/inferior view, the brain cavity lacks any prominent lucency at this stage of decomposition, suggesting that appearances shown in the previous view are indeed from overlying structures.

Soft tissues surrounding the mandible, neck and the ears can be seen. The plastic bag cannot be visualised. A laterality marker is noted.

Radiographic measurements differ from the previous view, indicating the effect of image distortion due to distance of anatomy from the x-ray detector.

Radiographic measurements:
Skull length – 25.0 cm
Cranial length – 8.1 cm
Nasal length – 13.8 cm | A comparable area of patchy lucency can be seen along inferior to the brain cavity. At its greatest points it measures 5.5 cm in length and 1.8 cm width. This seems to be the entry point of the bullet and associated route of travel, although the superimposition of structures cannot locate the exit point. In all likelihood this was posteriorly given the lack of an exit wound caused by the bullet.

No definitive evidence of other bone trauma can be seen on this view.

No bullet or other high-density object can be seen.

Laterality marker noted. Surrounding bags are not visualised. |

	Superior/inferior view	Observations of the sinuses are the same with this individual. No bone damage seen. As before, patchy lucencies can be seen within the cranium, depicting either overlying anatomy, voids or the early stages of brain decomposition. The point of head severance is similarly ragged in radiographic nature, showing an uneven distribution of densities. Soft tissues of the cheeks and ears are seen bilaterally. There is no discernible artefact by the plastic bag. Laterality markers are noted. Radiographic measurements: Skull length – 26.7 cm Skull width – 15.6 cm Cranial length – 9.7 cm Nasal length – 17.0 cm	As with the previous head, there is an increased apparent size of the soft tissues of the cheeks of the pig. Either the head has been placed differently from the initial radiographic examination or post-mortem changes have created different circumstances due to decomposition. The soft tissues of both sides appear larger, with increased radiolucencies seen predominantly within the left cheek. Was this due to storage conditions? Were the heads placed on one side? A similar linear line of irregular, patchy lucency can be seen through the brain cavity of this pig, although it can only be seen within the midline extending to the left side. The measurements of which are 8.8 cm in length and 1.5 cm in width. The left zygomatic arch demonstrates similar appearance to pig 1, with an interruption to the lateral border. Once again, there are overlying soft tissues and the confluence of various radiolucencies making this difficult to interpret. No definitive evidence of other bone trauma can be seen on this view. No bullet or other high-density object can be seen. Laterality markers are seen. Surrounding bags are seen but do not affect the quality of the image.
Pig head 2			

|			
	Lateral view	No new observations compared to previous head. No bone damage seen. Similar radiodensities seen within brain cavity. Soft tissues surrounding the mandible, neck and the ears can be seen. The plastic bag cannot be visualised. A laterality marker is noted. Radiographic measurements: Skull length – 25.6 cm Cranial length – 8.2 cm Nasal length – 14.2 cm	The contents of the brain cavity demonstrate considerably increased lucency when compared to the initial radiograph. There is a difference in radiodensity seen within the skull, presumably the brain showing as mid density and gas or air above showing as low density. Bone trauma cannot be seen, although it is plausible that these cannot be visualised but exist nonetheless. No bullet or other high-density object can be seen. Laterality marker noted. Surrounding bags seen but do not affect the quality of the image.
Pig head 3	Superior/inferior view	Observations of the sinuses are the same with this individual. No bone damage seen. Similar patchy lucencies seen within the brain cavity and uneven densities associated with the point of severance of the head. Soft tissues of the cheeks and ears are seen bilaterally. There is no discernible artefact by the plastic bag. Laterality markers are noted. Radiographic measurements: Skull length – 24.1 cm Skull width – 15.0 cm	A high-density object can be seen within the left zygomatic arche region. Measurements of the object are 1.8 cm in length, 9.7 cm in width. It has a rounded end and pointed end (which is pointing posteriorly). The shape adheres to the characteristics of a bullet. An irregular lucent line can be seen within the posterior portion of the cranium, extending from the midline to the left. A conservative measurement puts this at 4 cm in length, with variable width, throughout its course (1 – 2 mm). This is not seen on the contralateral side, suggesting it is a fracture. The alignment of bony anatomy at the point of bullet entry (right side) appears normal. There are no interruptions to the continuity of bone anatomy for the right zygomatic arche or adjacent anatomy. This is difficult to interpret though, as the underlying includes the junction between the mandible and the remainder of the skull.

		Cranial length – 10.9 cm Nasal length – 13.0 cm	The brain cavity has an increased amount of patchy lucencies which may be accounted for by the passage of the bullet or further decomposition. A pocket of lucency is seen alongside the bullet (medially), which could be cavitation or a similar result of the passage of the bullet. The plastic bags are visualised on this image. Laterality markers are noted.
	Lateral view	No new observations compared to previous head. No bone damage seen. Similar radiodensities seen within brain cavity. Soft tissues surrounding the mandible, neck and the ears can be seen. The plastic bag cannot be visualised. A laterality marker is noted. Radiographic measurements: Skull length – 23.0 cm Cranial length – 8.6 cm Nasal length – 14.6 cm	The high-density bullet is visualised in what appears to be the brain cavity, although the previous image confirms it to be more laterally. The increased radiolucency of the brain cavity is noticeable on the lateral image, further suggesting a cavitation of tissues, decomposition or a combination of the two. A lucent line can be seen within the posterior portion of the cranium, extending superiorly to inferiorly in what appears to be the full thickness of the skill vault. Radiographic measurements put it at 2.7 cm in length and variable thickness 1 – 2 mm. This has the characteristics of a fracture. It is difficult to discern other fractures within the maxilla, at the point of bullet entry. There are numerous irregularities in bone outlines and greater variability in radiodensity when compared to the initial radiographs. These could identify further areas of trauma. The plastic bags are visualised on this image. Laterality marker is noted.
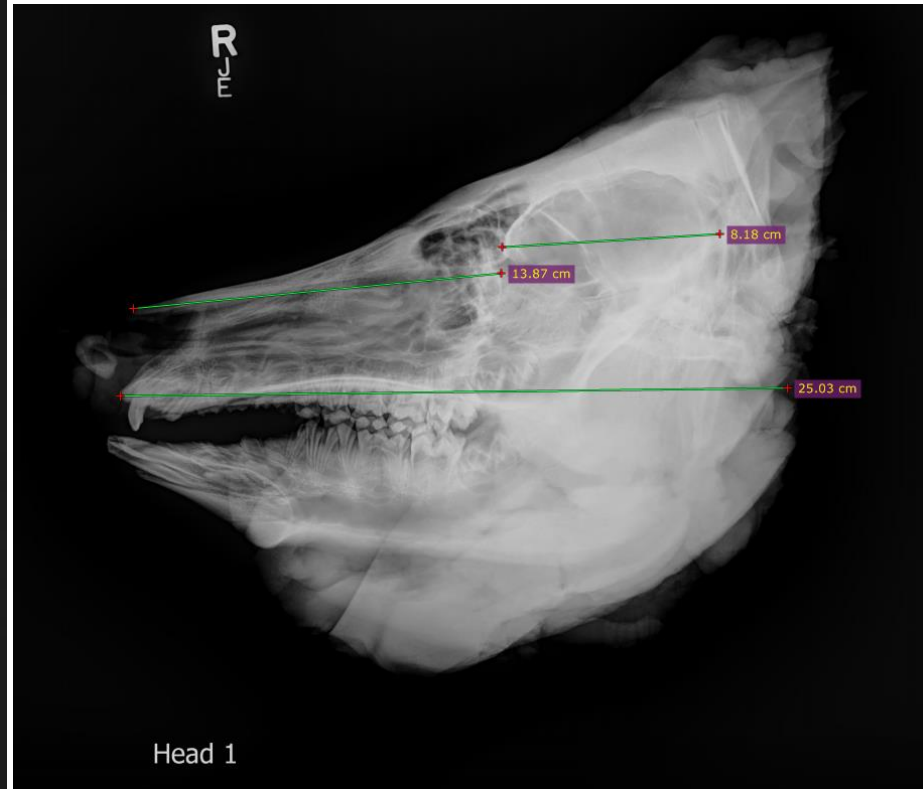
Pig Head 1 showing radiographic measurements examples .
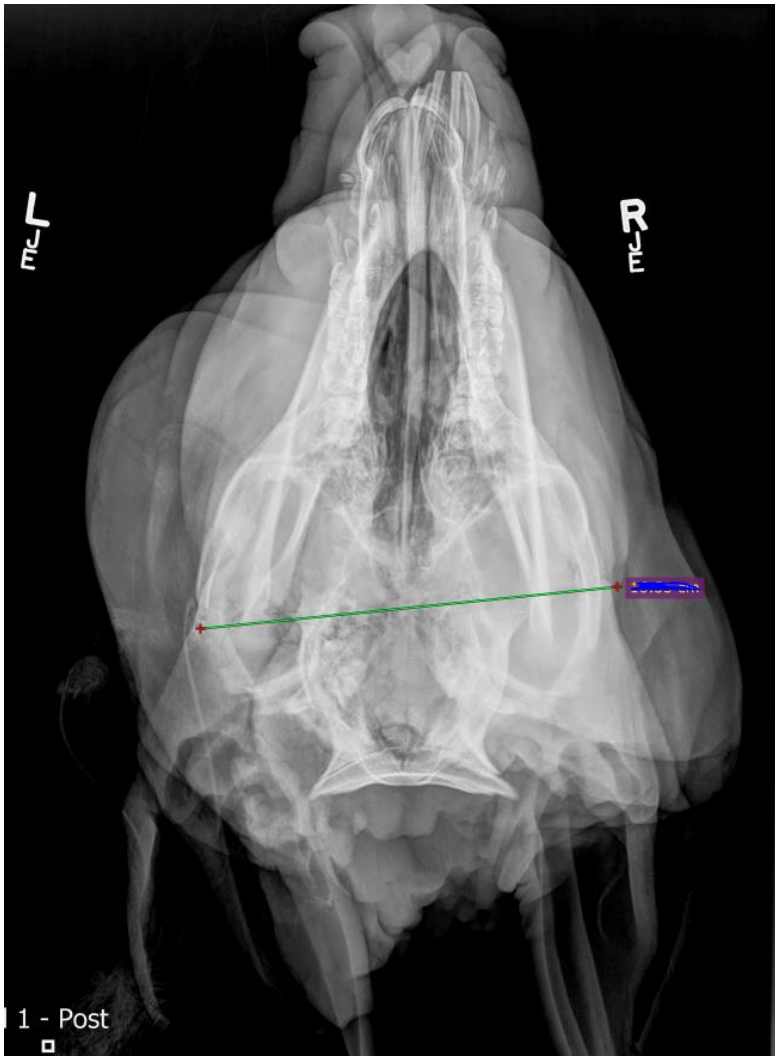
Head one with line to show possible path of bullet.

References:

Choudhary, O. P., Kalita, P. C., Doley, P. J. and Kalita, A. (2017) 'Applied Anatomy of the Head Region of the Indian Wild Pig (*Sus scrofa*) and its Clinical Value during Regional Anesthesia', *Journal of Animal Research*, 7(2), pp. 339-344

Bibliography

- Allen, G., 2020. *Knife Crime Statistics*. [online] House of Commons Library. Available at: <https://commonslibrary.parliament.uk/research-briefings/sn04304/> [Accessed 15 September 2020].
- Allen, G. and Audickas, L., 2020. *Firearm Crime Statistics: England & Wales*. [online] House of Commons Library. Available at: <https://commonslibrary.parliament.uk/research-briefings/cbp-7654/> [Accessed 15 September 2020].
- Allen, G. and Audickas, L., 2018. *Firearm Crime Statistics: England & Wales*. [online] Researchbriefings.parliament.uk. Available at: <https://researchbriefings.parliament.uk/ResearchBriefing/Summary/CBP-7654> [Accessed 23 December 2019].
- Allen, G., Audickas, L., Loft, P. and Bellis, A., 2020. *Knife Crime Statistics*. [online] House of Commons Library. Available at: <https://commonslibrary.parliament.uk/research-briefings/sn04304/> [Accessed 9 September 2020].
- Almirall, J., Trejos, T. and Lambert, K., 2020. Interpol review of glass and paint evidence 2016-2019. *Forensic Science International: Synergy*,.
- 1996. *Analytical Methods For Atomic Absorption Spectroscopy*. Waltham: The Perkin-Elmer Corporation.
- Andrade, T., 2017. *The Gunpowder Age*. Princeton: Princeton University Press.
- Antonov, A., Popova, N. and Voevodin, V., 2018. Computational science and HPC education for graduate students: Paving the way to exascale. *Journal of Parallel and Distributed Computing*, 118, pp.157-165.
- Arndt, J., 2010. *Matters Computational: Ideas, Algorithms, Source Code*. Nurenberg: Springer Science & Business Media.
- Arsenal, 2020. *Small Arms Ammunition 7.62X54mm Cartridges*. [image] Available at: <https://www.arsenal-bg.com/c/small-arms-ammunition-31/762x54-mm-cartridges-166> [Accessed 10 May 2020].
- Atterholt, J., 2018. *Section Of Pig Head*. [image] Available at: <https://svpow.files.wordpress.com/2018/12/pig-sectioning-4-head-left-half.jpg> [Accessed 07 May 2020].
- Baptista, M., d'Ávila, S. and d'Ávila, A., 2014. Histopathological detection of entry and exit holes in human skin wounds caused by firearms. *Journal of Forensic and Legal Medicine*, 25, pp.49-52.
- BERGHOF, 2020. *Speedwave XPERT*. [image] Available at: <https://www.berghof-instruments.com/en/product/speedwave-xpert/> [Accessed 26 May 2020].

- BERGHOF, 2020. *Berghof Gefäßvarianten Für Mikrowellenaufschlusssystem Speedwave XPERT*. [image] Available at: <https://www.analytica-world.com/en/products/43064/microwave-digestion-pressure-innovative-system.html> [Accessed 26 May 2020].
- Biau, G. and Scornet, E., 2016. A random forest guided tour. *TEST*, 25(2), pp.197-227.
- Blakey, L., Sharples, G., Chana, K. and Birkett, J., 2017. Fate and Behavior of Gunshot Residue-A Review. *Journal of Forensic Sciences*, 63(1), pp.9-19.
- Blakey, L., Sharples, G., Chana, K. and Birkett, J., 2019. Fate and Behavior of Gunshot Residue: Recreational Shooter Vehicle Distribution. *Journal of Forensic Sciences*, 64(6), pp.1668-1672.
- Bolouri, H., 2008. *Computational Modeling Of Gene Regulatory Networks: A Primer*. London: Imperial Collage Press.
- Botello, D., Botello, D., Staton, P., Rushton, C. and Copeland, J., 2013. *The Effects Of Powder, Barrel Length & Velocity On Distance Determination*. Research paper. WV: Marshall University.
- Bresson, F. and Franck, O., 2009. Estimating the shooting distance of a 9-mm Parabellum bullet via ballistic experiment. *Forensic Science International*, 192(1-3), pp.e17-e20.
- Brown, H., Cauchi, D., Holden, J., Allen, F., Cordner, S. and Thatcher, P., 1999. Image analysis of gunshot residue on entry wounds. *Forensic Science International*, 100(3), pp.179-186.
- Brożek-Mucha, Z., 2007. Comparison of cartridge case and airborne GSR—a study of the elemental composition and morphology by means of SEM-EDX. *X-Ray Spectrometry*, 36(6), pp.398-407.
- Brożek-Mucha, Z., 2014. Scanning Electron Microscopy and X-Ray Microanalysis for Chemical and Morphological Characterisation of the Inorganic Component of Gunshot Residue: Selected Problems. *BioMed Research International*, 2014, pp.1-11.
- Brożek-Mucha, Z., 2017. Trends in analysis of gunshot residue for forensic purposes. *Analytical and Bioanalytical Chemistry*, 409(25), pp.5803-5811.
- Bryce, T. and MacMillan, K., 2009. Momentum and kinetic energy: Confusable concepts in secondary school physics. *Journal of Research in Science Teaching*, 46(7), pp.739-761.
- Caldwell, M., 2019. *Development Of A Method To Estimate Measurement Uncertainty In The Creation Of Test Panels For GSR Distance Determination*. Masters Of Science. Boston University School Of Medicine.
- Campbell, J., Stipdonk, M., Wetzel, S. and Kohlhepp, B., 2018. Analysis of Metallic Components of GSR from Various Types of Ammunition and Firearms Utilizing an SEM-EDX. *Duquesne Scholarship Collection*.
- Carlucci, D. and Jacobson, S., 2018. *Ballistics: Theory And Design Of Guns And Ammunition*. 3rd ed. Boca Raton: Taylor & Francis Group.
- Carman, W., 2015. *A History Of Firearms: From Earliest Times To 1914*. 7th ed. Oxon: Routledge.

- Carter, F., Frank, T., Davies, P., McLean, D. and Cuschieri, A., 2001. Measurements and modelling of the compliance of human and porcine organs. *Medical Image Analysis*, 5(4), pp.231-236.
- Cecchetto, G., Giraudo, C., Amagliani, A., Viel, G., Fais, P., Cavarzeran, F., Feltrin, G., Ferrara, S. and Montisci, M., 2010. Estimation of the firing distance through micro-CT analysis of gunshot wounds. *International Journal of Legal Medicine*, 125(2), pp.245-251.
- Chan, O., 2013. *ABC Of Emergency Radiology*. 3rd ed. massachusetts: Wiley-Blackwell.
- Changmai, P., Bora, K., Suresh, R., Deb, N. and Mahanta, L.B., 2019. On the study of automated identification of firearms through associated striations. In *Proc. 31st Int. Symp. Ballistics*. [Accessed 10 June 2020].
- Chauhan, S., Rühaak, W., Khan, F., Enzmann, F., Mielke, P., Kersten, M. and Sass, I., 2016. Processing of rock core microtomography images: Using seven different machine learning algorithms. *Computers & Geosciences*, 86, pp.120-128.
- Eaton, R.M., 2009. 'Kiss My Foot,'Said the King: Firearms, Diplomacy, and the Battle for Raichur, 1520. *Modern Asian Studies*, *43*(1), pp.289-313.
- CHEMEUROPE, 2020. *Speedwave Xpert*. [image] Available at: <https://www.chemeurope.com/en/whitepapers/126497/efficient-quality-control-of-pharmaceutical-products.html> [Accessed 03 June 2020].
- Nibib.nih.gov. 2020. *Computational Modeling*. [online] Available at: <https://www.nibib.nih.gov/science-education/science-topics/computational-modeling> [Accessed 17 June 2020].
- Assets.publishing.service.gov.uk. 2020. *CONTROL OF HAZARDOUS SUBSTANCES IN INDOOR RANGES*. [online] Available at: <https://assets.publishing.service.gov.uk/government/uploads/system/uploads/attachment_data/file/138248/JSP403_Vol2_Chap30_DLRSC.pdf> [Accessed 02 may 2020].
- Ikuz.eu. 2020. *Convert CSV To ARFF Online*. [online] Available at: <https://ikuz.eu/csv2arff/> [Accessed 22 June 2020].
- Daghfous, A., Bouzaïdi, K., Abdelkefi, M., Rebai, S., Zoghlemi, A., Mbarek, M. and Rezgui Marhoul, L., 2015. Contribution of imaging in the initial management of ballistic trauma. *Diagnostic and Interventional Imaging*, 96(1), pp.45-55.
- Dalby, O., Butler, D. and Birkett, J., 2010. Analysis of Gunshot Residue and Associated Materials-A Review. *Journal of Forensic Sciences*, 55(4), pp.924-943.
- Darling, D., 2016. *Layers Of The Skin*. [image] Available at: <https://www.daviddarling.info/images/hypodermis.jpg> [Accessed 24 April 2020].
- HackerEarth. 2020. *Decision Tree Tutorials & Notes | Machine Learning | Hackerearth*. [online] Available at: <https://www.hackerearth.com/practice/machine-learning/machine-learning-algorithms/ml-decision-tree/tutorial/> [Accessed 27 July 2020].
- Ditrich, H., 2012. Distribution of gunshot residues – The influence of weapon type. *Forensic Science International*, 220(1-3), pp.85-90.

- Doi, K., Genant, H. and Rossmann, K., 1974. The Effect of Geometric Unsharpness upon Image Quality in Fine-Detail Skeletal Radiography. *Radiology*, 113(3), pp.723-725.
- DOWNEY, A., 2018. *Think complexity: complexity science and computational modeling.* 2nd ed. O'REILLY MEDIA, INC, USA.
- Dowsett, D., Kenny, P. and Johnston, R., 2006. *The Physics Of Diagnostic Imaging*. CRC Press.
- Du, S., Liu, C. and Huang, D., 2015. A shearlet-based separation method of 3D engineering surface using high definition metrology. *Precision Engineering*, 40, pp.55-73.
- Elkin, M., 2020. *Offences Involving The Use Of Weapons: Data Tables - Office For National Statistics*. [online] Ons.gov.uk. Available at: <https://www.ons.gov.uk/peoplepopulationandcommunity/crimeandjustice/datasets/offencesinvolvingtheuseofweaponsdatatables> [Accessed 15 July 2020].
- FBI. 2019. *Expanded Homicide Data Table 11*. [online] Available at: <https://ucr.fbi.gov/crime-in-the-u.s/2017/crime-in-the-u.s.-2017/tables/expanded-homicide-data-table-11.xls>[Accessed 18 March 2020]..
- FACKLER, M. and MALINOWSKI, J., 1985. The Wound Profile. *The Journal of Trauma: Injury, Infection, and Critical Care*, 25(6), pp.522-529.
- Fails, A. and Magee, C., 2018. *Anatomy And Physiology Of Farm Animals*. 8th ed. John Wiley & Sons.
- Farrukh, M.A. ed., 2012. *Atomic absorption spectroscopy*. BoD–Books on Demand.
- Cps.gov.uk. 2020. *Firearms | The Crown Prosecution Service*. [online] Available at: <https://www.cps.gov.uk/legal-guidance/firearms> [Accessed 19 April 2020].
- Gerard, R., McVicar, M., Lindsay, E., Randall, E. and Harvey, E., 2011. The Long Range Deposition of Gunshot Residue and the Mechanism of Its Transportation. *Canadian Society of Forensic Science Journal*, 44(3), pp.97-104.
- Goudsmits, E., Blakey, L., Chana, K., Sharples, G. and Birkett, J., 2019. The analysis of organic and inorganic gunshot residue from a single sample. *Forensic Science International*, 299, pp.168-173.
- Grahm, T.W., Williams, F.C., Harrington, T. and Spetzler, R.F., 1990. Civilian gunshot wounds to the head: a prospective study. *Neurosurgery*, *27*(5), pp.696-700.
- GRAMLICH, J., 2019. *What The Data Says About Gun Deaths In The U.S.*. [online] Pew Research Center. Available at: <https://www.pewresearch.org/fact-tank/2019/08/16/what-the-data-says-about-gun-deaths-in-the-u-s/>[Accessed 16 January 2020].
- Gribel, B., Gribel, M., Frazão, D., McNamara, J. and Manzi, F., 2011. Accuracy and reliability of craniometric measurements on lateral cephalometry and 3D measurements on CBCT scans. *The Angle Orthodontist*, 81(1), pp.26-35.
- Pbs.org. 2018. *Gun Timeline | History Detectives | PBS*. [online] Available at: <http://www.pbs.org/opb/historydetectives/technique/gun-timeline/> [Accessed 23 December 2019].

- Hamamoto, Y., Uchimura, S., Watanabe, M., Yasuda, T., Mitani, Y. and Tomita, S., 1998. A gabor filter-based method for recognizing handwritten numerals. *Pattern Recognition*, 31(4), pp.395-400.
- Hamidi, H., 2017. *Bullet In Lung*. [image] Available at: <https://prod-images-static.radiopaedia.org/images/37576160/dc107212c8bb116763ac304ade80e6_jumbo.jpeg> [Accessed 15 march 2020]..
- Hare, E., Hofmann, H. and Carriquiry, A., 2017. Automatic matching of bullet land impressions. *The Annals of Applied Statistics*, 11(4), pp.2332-2356.
- Heard, B., 2013. *Handbook Of Firearms And Ballistics*. Hoboken, N.J.: Wiley.
- heckler & koch, 2020. *MP5*. [image] Available at: <https://www.heckler-koch.com/en/products/military/submachine-guns/mp5/mp5/overview.html> [Accessed 12 April 2020].
- Hinrichs, R., Frank, P. and Vasconcellos, M., 2017. Short range shooting distance estimation using variable pressure SEM images of the surroundings of bullet holes in textiles. *Forensic Science International*, 272, pp.28-36.
- Hofer, R. and Wyss, P., 2017. The use of unburned propellant powder for shooting-distance determination. Part II: Diphenylamine reaction. *Forensic Science International*, 278, pp.24-31.
- Hofstetter, C., Maitre, M., Beavis, A., Roux, C., Weyermann, C. and Gassner, A., 2017. A study of transfer and prevalence of organic gunshot residues. *Forensic Science International*, 277, pp.241-251.
- howstuffworks, 2005. *How Shotguns Work*. [image] Available at: <https://science.howstuffworks.com/shotgun8.htm> [Accessed 25 April 2020].
- Hsu, C., Huang, Y. and Chang, K., 2008. Extended Naive Bayes classifier for mixed data. *Expert Systems with Applications*, 35(3), pp.1080-1083.
- Hughes, N. and Baker, M., 1997. The use of radiography in forensic medicine. *Radiography*, 3(4), pp.311-320.
- Humphrey, C., Henneberg, M., Wachsberger, C. and Kumaratilake, J., 2018. Comparison of porcine organs and commonly used ballistic simulants when subjected to impact from steel spheres fired at supersonic velocities. *Forensic Science International*, 288, pp.123-130.
- Imandoust, S. and Bolandraftar, M., 2013. Application of K-nearest neighbor (KNN) approach for predicting economic events theoretical background. *Int. Journal of Engineering Research and Applications*, [online] 3(5), pp.605-610. [Accessed 05 August 2020].
- Jalanti, T., Henchoz, P., Gallusser, A. and Bonfanti, M., 1999. The persistence of gunshot residue on shooters' hands. *Science & Justice*, 39(1), pp.48-52.
- Jin, Y., Mai, R., Wu, C., Han, R. and Li, B., 2018. Comparison of ballistic impact effects between biological tissue and gelatin. *Journal of the Mechanical Behavior of Biomedical Materials*, 78, pp.292-297.
- Johnson, C., Timmons, D. and Hall, P., 2003. *Essential Laboratory Mathematics*. 2nd ed. Clifton Park, N.Y.: Delmar Learning.

- Kereiakes, J. and Rosenstein, M., 2019. *Handbook Of Radiation Doses In Nuclear Medicine And Diagnostic X-Ray*. Boca Raton: CRC Press.
- Knoll, R., Reinshagen, K., Barber, S., Ghanad, I., Swanson, R., Smith, D., Abdullah, K., Jung, D., Remenschneider, A. and Kozin, E., 2019. High Resolution Computed Tomography Atlas of the Porcine Temporal Bone and Skull Base: Anatomical Correlates for Traumatic Brain Injury Research. *Journal of Neurotrauma*, 36(7), pp.1029-1039.
- Knudsen, P., Vigsnãs, J., Rasmussen, R. and Nissen, P., 1995. Terminal ballistics of 7.62 mm NATO bullets: experiments in ordnance gelatin. *International Journal of Legal Medicine*, 108(2), pp.62-67.
- Kr. Singh, B. and Mazumdar, B., 2010. Content Retrieval From X-RAY Images Using Color & Texture Features. *International Journal of Electronics Engineering*, 2(1), pp.25-28.
- Kramer, O., 2013. *Dimensionality Reduction With Unsupervised Nearest Neighbors*. 51st ed. Berlin: Springer.
- Kyllar, M., Štembírek, J., Putnová, I., Stehlík, L., Odehnalová, S. and Buchtová, M., 2013. Radiography, Computed Tomography and Magnetic Resonance Imaging of Craniofacial Structures in Pig. *Anatomia, Histologia, Embryologia*, 43(6), pp.435-452.
- Lee, C. and Wang, S., 1999. Fingerprint feature extraction using Gabor filters. *Electronics Letters*, 35(4), p.288.
- Lee, L. and Grimson, W., 2002. Gait analysis for recognition and classification. *Proceedings of Fifth IEEE International Conference on Automatic Face Gesture Recognition*, [online] Available at: <https://ieeexplore.ieee.org/abstract/document/1004148> [Accessed 05 June 2020].
- Lesmana, D., Arifurrahman, F., Hameed, A., Appleby-Thomas, G. and Santosa, S., 2020. On the importance of the bullet jacket during the penetration process: Reversed-ballistic experimental and numerical study. *Journal of Mechanical Science and Technology*,.
- Locard, E., 1920. *Dr Edmond Locard. L'enquête Criminelle Et Les Méthodes Scientifiques*. Paris: E. Flammarion.
- Lyle, D., 2019. *Forensics For Dummies*. 2nd ed. A Wiley Brand.
- M. Saloom, J., 2015. *Bullet Diagram*. [image] Available at: <https://slideplayer.com/slide/1677042/7/images/9/CARTRIDGE+CASE+PRIMER+CUP+BULLET+POWDER+ANVIL+FLASH+HOLE+J.M.+Saloom.jpg>[Accessed 14 January 2020].
- Mabbott, A., Carr, D., Champion, S. and Malbon, C., 2016. Comparison of porcine thorax to gelatine blocks for wound ballistics studies. *International Journal of Legal Medicine*, 130(5), pp.1353-1362.
- Maitre, M., Horder, M., Kirkbride, K., Gassner, A., Weyermann, C., Roux, C. and Beavis, A., 2018. A forensic investigation on the persistence of organic gunshot residues. *Forensic Science International*, 292, pp.1-10.
- Maltz, J., Sprenger, F., Fuerst, J., Paidi, A., Fadler, F. and Bani-Hashemi, A., 2009. Fixed gantry tomosynthesis system for radiation therapy image guidance based on a

multiple source x-ray tube with carbon nanotube cathodes. *Medical Physics*, 36(5), pp.1624-1636.

- Marsden, E., 1999. *Greek And Roman Artillery*. London: Sandpiper Books.

- McCue, C., 2015. *Data Mining And Predictive Analysis: Intelligence Gathering And Crime Analysis*. 2nd ed. Oxford: Butterworth-Heinemann.

- Mikołajczyk, A. and Grochowski, M., 2018. Data augmentation for improving deep learning in image classification problem. In: *2018 International Interdisciplinary PhD Workshop (IIPhDW)*. Gdańsk, Poland: IEEEE, pp.122-177.

- Miranda, K., Ortega-Ojeda, F., García-Ruíz, C. and Martínez, P., 2019. Shooting distance estimation based on gunshot residues analyzed by XRD and multivariate analysis. *Chemometrics and Intelligent Laboratory Systems*, 193, p.103831.

- Motta, L., Vanini, G., Chamoun, C., Costa, R., Vaz, B., Costa, H., Bassane, J., Carneiro, M. and Romão, W., 2015. Detection of Pb, Ba, and Sb in Blowfly Larvae of Porcine Tissue Contaminated with Gunshot Residue by ICP OES. *Journal of Chemistry*, 2015, pp.1-6.

- Munisami, T., Ramsurn, M., Kishnah, S. and Pudaruth, S., 2015. Plant Leaf Recognition Using Shape Features and Colour Histogram with K-nearest Neighbour Classifiers. *Procedia Computer Science*, 58, pp.740-747.

- Myer, W., 1977. Radiography Review: Radiographic Density. *Veterinary Radiology*, 18(5), pp.138-140.

- Mythbusters, 2015. *An Incredible Super Slow Motion Video Of A Pistol Being Fired Recorded At 73,000 Frames Per Second*. [image] Available at: <https://i.ytimg.com/vi/7y9apnbI6GA/maxresdefault.jpg> [Accessed 11 March 2020].

- Federal Bureau of Investigation. 2020. *National Instant Criminal Background Check System (NICS) | Federal Bureau Of Investigation*. [online] Available at: <https://www.fbi.gov/services/cjis/nics> [Accessed 25 February 2020].

- Nikolić, S., Juković, F., Živković, V. and Cvetković, D., 2017. *Double Suicidal Gunshot Wounds To The Heart*. [image] Available at: <https://www.semanticscholar.org/paper/Double-suicidal-gunshot-wounds-to-the-heart-Cvetkovi%C4%87-%C5%BDivkovi%C4%87/1d4869ca9ad7343059405823d3a0966c4a9d6d20/figure/0> [Accessed 01 March 2020].

- Nordin, F., Bominathan, U., Abdullah, A. and Chang, K., 2019. Forensic Significance of Gunshot Impact Marks on Inanimate Objects: The Need for Translational Research. *Journal of Forensic Sciences*, 65(1), pp.11-25.

- Oswatitsch, K., Platzer, M. and Schneider, W., 1980. *Contributions To The Development Of Gasdynamics*. Braunschweig: Wieweg.

- Park, S. and Carriquiry, A., 2019. Learning algorithms to evaluate forensic glass evidence. *The Annals of Applied Statistics*, 13(2), pp.1068-1102.

- PHILLIPS, B., 2011. *THE CHARACTERIZATION OF GUNSHOT RESIDUE IN GREEN BULLETS USING LASER INDUCED BREAKDOWN SPECTROSCOPY*. Msc. University of Alabama, Birmingham.

- PHILLIPS, G., 2020. *BIOMEDICAL APPLICATIONS OF LAMINAR AIRFLOW*. [S.l.]: CRC PRESS.
- PhysicsOpenLab, 2017. *Relative Intensity Of X-Rays And Photon Energy Graphy*. [image] Available at: <http://physicsopenlab.org/2017/08/02/bremsstrahlung-radiation/> [Accessed 05 June 2020].
- Plaats, G. and Van der Plaats, G., 1980. *Medical X-Ray Techniques In Diagnostic Radiology. A Textbook For Radiographers And Radiological Technicians. 4.Ed*. London: MacMillan.
- Powers, D. and Delo, R., 2015. *Maxillofacial Ballistic And Missile Injuries*. [image] Available at: <https://pocketdentistry.com/wp-content/uploads/285/B9781455705542000277_f027-005a-9781455705542.jpg>. [Accessed 15 January 2020].
- Radiantviewer.com. 2020. *Radiant DICOM Viewer*. [online] Available at: <https://www.radiantviewer.com/> [Accessed 21 September 2020].
- Ranganathan, S., Gribskov, M., Nakai, K. and Schönbach, C., 2018. *Encyclopedia Of Bioinformatics And Computational Biology*. 1st ed. Elsevier, 2018.
- Reeves, P. and Decker, S., 2012. Diagnostic radiography: A study in distancing. *Radiography*, 18(2), pp.78-83.
- Rosenberg, Z. and Dekel, E., 2012. *Terminal Ballistics*. 3rd ed. Cham: Springer.
- Roux, C., Crispino, F. and Ribaux, O., 2018. From Forensics to Forensic Science. *Forensic Science and Justice: From Crime Scene to Court and Beyond*, 24(1).
- Russo, P., 2017. *Handbook Of X-Ray Imaging*. CRC Press, pp.327-330.
- Saad Hussein, A., Li, T., Yohannese Chubato, W. and Bashir, K., 2019. A-SMOTE: A New Preprocessing Approach for Highly Imbalanced Datasets by Improving SMOTE. *International Journal of Computational Intelligence Systems,*, *12*(2), pp.1412-1422.
- Sahu, K., Kennao, P., Gupta, A., Saran, V. and Waghmare, N., 2018. Study of 9mm Improvised Pistol Pattern and Gunshot Residue with respect to Different Range. *International Journal of Computer Sciences and Engineering*, 6(5), pp.155-160.
- Santos, A., Magalhães, T., Vieira, D., Almeida, A. and Sousa, A., 2007. Firing Distance Estimation Through the Analysis of the Gunshot Residue Deposit Pattern Around the Bullet Entrance Hole by Inductively Coupled Plasma Mass Spectrometry. *The American Journal of Forensic Medicine and Pathology*, 28(1), pp.24-30.
- Schweinberger, M., 2011. Statistical modelling of network panel data: Goodness of fit. *British Journal of Mathematical and Statistical Psychology*, 65(2), pp.263-281.
- Gov.uk. 2020. *Shotgun And Firearm Certificates - GOV.UK*. [online] Available at: <https://www.gov.uk/shotgun-and-firearm-certificates> [Accessed 20 February 2020].
- Javatips.net. 2020. *Simplecolorhistogram.Java Example*. [online] Available at: <https://www.javatips.net/api/lire-master/src/main/java/net/semanticmetadata/lire/imageanalysis/features/global/SimpleColorHistogram.java> [Accessed 19 June 2020].

- Smyth Wallace, J., 2018. *Chemical Analysis Of Firearms, Ammunition, And Gunshot Residue, Second Edition*. Milton: Chapman & Hall/CRC Press.
- Sookaromdee, P. and Wiwanitkit, V., 2017. Quality assurance training course on chest radiography in Laos. *International Journal of Mycobacteriology*, 6(4), p.414.
- Spathis, V., 2017. *FEG-SEM Image Of Impact-Disrupted GSR Showing The Imaging Capabilities Of A Cold Field Emission SEM. Scale On Zoomed In Image: 1 Mm HV 1.5 Kv.*. [image] Available at: <https://www.sciencedirect.com/science/article/pii/S2214914717300570> [Accessed 02 February 2020].
- Srivastava, S., 2014. Weka: A Tool for Data preprocessing, Classification, Ensemble, Clustering and Association Rule Mining. *International Journal of Computer Applications*, 88(10), pp.26-29.
- Stefanopoulos, P., Soupiou, O., Pazarakiotis, V. and Filippakis, K., 2015. Wound ballistics of firearm-related injuries—Part 2: Mechanisms of skeletal injury and characteristics of maxillofacial ballistic trauma. *International Journal of Oral and Maxillofacial Surgery*, 44(1), pp.67-78.
- Stentiford, F., 2004. A Visual Attention Estimator Applied to Image Subject Enhancement and Colour and Grey Level Compression. In: *17th International Conference on Pattern Recognition*. [online] Cambridge, UK: IEEE Computer Society [Accessed 26 July 2020].
- Sun, J., Chen, G., Qian, L. and Liu, T., 2017. Analysis of gun barrel rifling twist. In: *Analysis of gun barrel rifling twist*. [online] Nanjing: Nanjing University of Science and Technology. Available at: <https://doi.org/10.1063/1.4982461> [Accessed 11 August 2020].
- Sutton, O., 2012. Introduction to k nearest neighbour classification and condensed nearest neighbour data reduction. *University lectures, University of Leicester*, *pp.1-10*.
- GOV.UK. 2020. *Table 1: Types Of Firearms*. [online] Available at: <https://www.gov.uk/government/publications/deactivated-firearms-implementing-regulation-eu-20152403/table-1-types-of-firearms> [Accessed 15 July 2020].
- Tang, Z., Tu, W., Zhang, G., Chen, Y., Lei, T. and Tan, Y., 2012. Dynamic simulation and preliminary finite element analysis of gunshot wounds to the human mandible. *Injury*, 43(5), pp.660-665.
- Taudte, R., Roux, C., Blanes, L., Horder, M., Kirkbride, K. and Beavis, A., 2016. The development and comparison of collection techniques for inorganic and organic gunshot residues. *Analytical and Bioanalytical Chemistry*, 408(10), pp.2567-2576.
- Team, D., 2020. *Txdps - Handgun Licensing*. [online] Dps.texas.gov. Available at: <https://www.dps.texas.gov/rsd/ltc/index.htm> [Accessed 20 February 2020].
- 1929. *Textbook Of Small Arms*. London: Naval and Military Press.
- Thali, M., Viner, M. and Brogdon, B., 2011. *Brogdon's Forensic Radiology*. 2nd ed. Boca Raton: CRC Press.
- Tortora, G. and Derrickson, B., 2009. *Principles Of Anatomy And Physiology*. 12th ed. Hoboken: John Wiley & Sons.

- Tucker, W., Lucas, N., Seyfang, K., Kirkbride, K. and Popelka-Filcoff, R., 2017. Gunshot residue and brakepads: Compositional and morphological considerations for forensic casework. *Forensic Science International*, 270, pp.76-82.
- Van Loon, J., 2012. *Analytical Atomic Absorption Spectroscopy*. New York: Acad. Press.
- Vanini, G., Destefani, C., Merlo, B., Carneiro, M., Filgueiras, P., Poppi, R. and Romão, W., 2015. Forensic ballistics by inductively coupled plasma-optical emission spectroscopy: Quantification of gunshot residues and prediction of the number of shots using different firearms. *Microchemical Journal*, 118, pp.19-25.
- Vorburger, T., Song, J. and Petraco, N., 2015. Topography measurements and applications in ballistics and tool mark identifications. *Surface Topography: Metrology and Properties*, 4(1), p.013002.
- Wallace, J., 2018. *Chemical Analysis Of Firearms, Ammunition, And Gunshot Residue*. 2nd ed. Boca Raton: CRC Press.
- Warlow, T., 2016. *Firearms, The Law, And Forensic Ballistics*. 3rd ed. Boca Raton: Taylor & Frances Group.
- Wen, Y., Xu, C., Jin, Y. and Batra, R., 2017. Rifle bullet penetration into ballistic gelatin. *Journal of the Mechanical Behavior of Biomedical Materials*, 67, pp.40-50.
- Werner, D., Gassner, A., Marti, J., Christen, S., Wyss, P. and Weyermann, C., 2020. Comparison of three collection methods for the sodium rhodizonate detection of gunshot residues on hands. *Science & Justice*, 60(1), pp.63-71.
- Wong, S., Gatt, A., Stamatescu, V. and McDonnell, M., 2016. Understanding data augmentation for classification: when to warp?. In: *In 2016 international conference on digital image computing: techniques and applications*. [online] IEEE. Available at: <https://ieeexplore.ieee.org/abstract/document/7797091> [Accessed 27 JuneHGac 2020].
- Xiao-ling, X., Chun-yue, J. and Zhe-tang, C., 2009. Study on the relation between gunshot distance and gunshot residues distribution of 92 pistol [J]. *Forensic Science and Technology*, *3*.
- Xiao-yong, L.I., 2004. The Relations between the Remains of Gunshot and the Distance of Gunshot. *Journal of Shanxi Police Academy*, *3*.
- Yacob, N., Mohamed, M. and Megat Hanafiah, M., 2016. *Regional Conference On Science, Technology And Social Sciences (RCSTSS 2014)*. 1st ed. Singapore: Springer; 1st ed. 2016 edition, pp.241-249.
- YANG, J., 2011. XML Document Classification Based on Kernel Method. *Chinese Journal of Computers*, 34(2), pp.353-359.
- You, H., Lee, S., Ok, Y., Kang, H., Sung, H., Lee, J., Kang, S. and Hyun, S., 2019. Influence of swabbing solution and swab type on DNA recovery from rigid environmental surfaces. *Journal of Microbiological Methods*, 161, pp.12-17
- Zhang, Z. and Sejdić, E., 2019. Radiological images and machine learning: Trends, perspectives, and prospects. *Computers in Biology and Medicine*, 108, pp.354-370.